DEVELOPMENT OF THIN FILM COMPOSITE HOLLOW FIBRE MEMBRANES FOR ORGANIC SOLVENT APPLICATIONS

GOH KENG SIANG

Interdisciplinary Graduate School

Singapore Membrane Technology Centre / Nanyang Environment and Water Research Institute

2022

DEVELOPMENT OF THIN FILM COMPOSITE HOLLOW FIBRE MEMBRANES FOR ORGANIC SOLVENT APPLICATIONS

GOH KENG SIANG

Interdisciplinary Graduate School

Singapore Membrane Technology Centre / Nanyang Environment and Water Research Institute

A thesis submitted to the Nanyang Technological University in partial fulfilment of the requirement for the degree of

Doctor of Philosophy

2022

Statement of Originality

I hereby certify that the work embodied in this thesis is the result of original research, is free of plagiarised materials, and has not been submitted for a higher degree to any other University or Institution.

31/07/2021

Date

Goh Keng Siang

Supervisor Declaration Statement

I have reviewed the content and presentation style of this thesis and declare it is free of plagiarism and of sufficient grammatical clarity to be examined. To the best of my knowledge, the research and writing are those of the candidate except as acknowledged in the Author Attribution Statement. I confirm that the investigations were conducted in accord with the ethics policies and integrity standards of Nanyang Technological University and that the research data are presented honestly and without prejudice.

31/7/2021

Date

Wang Rong

Authorship Attribution Statement

This thesis contains material from 3 papers published in the following peer-reviewed journals where I was the first and/or corresponding author.

Chapter 3 is published as K.S. Goh, J.Y. Chong, Y. Chen, W. Fang, T.-H. Bae, R. Wang, Thin-film composite hollow fibre membrane for low pressure organic solvent nanofiltration, Journal of Membrane Science, 597 (2020) 117760. https://doi.org/10.1016/j.memsci.2019.117760

The contributions of the co-authors are as follows:

- Prof Wang provided the initial project direction, obtained the funding for the project and edited the manuscript drafts.
- Prof Bae provided initial direction on project and provided analysis tools.
- I prepared the manuscript drafts while Dr Chong and Dr Chen revised the manuscript.
- I co-designed the study with Dr Chong and Dr Chen and performed all the laboratory work at Singapore Membrane Technology Centre. I also analysed all the data.

Chapter 4 is published as K.S. Goh, Y. Chen, J.Y. Chong, T.H. Bae, R. Wang, Thin film composite hollow fibre membrane for pharmaceutical concentration and solvent recovery, Journal of Membrane Science, 621 (2021) 119008. https://doi.org/10.1016/j.memsci.2020.119008

The contributions of the co-authors are as follows:

- Prof Wang edited the manuscript drafts and obtained the funding for the project.
- Prof Bae provided initial direction on project and provided analysis tools.
- Dr Chong provided the initial project direction.
- I prepared the manuscript drafts while Dr Chong and Dr Chen revised the manuscript.
- I co-designed the study with Dr Chong and Dr Chen and performed all the laboratory work at Singapore Membrane Technology Centre. I also obtained all characterisation and analysed all the data.

Chapter 6 is published as K. S. Goh, Y. Chen, D. Y. F. Ng, J. W. Chew, and R. Wang, "Organic solvent forward osmosis membranes for pharmaceutical concentration," Journal of Membrane Science, 642 (2022) 119965. https://doi.org/10.1016/j.memsci.2021.119965

The contributions of the co-authors are as follows:

- Prof Wang and Dr Chen provided the initial project direction and edited the manuscript drafts.
- Prof Chew provided initial direction on project and provided analysis tools.
- I prepared the manuscript drafts while Dr Ng and Dr Chen revised the manuscript.
- I co-designed the study with Dr Ng and performed all the laboratory work at Singapore Membrane Technology Centre. I also obtained all characterisation and analysed all the data.

31/07/2021

Date

Goh Keng Siang

ACKNOWLEDGEMENTS

I would like to take this opportunity to thank Nanyang Technological University for awarding me the Nanyang President's Graduate Scholarship to pursue my doctorate. I would also like to thank Interdisciplinary Graduate Program, Nanyang Environmental Water and Research Institute and Singapore Membrane Technology Centre for their material and financial support.

I would like to express my utmost gratitude to my supervisor, Professor Wang Rong, for her words of encouragement and guidance throughout my PhD. Her expertise in the field of membrane science and her resourcefulness has been very helpful in my research. I would also like to thank my co-supervisors Dr. Bae Tae-Hyun and Associate Professor Chew Jia Wei for their guidance on my research.

I would like to acknowledge the indispensable support from Dr. Chen Yun Feng, Dr. Chong Jeng Yi and Dr. Ng Yee Fan whom I have worked very closely with throughout my PhD. Your guidance on numerous subject matters helped me immensely throughout my PhD. I would also like to extend my appreciation to Zhang Li Zhi and the NEWRI team for their help in the lab.

I would also like to thank my undergraduate research supervisor and mentor, Associate Professor Cao Bin and Dr. Ng Chun Kiat, for kindling my interest in research. Special thanks to my lunch buddies, Jeremine and Jing Wee, for keeping the office lively throughout my PhD.

Last but not least, I would like to express my deepest appreciation to my family and girlfriend, Ms. Yi Yong, for their endless love, understanding and encouragement they have shown me throughout my journey in pursuing the doctorate degree.

LIST OF PUBLICATIONS

K. S. Goh, J. Y. Chong, Y. Chen, W. Fang, T. H. Bae, R. Wang, "Thin film composite hollow fibre membranes for organic solvent nanofiltration", Journal of Membrane Science, 597, 117760, 2020

K. S. Goh, Y. Chen, J. Y. Chong, T. H. Bae, R. Wang, "Thin film composite hollow fibre membrane for pharmaceutical concentration and solvent recovery", Journal of Membrane Science, 621, 119008, 2021

K. S. Goh, Y. Chen, D. Y. F. Ng**,** J. W. Chew, R. Wang, "Organic solvent forward osmosis membranes for pharmaceutical concentration", Journal of Membrane Science, Journal of Membrane Science, 642, 119965, 2022

X. You, J. Y. Chong, **K. S. Goh**, M. Tian, J. W. Chew, R. Wang. "Electrospun polyimide-based thin-film composite membranes for organic solvent nanofiltration", Journal of Membrane Science, 640, 119825, 2021

TABLE OF CONTENTS

ACKNOWLEDGEMENTS vii

LIST OF PUBLICATIONS viii

TABLE OF CONTENTS ix

SUMMARY xiii

LIST OF TABLES xvi

LIST OF FIGURES xvii

Chapter 1 Introduction 1

1.1 Background 1

1.1.1 Membrane technology 1

1.1.2 Organic solvent nanofiltration and its challenges 3

1.1.3 Organic solvent forward osmosis and its challenges 7

1.2 Research objectives 11

1.3 Thesis outline 12

Chapter 2 Literature review 13

2.1 Fundamentals of membrane separation processes 13

2.1.1 Pore-flow model 13

2.1.2 Solution diffusion model 14

2.1.3 Concentration polarisation 16

2.2 Solvent resistant polymeric membranes 18

2.2.1 Polymeric membranes 18

2.2.2 Crosslinking 24

2.3 Membrane fabrication 25

2.3.1 Phase inversion 25

2.3.2 Fabrication of integrally skinned asymmetric membrane 29
2.3.3 Fabrication of OSN TFC membrane 31
2.3.4 Fabrication of OSFO TFC membrane 33
2.3.5 Membrane configurations and module design 34
2.4 Membrane application in pharmaceutical industry (include OSFO) 39
2.4.1 Solvent exchange 39
2.4.2 Solvent recovery 46
2.4.3 Separation and purification of active pharmaceutical ingredients 47
Chapter 3 Thin film composite hollow fibre membrane for low pressure organic solvent nanofiltration 50
3.1 Introduction 50
3.2 Materials and methods 52
3.2.1 Materials and chemicals 52
3.2.2 Spinning of polyimide hollow fibre membranes and cross-linking 53
3.2.3 Synthesis of TFC layer by interfacial polymerisation 55
3.2.4 Membrane characterisation 55
3.2.5 Membrane separation properties 57
3.3 Results and discussion 59
3.3.1 Fabrication of solvent resistant polyimide hollow fibre substrates 59
3.3.2 Solvent resistant properties of polyimide hollow fibre substrates 61
3.3.3 Polyamide synthesis on cross-linked polyimide hollow fibres 65
3.3.4 Performance of TFC hollow fibre membranes 70
3.4 Conclusions 77
Chapter 4 Thin film composite hollow fibre membrane for pharmaceutical concentration and solvent recovery 78
4.1 Introduction 78

4.2 Materials and methods 80
4.2.1 Materials and chemicals 80
4.2.2 Fabrication of hollow fibre membrane module 80
4.2.3 Membrane characterisation and performance evaluation 82
4.2.4 Effect of solvent activation on membrane separation properties 83
4.2.5 7-day stability test and concentration of active pharmaceutical ingredients 83
4.3 Results and discussion 84
4.3.1 Characterisation of P84 hollow fibre substrate 84
4.3.2 Characterisation of polyamide thin-film composite membrane 88
4.3.3 Scalability of hollow fibre membrane 92
4.3.4 Extended filtration test for pristine 100-piece module 95
4.3.5 Solvent activation of 100-piece module 96
4.3.6 Concentration of levofloxacin and solvent recovery 101
4.3.7 Performance comparison of solvent-activated membrane and commercial membranes 103
4.4 Conclusions 107
Chapter 5 Thin film composite hollow fibre membrane: Upscaling 108
5.1 Introduction 108
5.2 Materials and methods 109
5.2.1 Fabrication of hollow fibre membranes and modules 109
5.2.2 Defect identification and repair 112
5.2.3 Membrane characterisation and performance evaluation 113
5.2.4 Simultaneous pharmaceutical concentration and solvent recovery 113
5.3 Results and discussion 114
5.3.1 Characterisation of polyamide thin-film composite membrane 114
5.3.2 Effect of upscaling on membrane performances 116

5.3.3 Extended filtration test for P500 122
5.3.4 Performance in OSN application 123
5.4 Conclusions 125
Chapter 6 Organic solvent forward osmosis membrane 126
6.1 Introduction 126
6.2 Materials and methods 127
6.2.1 Materials and chemicals 127
6.2.2 Fabrication of thin-film composite hollow fibre membrane 127
6.2.3 Membrane characterisation and performance evaluation 129
6.2.4 Organic solvent forward osmosis application 132
6.3 Results and discussion 133
6.3.1 Characterisation of polyimide substrate 133
6.3.2 Characterisation of selective layer 138
6.3.3 FO performance of lab-scale and scaled-up modules 142
6.3.4 OSFO performance tests for P500 module 144
6.4 Conclusions 151
Chapter 7 Conclusions and recommendations 152
7.1 Overall conclusion 152
7.2 Recommendations for future research 154
7.2.1 OSN performance tests 154
7.2.2 Concentration polarisation 155
7.2.3 Draw solution for OSFO 155
References 157

SUMMARY

Membrane technology has seen significant growth in the past few decades and been implemented in various industries like water treatment and food processing. In recent years, there is an increased demand for greener purification processes for the pharmaceutical industry, and membrane separation technology is at the forefront of this transformation. Organic solvent nanofiltration (OSN) and more recently, organic solvent forward osmosis (OSFO), have attracted much attention due to their potential economic and environmental benefits. The technology typically can achieve separation with much lower energy requirements, compared to conventional processes such as distillation. In addition, these athermal processes reduce the likelihood of damaging thermally sensitive compounds in the feed stream, thereby improving product quality. However, these membrane separation processes face several obstacles. The membrane has to be chemically stable in a wide range of organic solvents and maintain its performance over long period of time. This narrows down the type of polymers that can be used to fabricate these membranes. The membrane fabricated should also be relatively easy to scale-up and replicable. In addition, the purification of high-value pharmaceutical products should achieve high yield and purity. Therefore, the design of OSN and OSFO membranes should focus on high selectivity and robustness.

To address these challenges, a solvent resistant hollow fibre thin-film composite (TFC) membrane was fabricated via a non-solvent induced phase separation process. Cross-linked P84 polyimide was used as the substrate due to its excellent chemical stability in a wide range of organic solvents commonly used in the pharmaceutical industry. To achieve solvent resistance, the polyimide substrate was chemically cross-linked with a diamine. TFC membrane was prepared via an interfacial polymerisation (IP) process and the selective layer was formed in the lumen. A mixture of piperazine (PIP) and polyetherimide (PEI) was used as

the monomers to improve solvent flux for low pressure OSN process. The membranes then underwent OSN performance tests to evaluate its performance. In general, the tests were performed on a cross-flow setup at 2 – 5 bar. Dyes of various molecular weights were added into organic solvents at 50 ppm concentrations to evaluate selectivity of the fabricated membranes. From the OSN performance tests, the TFC membrane exhibited high solvent permeabilities of 11.6 and 4.5 LMH/Bar for acetone and isopropanol, respectively. In addition, the membrane achieved a molecular weight cut-off (MWCO) of about 585 Da, showing promising performance in the nanofiltration range.

The TFC hollow fibre membrane was further improved by optimising the dope composition and spinning parameters of the substrate. The mixture of amine monomers for IP was replaced with m-phenylenediamine (MPD) to obtain a more selective membrane for active pharmaceutical ingredients (APIs) with smaller molecular weights (<300 Da). To maintain its high solvent permeability, the TFC membrane was solvent-activated with n,n-dimethylformamide. Moreover, a feasibility study was done on its scalability by fabricating a 100-piece membrane module. The TFC membrane achieved high solvent permeabilities of 24.3 and 2.33 LMH/Bar for acetone and ethanol, respectively. In addition, it achieved an even higher selectivity with an MWCO of about 269 Da. The scaling-up process also demonstrated that much of the membrane performance was maintained, showing promising potential for further scale-up. The membrane was further tested by concentrating levofloxacin (361 Da), an API, in acetone, to simulate the concentration of pharmaceutical products and recovery of organic solvents. The membrane maintained excellent selectivity (>99%) but gradually diminished due to concentration polarisation.

Subsequently, the membrane was scaled-up to match that of a small commercial membrane module (2 inch). The scale-up module featured a membrane area of about 1.4 m^2 with superior

packing density compared to spiral wound modules. The performance of the scale-up module was also similarly tested and exhibited slightly lower solvent permeabilities, while the selectivity was maintained. On closer inspection, this indicated that the IP process was scalable for hollow fibre membranes on a much larger scale but with a thicker selective layer. The increase in mass transport resistance resulted in the low solvent permeability achieved. Nonetheless, selectivity is much more important in pharmaceutical industry when processing of high-value APIs. Therefore, the study demonstrated that the fabrication method for the TFC hollow fibre membrane is facile and scalable.

Lastly, the hollow fibre substrate was further modified for OSFO application. Through the optimisation of spinning parameters and dope composition, the resulting substrate possessed significantly higher porosity, thinner and overall, lower structural parameter. A similar MPD-based selective layer was synthesized via IP and demonstrated excellent selectivity with 92.1% rejection for methyl red (269 Da) in ethanol. Similarly, the TFC hollow fibre membrane was scaled-up to 2 inch modules and tested for OSFO performance. The membrane displayed high isopropanol and acetone fluxes of 0.63 and 13.9 LMH, respectively, using 2 M polyethylene glycol (PEG) 400 as draw solute. The membrane also exhibited low specific reverse solute flux when PEG 400 was used as draw solute for both solvent systems. In the pharmaceutical concentration experiment, levofloxacin in acetone was concentrated with 2 M PEG 400 as draw solution. The membrane was able to concentrate the API from 1000 ppm to 16,000 ppm while maintaining high selectivity (>95%). Overall, this study demonstrated promising potential of OSFO to be used in the pharmaceutical industry for API concentration.

LIST OF TABLES

Table 2-1 Summary of polymers used in OSN membrane fabrication 22

Table 2-2: Summary of commercial membrane configurations and their advantages and disadvantages [40] 38

Table 2-3: Commercial OSN membranes 41

Table 3-1 Dope composition for fabricating polyimide hollow fibre membranes 53

Table 3-2 Spinning parameters for polyimide hollow fibre membrane 54

Table 3-3 Membrane properties of substrate before and after cross-linking 62

Table 3-4 Swelling factor and weight loss for the cross-linked membrane 65

Table 3-5 Surface chemical composition of cross-linked polyimide substrate and polyamide TFC membrane by XPS wide-scan analysis 68

Table 3-6 OSN performance of polymeric hollow fibre membranes reported in literature 75

Table 4-1 Spinning condition for P84 hollow fibre 81

Table 4-2 Properties of membrane substrate before and after cross-linking 85

Table 4-3 Swelling degree and weight loss for cross-linked membranes in organic solvents for 7 days 87

Table 4-4 Elemental composition of substrate and thin-film composite surface by XPS wide scan 92

Table 4-5 OSN membrane performance of recent works and 100-piece module developed in this work 105

Table 5-1: Dimensions of hollow fibre modules 111

Table 5-2: Module properties 117

Table 5-3: Performances of various commercial OSN membranes 121

Table 6-1: Spinning parameters of hollow fibre substrate 128

Table 6-2: Dimensions of module for hollow fibre FO membranes 128

Table 6-3: Physical properties of polyimide substrate before and after cross-linking 134

Table 6-4: Viscosity of different solutions 146

Table 6-5: Concentrating feed in solvent streams using membrane-based separation processes 150

LIST OF FIGURES

Figure 1-1: Schematic illustration of a semi-permeable membrane separation process 2
Figure 1-2: Types of pressure-driven membrane separation technology 3
Figure 1-3: Publications in Web of Science relating to OSN 7
Figure 1-4: Schematic illustration of forward osmosis membrane process 8
Figure 2-1: Concentration gradient profile and effect of concentration polarisation for a typical TFC membrane. (a) RO mode; (b) AL-FS mode; (c) AL-DS 17
Figure 2-2: Ternary phase diagram. Mechanism of phase separation for membrane fabrication 26
Figure 2-3 (a) Support layer with finger-like structures (macrovoids) (b) Support layer with sponge-like structures (interconnected pores) 27
Figure 2-4: Schematic drawing of hollow fibre membrane fabrication using dry-jet wet spinning. (a) Spinning setup; (b) cross-section of spinneret 28
Figure 2-5: Integrally-skinned asymmetric membrane 29
Figure 2-6: Interfacial Polymerisation 32
Figure 2-7: Schematic illustration of membrane configurations. (a) Plate-and-frame; (b) Spiral wound; (c) Tubular / Hollow fibre. Modified from [141] 36
Figure 2-8: Flow diagram of active pharmaceutical ingredient synthesis process 40
Figure 2-9: Schematic diagram of solvent recovery unit 47
Figure 2-10: Schematic drawing of concentration and purification of active pharmaceutical ingredient 49
Figure 3-1 SEM images of hollow fibre substrate. (a-d) cross-section, inner surface, outer surface and enlarged cross-section of inner surface of the substrate with LiCl as pore former; (A-D) cross-section, inner surface, outer surface and enlarged cross-section of inner surface of the substrate with DG as pore former 60
Figure 3-2 water permeability and MWCO for hollow fibre substrate 61
Figure 3-3 SEM images of hollow fibre substrate. (a) cross-section of uncross-linked; (A) inner surface of uncross-linked; (b) cross-section of cross-linked; (B) inner surface of cross-linked 63
Figure 3-4 FTIR of uncross-linked and cross-linked polyimide substrate 64
Figure 3-5 SEM images of TFC. (a) inner surface; (b) enlarged cross-section 66

Figure 3-6 XPS narrow scan spectra on the surface of (a): N1s cross-linked polyimide substrate, (b) N1s polyamide thin film composite, (c) O1s cross-linked polyimide substrate, (d) O1s polyamide thin film composite 67
Figure 3-7: Effect of PEI concentration on acetone permeability and dye rejection. (a) RB; (b) MO (amine solution pH=11; rejection of 35 μM dyes at pressure of 2 bar) 69
Figure 3-8: Solvent permeability of thin film composite membrane 71
Figure 3-9 Comparison of rejection and with different molecular weights 72
Figure 3-10 72-h filtration test (35 μM acid fuchsin in acetone at 2 bar for 72 hours)[a]: The permeabilities are obtained from acetone feed with acid fuchsin rather than pure acetone. 73
Figure 4-1: SEM images of hollow fibre substrate. (a) cross-section; (b) enlarged cross-section near lumen; (c) inner surface 85
Figure 4-2 FTIR spectrum of uncross-linked and cross-linked polyimide substrate 86
Figure 4-3: Solvent permeability of substrate 88
Figure 4-4 SEM images of TFC membranes, (a) inner surface; (A) enlarged inner surface; (b) cross-section; (B) enlarged cross-section 89
Figure 4-5 (a) XPS wide scan of polyimide substrate and polyamide TFC membrane, XPS spectra of (b) substrate N1s, (c) TFC N1s, (d) substrate O1s and (e) TFC O1s 91
Figure 4-6: Outside view and cross-section of hollow fibre membrane modules; (a) Outside view of 5-piece and 100-piece modules; (b) Cross-section of 5-piece and 100-piece modules 93
Figure 4-7 Solvent permeability comparisons for 5-piece and 100-piece modules 93
Figure 4-8 Solute rejections comparisons for 5-piece and 100-piece modules in acetone 94
Figure 4-9 SEM images of the inner surface of the 100-piece module. (a) inlet of the module; (b) outlet of the module 95
Figure 4-10 7-day filtration test for 100-piece module (50 ppm of methyl red in acetone at 2 bar) 96
Figure 4-11: SEM images of pristine and solvent-activated membrane. (a) and (A) Inner surfaces of solvent-activated and pristine membranes; and (b) and (B) cross-sections of solvent-activated and pristine membranes 97
Figure 4-12 Solvent permeability of pristine and solvent-activated membranes 98
Figure 4-13 Solute rejection of pristine and solvent-activated membranes 99
Figure 4-14 7-day filtration test for solvent-activated 100-piece module (50 ppm of methyl red in acetone at 2 bar) 100

Figure 4-15: Levofloxacin concentration and solvent recovery - rejection and permeability for pristine and solvent-activated 100-piece module 102
Figure 5-1: Potting of 2-inch module 110
Figure 5-2: Spacer configuration for 2-in module. (a) cross-section of spacer; (b) location of space along fibre bundle 111
Figure 5-3: Schematic drawing of defect identification and repair 112
Figure 5-4: Schematic drawing of pharmaceutical concentration and solvent recovery system 114
Figure 5-5: SEM images of the polyamide selective layer from modules with various scales. (a) P5; (b) P500; (c) P1500 115
Figure 5-6: XPS spectra of (a) P5 N1s; (b) P500 N1s; (c) P1500 N1s; (d) P5 O1s; (e) P500 O1s; (f) P1500 O1s 116
Figure 5-7: Cross-section of scaled-up hollow fibre module. (a) P1500; (b) P500 117
Figure 5-8: Solvent permeabilities of thin film composite membranes 120
Figure 5-9: Rejection of dyes in ethanol 120
Figure 5-10: Stability test of P500 module for OSN performance. 50 ppm methyl red dissolved in ethanol 122
Figure 5-11: Simultaneous pharmaceutical concentration and solvent recovery for P5 and P500 modules 124
Figure 6-1: Schematic diagram of forward osmosis experimental setup 131
Figure 6-2: SEM images of cross-linked hollow fibre substrate. (a) Cross-section; (b) enlarged cross-section; (c) cross-section of inner surface; (d) inner surface; (e) cross-section of outer surface; (f) outer surface 135
Figure 6-3: Solvent permeability of hollow fibre substrates in various solvents 136
Figure 6-4: FTIR spectrum of uncross-linked and cross-linked polyimide substrates. 137
Figure 6-5: SEM images of thin-film composite hollow fibre membranes, (a) inner surface; (b) enlarged inner surface; (c) cross-section 138
Figure 6-6: XPS spectra of (a) substrate N1s, (b) TFC N1s, (c) substrate O1s and (d) TFC O1s 139
Figure 6-7: Solvent permeabilities for P5 and P500 thin-film composite modules 141
Figure 6-8: Solute rejections of P5 and P500 modules in ethanol and water 141
Figure 6-9: FO performance of P5 and P500 modules in AL-FS orientation. (a) and (A) Water flux (*Jw*) and RSF (*Js*); (b) and (B) Specific RSF (*Js/Jw*) 143

Figure 6-10: Effect of draw solution concentration on organic solvent forward osmosis performance. (a) Acetone flux (J_{ace}) and RSF ($J_{PEG\ 400}$); (A) IPA flux (J_{IPA}) and RSF ($J_{PEG\ 400}$); (b) and (B) Specific solute flux of PEG 400 145
Figure 6-11: Concentration of levofloxacin in AL-FS orientation. Effects of feed concentration on (a) solvent and RSF; (b) specific RSF 148

Chapter 1 Introduction

1.1 Background

1.1.1 Membrane technology

Semi-permeable membranes have been used as a separation technology for a wide range of applications. A schematic illustration of a cross-flow membrane separation process is shown in Figure 1-1. A feed (solute-solvent mixture) is separated at the membrane interface into retentate (higher concentration of solute) and permeate (lower concentration of solute) using a driving force [1]. Depending on its applications and properties of the fluid mixture, the primary driving force used can be the differences in pressure, concentration, thermal gradient, as well as electric potential across the semi-permeable barrier [2-5]. There are several advantages for using membrane for separation and purification compared to conventional technology such as distillation and crystallisation. In general, membrane filtration processes do not require a change in phase of the feed stream. As a result, lower energy is usually required to accomplish the separation [6]. In addition, membranes can be fabricated using a wide range of polymers and inorganic materials, allowing membranes to be designed with application-specific properties.

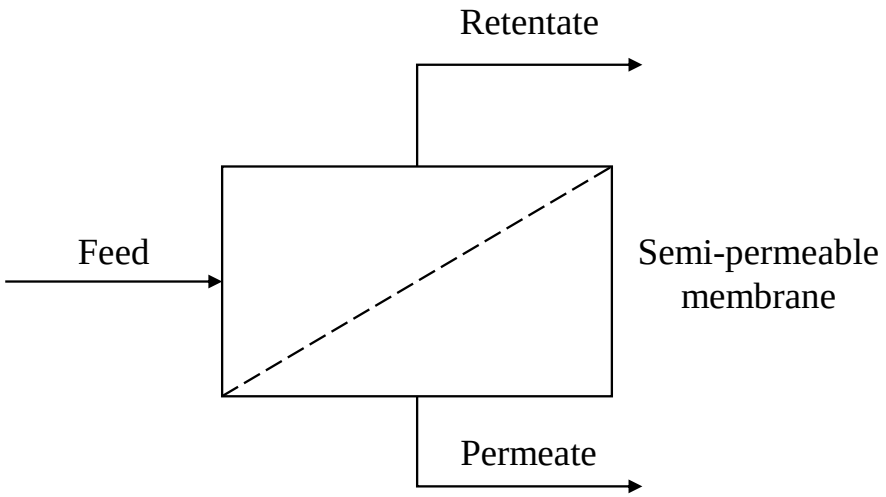

Figure 1-1: Schematic illustration of a semi-permeable membrane separation process

Since the advent of the first anisotropic reverse osmosis (RO) membrane by Loed and Sourirajan via phase inversion process in early 1960s [4], membrane technology has progressed drastically. Subsequent development of commercial microfiltration (MF), ultrafiltration (UF) and nanofiltration (NF) membranes in the 1970s led to even broader applications in wastewater treatment and water softening [7-10]. Since then, new membrane configurations have been developed and this allowed wider adoption of membrane technology by various industries (Figure 1-2). For example, the development of composite RO membranes significantly improved separation performance, which readily substituted energy intensive thermal desalination processes in water purification [11]. In addition, the exploration of novel membrane processes such as forward osmosis, membrane distillation and gas separation have opened the field of membrane separation and its potential applications [6, 12-14]. In recent decades, the development of more robust and chemically resistant membranes enabled membrane separation processes to be used in industries like chemical, pharmaceutical and food industries. As such, a new branch of membrane technology has emerged, with the aim of improving energy and material recovery efficiencies in these industrial processes.

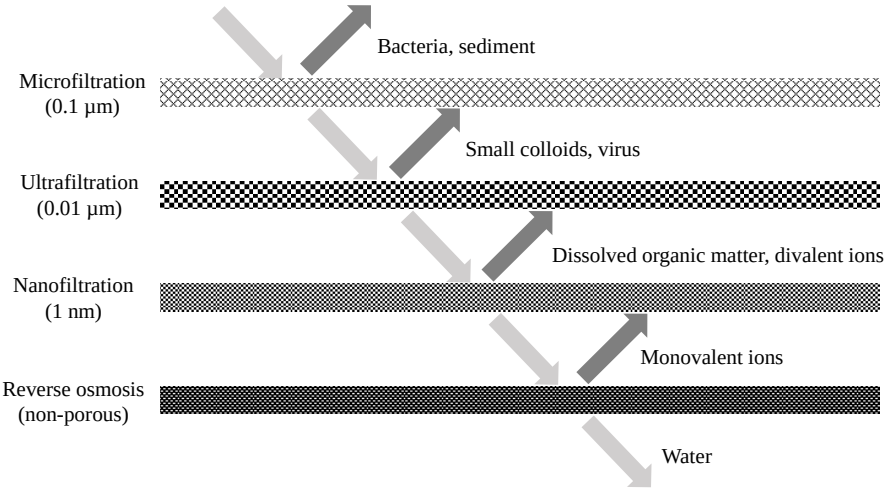

Figure 1-2: Types of pressure-driven membrane separation technology

1.1.2 Organic solvent nanofiltration and its challenges

Organic solvent nanofiltration (OSN) technology addresses the limitations of distillation and evaporative processes used in purification and recovery systems, where high energy consumption and intense processing conditions are required [15]. OSN, a pressure-driven membrane process, enables thermally sensitive products in the feed stream to be refined to high levels without the risk of thermal degradation [16-21]. In addition, the energy consumption is also significantly lesser as there is no change in phase of the feed stream. The milder operating conditions of the system also mean that the cost of constructing the system can be kept low. Furthermore, OSN membrane systems can be installed modularly along existing separation processes to form a hybrid system, thereby encouraging the uptake of such technology in existing plants [19, 21].

New types of polymers were developed for OSN applications over the past few decades. Polymeric membranes made of polybenzimidazole (PBI), polyether ether ketones (PEEK), polymer with intrinsic microporosity (PIM) and polyimides exhibit excellent chemical and

thermal stability, vastly expanding their industrial applications [16, 19, 21-24]. New fabrication and treatment techniques have also enhanced the tuneable properties of the membranes, increasing both permeability and selectivity. One such technique is the cross-linking of polymeric membranes, which was frequently discussed in literature and eventually used in commercialised membranes [20, 25, 26]. This process enhances the chemical and thermal stability of polymeric membranes and made them suitable for feed streams with harsh conditions.

Another method was also developed to prepare highly permeable OSN membranes in one-step process. Cross-linked polymeric membranes with low permeability underwent solvent annealing, resulting in several times higher solvent permeances with little compromise on selectivity [20, 26, 27]. This method has been applied for improving the performance of commercial membranes such as the Duramem™ series from Evonik [26]. In addition, studies on membrane surface modifications were reported to improve the selectivity and permeability of OSN membranes. Membrane surfaces were functionalised or altered through methods such as grafting, radiation, plasma-induced treatment and interfacial polymerisation [3, 28]. One of the more established modification techniques, interfacial polymerisation (IP), has been implemented in RO membranes for water desalination and proves to be a viable modification technique for OSN membranes [27, 29-32]. With the increasing interest in the field of OSN membrane, more of such membranes will soon be commercialised and used in various industries.

There are several key challenges that researchers face when developing OSN membranes. Compared to membranes made for water applications, OSN membranes are far more complex to produce. Several post treatment steps are required to achieve the desired solvent resistance and separation performance. The swelling of membranes in harsh organic solvents are also much more significant due to the interaction between the polymer chains and the organic solvents [16, 21]. This negatively affects the performance of the membrane in the long run, which is critical for industrial processes. In addition, industries like pharmaceutical and petrochemical requires high product purity, and current selectivity of OSN membranes are unable to achieve such performance reliably [33]. Another challenge that OSN membranes face is that a wide range of organic solvents are used in the industry, and each has different interactions with the membranes [15, 16, 19]. This means that it is crucial for researchers to design and choose application-specific membranes that are suitable for use, adding to the complexity of developing an OSN membrane.

Another challenge researchers face when working on OSN membranes is the lack of comparable data in literature [34-36]. Though research on OSN has been increasing over the past decades, performance data from literatures are usually application-specific and have varying solute-solvent systems. The difficulty in finding comparable data lies in the vast combination of solvents and solutes that are used in each study. A particular polymeric membrane may exhibit excellent performance in a particular solute-solvent system while another polymeric membrane might not be suitable for the same set of test conditions. Moreover, there are no widely accepted experimental performance tests that can be used to evaluate and compare membranes equally due to this nature. Thus, many studies on OSN membrane focus on application-specific performance tests to evaluate their membranes.

Since the membranes fabricated are application-specific, the selectivity of the membrane must be tuned to achieve high solute separation. This is especially crucial in the pharmaceutical industries where high purity of active pharmaceutical ingredients (APIs) is required. Industries are also reluctant to implement OSN membrane for their processes due to the lack of robustness of many OSN membranes. The lack of long-term performance tests on OSN membranes is also one of the key challenges. Combined with the requirement of high purity for certain industries, many OSN membranes are unable to enter the commercialisation stage.

Finally, typical issues associated with membrane separation processes such as fouling and concentration polarisation continues to plague OSN and needs to be addressed before it can be moved to large-scale processes. Researchers would need to find insights from studies developed in water research to aid them in solving these issues.

Fortunately, there has been an increasing trend in research for OSN membranes in recent decade. A quick look-up on Web of Science database and one can find that an exponential increase of publications relating to OSN from less than 10 in 1999 to more than 1200 since 2020 (Figure 1-3). This means that researchers are picking up interest in OSN and continual innovations will be made in this field. The challenges faced by polymeric OSN membranes are constantly being highlighted in literatures and researchers are constantly finding solutions to them. Researchers in this field do not have to start from scratch to develop such technology. Membrane separation processes have been used for water purification way before the introduction of OSN. The amount of literatures published for water research overshadows that of OSN process. Key characteristics and parameters that makes a membrane perform well has also been well documented in literatures thus, it is important for researchers to harness the knowledge and apply them to in the field of OSN.

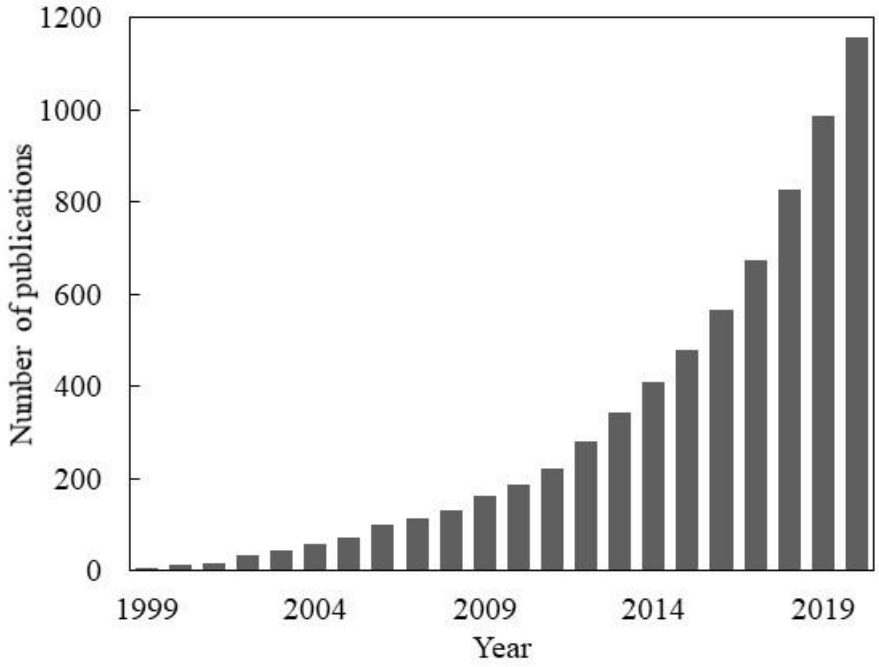

Figure 1-3: Publications in Web of Science relating to OSN

1.1.3 Organic solvent forward osmosis and its challenges

With the advent of membrane separation processes in pharmaceutical industry, a new field of organic solvent forward osmosis (OSFO) has also been suggested as a potential alternative. Fundamentally, separation by OSFO process is achieved through a chemical gradient between the draw solution and feed solution (Figure 1-4). The driving force is provided by the draw solution, which contains solutes of much higher concentration than the targeted feed solution. With a suitable draw solute and a highly selective membrane, preferential transport of the solvent can be achieved. OSFO is also an athermal process, which prevents thermal damage from occurring to sensitive feed solutions. Furthermore, physical properties such as colour, taste and nutrition of feed in food processing will not be damaged. In addition, forward osmosis (FO) processes are able to achieve high product quality at potentially lower energy requirements. Hence, the technology has been utilised in water purification, food processing and pharmaceutical [37-47].

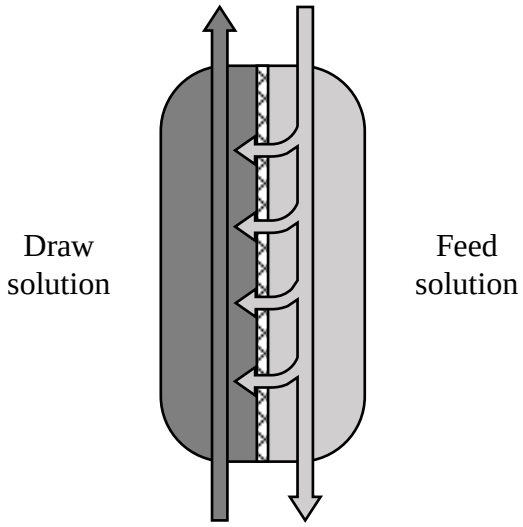

Figure 1-4: Schematic illustration of forward osmosis membrane process

There are several advantages of OSFO process compared to other membrane separation processes. Firstly, OSFO processes operates at very low or no hydraulic pressure, leading to lower fouling tendencies as compared to pressure driven processes like OSN [48, 49]. Moreover, this results in lower costs and energy requirements to operate the system. The lower requirement for mechanical strength of FO membranes also means that it can also be fabricated to be as thin and porous as possible, thereby reducing mass transport resistance of the membrane [50]. Another advantage of OSFO compared to pressure-driven membrane separation processes is that it can be used for applications where the osmotic pressure of the feed stream is exceedingly high. For example, it has been proposed to combine the use of FO and RO in desalination of seawater and brackish water to reduce energy consumption [13, 48, 51-53]. This shows promising potential for OSFO to be used in the pharmaceutical industry. Given these advantages, researchers have started to explore the utilisation of FO in organic solvent systems [15, 54, 55]. However, since OSFO is still a relatively new field, there are several challenges that needs to be addressed.

Concentration polarisation is a potential issue in OSFO due to the huge difference in concentration between the draw solution and feed solution. This phenomenon can occur at the membrane surface or within the membrane matrix and generally result in lower net driving force, decreasing solvent flux. In addition, the accumulation of solutes at the membrane interface increases the transport of solute across the membrane, potentially lowering product quality. The aggravation of concentration polarisation can also lead to membrane fouling, which is another unavoidable phenomenon in membrane separation processes. Membrane fouling can be caused by precipitation of solutes at the membrane interface due to concentration polarisation. It is also often caused by intermolecular adhesion of foulant as well as chemical and hydrodynamic interactions between the membrane and solutes [56, 57]. Membrane fouling in FO have been studied extensively and was observed to modify its selectivity. In cases where foulants are charged, it can potentially improve the rejection of ionic compounds [58]. However, the interaction of solute, solvent and membrane for OSFO are much more diverse and complex than for FO due to the wide range of organic solvents being used. Thus, more research should focus on studying the interactions to better understand the mass transport in OSFO.

Another challenge that needs to be address in OSFO process is reverse solute diffusion. This phenomenon occurs when the solute from the draw solution diffuses through the membrane to the feed solution. When large amount of draw solute diffuses into the feed, it needs to be replenished to maintain the osmotic pressure, thereby adding to operating costs. Furthermore, the diffusion of draw solution into the feed solution can potentially contaminate the feed solution. Studies have shown that this is a prevalent issue if an inappropriate draw solute is chosen for the process [44, 51, 59]. Since there are many combinations of solute-solvent systems in OSFO process, research should be done to find suitable application-specific draw solute. Incidentally, breakthroughs in the development of draw solutions are also required to

enable practical use of OSFO. A desirable draw solution should exhibit high osmotic pressure, be regenerated easily and economically and impervious to reverse solute diffusion.

1.2 Research objectives

The objectives of the research are to develop polymeric hollow fibre thin-film composite membranes for organic solvent membrane separation processes, and ultimately to demonstrate the scalability of this technology. The study can be subdivided into the following sections:

i. Fabricate solvent resistant thin-film composite hollow fibre membrane for low pressure OSN processes.
ii. Modify the fabrication process of the substrate to improve selectivity and scalability of the hollow fibre membrane.
iii. Tune the selective layer to achieve higher selectivity for pharmaceutical application.
iv. Demonstrate the scalability and long-term stability of fabricated hollow fibre thin film composite membranes.
v. Develop a thin-film composite hollow fibre membrane for organic solvent forward osmosis in pharmaceutical application.

1.3 Thesis outline

The thesis consists of 7 chapters in total to study the development of thin-film composite hollow fibre membrane for organic solvent applications. Chapter 1 provides a brief background of OSN and OSFO membrane processes and their potential challenges. Chapter 2 reviews the literature available on OSN and OSFO, focusing on the fabrication of polymeric membranes, its modifications, as well as its potential applications and challenges.

Chapter 3 to Chapter 6 encompass the experimental works carried out in this study to address the main objectives presented. In Chapter 3, a hollow fibre thin-film composite hollow fibre membrane was fabricated for low pressure OSN application. In Chapter 4, the substrate was further improved for scalability and the selective layer was tuned for increased selectivity for pharmaceutical product concentration. Chapter 5 demonstrates the scalability of the thin-film composite hollow fibre membrane by comparing it with commercially available module of equivalent dimensions. In Chapter 6, the substrate was further modified to improve membrane characteristics favourable for organic solvent forward osmosis processes. Finally, Chapter 7 concludes the thesis and provides some recommendation for future work.

Chapter 2 Literature review

2.1 Fundamentals of membrane separation processes

2.1.1 Pore-flow model

In general, there are 2 types of transport mechanisms that are often used to describe the movement of solvent and solute across a semi-permeable membrane. One such model is the pore-flow model, where the separation of solutes is governed by molecular sieving. Larger molecules are prevented from permeating through the membrane while smaller molecules can pass through, thus achieving separation [1, 60]. This permeation of molecules is determined by the size of the solute, pore size and pore size distribution of the membrane as well as the porosity of the membrane [1]. An equation that accurately describes the relationships is known as the Hagen-Poiseuille equation. A simplified mathematical representation of the relationship can be shown as equation 2.1, where J is the solvent flux (l m^{-2} h^{-1}), ε is surface porosity, r_p is pore radius, η is viscosity of liquid, τ is tortuosity of membrane, Δx is thickness of membrane and ΔP is pressure difference across the membrane.

$$J = \frac{\varepsilon r_p^2}{8\eta\tau\Delta x}\Delta P \qquad (2.1)$$

In this model, the viscosity of the solvent is the only property that is considered while the other parameters are membrane specific. Experimental studies have shown that this equation is useful for predicting selectivity of MF and UF membranes. However, in membranes such as NF and RO, several parameters start to affect the transport of solute [1, 60, 61]. With smaller pore size of less than 10 nm, surface forces such as charge, polarity and membrane-solvent interactions become more pronounced and classical fluid dynamics no longer holds [62]. As such, a

different branch of transport mechanism was used to describe molecular separation for membranes with small pore sizes.

2.1.2 Solution diffusion model

While the pore-flow model describes the transport mechanism in porous membranes, it does not correctly predict the transport of molecules through non-porous membranes. In the 1940s, the solution-diffusion model gained traction and eventually became a popular choice to describe RO FO and NF separation processes [2, 5, 63, 64]. The theory was based on Fick's law of molecular diffusion and Henry's law of solubility and few assumptions were made to simplify the model [2, 64]. Firstly, the membrane morphology is said to be homogenous and non-porous. Secondly, the solvent and solute dissolve in the membrane matrix and diffuse across their respective concentration gradient. In addition, the diffusions of solute and solvent were assumed to be independent of one another. Lastly, the chemical gradients developed were the results of a concentration or pressure gradient across the membrane [63-66]. A good approximation for this transport mechanism can be written as equation 2.2, where J_i is solvent flux, $D_{i,m}$ is diffusion coefficient of solvent in membrane, $c_{i,m}$ is concentration of solvent in membrane, V_i is partial molar volume of solvent, Δx is the membrane thickness, ΔP and $\Delta\pi$ are the hydraulic and osmotic pressure difference across the membrane, respectively. The osmotic pressure, $\Delta\pi$, of a solution can be estimated by Van't Hoff equation as shown in equation 2.3, where n is the number of dissociated species and c is the solution concentration.

$$J_i = \frac{D_{i,m} c_{i,m} v_i (\Delta p - \Delta\pi)}{\Delta x RT} \qquad (2.2)$$

$$\Delta\pi = nRTc \qquad (2.3)$$

The derivation of this equation has been done elsewhere [2, 67] and it can be simplified to equation 2.4.

$$J_i = A(\Delta P - \Delta\pi) \qquad (2.4)$$

where the term $D_{i,m}c_{i,m}v_i/\Delta xRT$ is replaced by A. In literatures, the constant A is referred to as water permeability constant and it is a key membrane performance parameter that is frequently compared. From this equation, we can see that the volumetric water flux through the membrane is dependent on the hydrostatic pressure, ΔP, across the membrane for pressure driven processes. Particularly, ΔP must be greater than that $\Delta\pi$ to have water flux. In the case of forward osmosis process, the main driving force is the osmotic pressure difference, $\Delta\pi$, across the membrane. The driving force is typically provided by a draw solution of high solute concentration, where the osmotic pressure is greater than that of the feed solution. Meanwhile, ΔP as the driving force is typically reduced to be very low, or otherwise insignificant.

On the other hand, the equation used to describe the permeation of solute in non-porous membrane is expressed by equation 2.5, where J_j is the solute flux, D_j is diffusion coefficient of solute in the membrane, K_j is the partition coefficient, $c_{j,m}$ is the concentration of solute at the membrane interface, $c_{j,p}$ is the concentration of solute in the permeate.

$$J_j = \frac{D_j K_j}{\Delta x}(c_{j,m} - c_{j,p}) \qquad (2.5)$$

Similarly, the equation has been derived by previous publications [2, 67] and subsequently simplified to equation 2.6.

$$J_j = B(c_{j,m} - c_{j,p}) \quad (2.6)$$

where $D_jK_j/\Delta x$ is replaced by B and frequently referred to as the salt permeability constant in RO literature. According to this equation, solute transport is only dependent on the concentration gradient, ($c_{j,m} - c_{j,p}$), across the membrane at the interface.

As for FO membranes, another phenomenon known as reverse solute diffusion is also present. Due to the concentration difference of the draw solution across the membrane, a small amount of draw solute tends to diffuse into the feed solution. Consequently, the osmotic pressure of the draw solution decreases while the feed is contaminated with the draw solute. Furthermore, reverse solute diffusion may indirectly contribute to lower solvent flux by promoting internal concentration polarisation [53, 59]. The impact of reverse solute diffusion can be determined by measuring reverse solute flux (RSF), which is modelled according to equation 2.6. For RSF, ($c_{j,m} - c_{j,p}$) is replaced by $c_{j,d}$, the concentration of solute at the draw solution.

2.1.3 Concentration polarisation

One of the main challenges that all membrane-based separation processes encounter is concentration polarisation [2, 63-66, 68-72]. The effects of this phenomenon are illustrated in Figure 2-1 and can be divided into two components, external and internal concentration polarisation. External concentration polarisation (ECP) occurs when the rejected solutes in the feed solution accumulates at the membrane-feed interface (Figure 2-1 (a and b)). The general equation describing this phenomenon can be expressed as equation 2.7, where k is the mass transfer coefficient, c_m and c_b are the concentrations of feed solution at the membrane surface and bulk, respectively.

$$\frac{c_m}{c_b} = exp\,(\frac{J_i}{k}) \qquad (2.7)$$

Preferential transport of solvent in the feed solution occurs due to the selectivity of the membrane. Gradually, the concentration of solutes at the membrane interface increases and eventually leading to larger driving forces required to achieve the same solvent flux. In cases where the concentration of solute is extremely high, solute precipitation may occur and result in excessive fouling of the membrane. Furthermore, ECP also affects the selectivity of the membrane, resulting in a lower apparent solute rejection. As such, numerous research has been focused on mitigating this phenomenon by improving process design and membrane properties [70, 72-76].

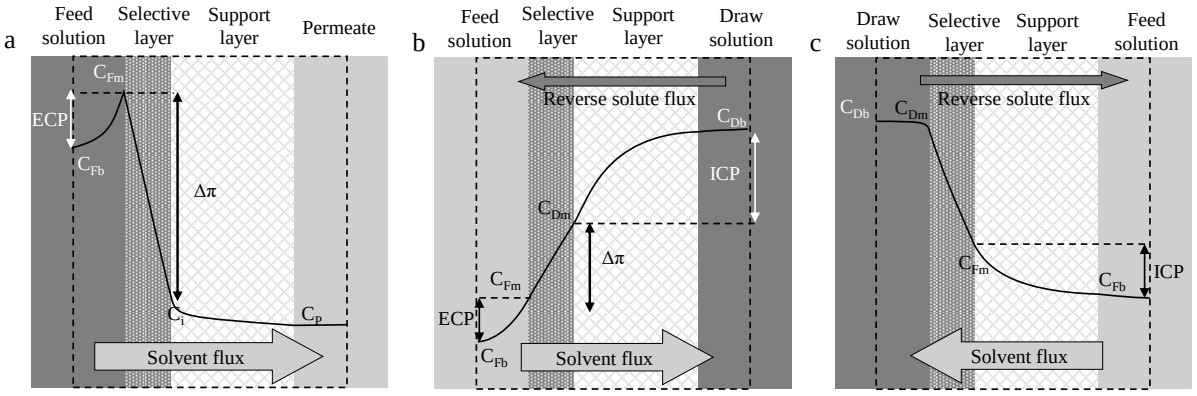

Figure 2-1: Concentration gradient profile and effect of concentration polarisation for a typical TFC membrane. (a) RO mode; (b) AL-FS mode; (c) AL-DS

Another type of concentration polarisation that impairs membrane performance is internal concentration polarisation (ICP). This phenomenon is particularly apparent in osmotically-driven membrane processes such as FO. ICP can be further subdivided into dilutive and concentrative ICPs. These occurs when solutes accumulate in the membrane substrate due to hinderance of mass transport. The solute transport within the membrane support layer can be

determined by solute resistivity, K, as expressed in equation 2.8, where τ, ε and S are the membrane tortuosity, porosity and structural parameter, respectively.

$$K = \frac{\Delta x \tau}{\varepsilon D} = \frac{S}{D} \qquad (2.8)$$

Figure 2-1 (b) illustrates dilutive ICP in a thin-film composite membrane when it is used in the active layer facing feed solution (AL-FS) orientation. Draw solution from the bulk phase diffuse towards the selective layer through the membrane substrate. As solvent from the feed solution is drawn towards the draw solution, it dilutes the draw solution over time. In cases where the solvent flux is very high, the diluted draw solution at the membrane interface cannot be replenished sufficiently to maintain the osmotic pressure. In the active layer facing draw solution (AL-DS) orientation (Figure 2-1 (c)), concentrative ICP occurs instead. Solute in the feed solution accumulates in the substrate due to hindered diffusion, decreasing the effective osmotic pressure across the membrane. In both cases of ICP, the effective osmotic pressure across the selective layer is reduced thus, the overall solvent flux gradually decreases.

2.2 Solvent resistant polymeric membranes

2.2.1 Polymeric membranes

Numerous polymers have been studied for use in membrane separation over the past several decades [77]. Ceramic membranes are also concurrently being studied for use in OSN. Generally, ceramic membranes have superior physical and chemical stability as compared to polymeric membranes [78]. The main advantages of ceramic OSN membranes are that they remain stable after long operations at high temperature of up to 300°C and can withstand high pressure without compaction [79]. In addition, they can be cleaned easily with harsh chemical

and physical processes and maintain their performance characteristics even after many cycles [79]. In particular, they do not swell in organic solvents, which plagues polymeric membranes in general [78]. However, ceramic membranes are usually several times more expensive than polymeric membranes and much harder to manufacture in large volumes. The fabrication process is also more energy intensive due to the high sintering temperatures. Polymeric membranes are less brittle than ceramic membranes, which makes them much more versatile in packing and scaling up [80]. However, it is important to choose the right polymer for OSN application, depending on their chemical and thermal stability. Typical polymers used in aqueous systems such as polysulfone (PSF) and polyethersulfone (PES) are prone to swelling in organic solvents and do not maintain its mechanical properties under prolonged use. This restricts the type of polymers that can be used for OSN applications. Thus, studies have been done to find polymeric membrane with better chemical and thermal stability for OSN applications that were once impossible. A review paper [81] has summarised the types of polymers frequently used to fabricate OSN membranes as illustrated in Table 2-1. Generally, these polymers exhibit excellent chemical stability in a wide range of organic solvents and have relatively high thermal stability, which are suitable for use in OSN applications.

Polyimide is stable in a wide range of organic solvents and readily dissolves in frequently used solvents for dope preparation like NMP and dimethylacetamide (DMAc). In addition, the aromatic structure of polyimide also results in a high glass transition temperature (T_g), making them suitable for thermal membrane separation processes like membrane distillation. P84 and Matrimid are 2 types of polyimides that are generally used for OSN membrane fabrication [20, 24, 82-86]. This is due to their commercial availability as well as excellent solvent resistance. As such, polyimides are widely used as asymmetric OSN membranes as well as ultrafiltration (UF) support for composite membranes [87]. For example, highly cross-linked polyimide and PA are ideal for use in strong solvents such as methanol and acetonitrile. These polymers are

chosen for their high stability in organic solvents as well as an acceptable level of rejection in the NF range [87-89].

Another type of polymer frequently used for OSN membrane fabrication is polydimethylsiloxane (PDMS). PDMS consists of a siloxane (Si-O) backbone with methyl groups, giving it a higher free volume fraction. This characteristic is especially beneficial in applications like gas separation, where a high diffusion coefficient for solvent and gases are advantageous [90]. However, the membrane undergoes severe swelling in non-polar solvents such as alkanes [91-93]. If they are used as support for selective layers in OSN, delamination can occur and this negatively impacts its selectivity and therefore are not used in such applications. To reduce the swelling of PDMS in non-polar solvents, it can also be cross-linked through various methods [19, 91, 93, 94]. Recent studies also have demonstrated that swelling can be minimised by the incorporation of fillers such as zeolites into the membrane matrix and selectivities improved [92, 94, 95].

Other polymers such as PAN, PEEK and PBI have been studied for OSN applications [96, 97]. These polymers are studied for use in OSN applications as they exhibit different properties that performs better at specific OSN systems. For example, PAN is commonly used as UF support due to its relatively lower cost than PEEK and PBI. In addition, the simplicity of cross-linking a PAN support layer provide a cost effective way to produce OSN membranes [98]. On the other hand, PBIs and PEEK exhibits superior chemical stability in n,n-dimethylformamide (DMF) and harsh pH conditions, which many polymers are unable to achieve at the moment [99]. In recent years, polybenzimidazole (PBI) has been touted to have not only excellent organic solvent resistance, but also is stable in a wide range of pH conditions [100]. Just like polyimide, PBI can be dissolved in polar aprotic solvents like NMP and DMSO from which membrane can be made through phase inversion. The membrane then undergoes chemical

cross-linking and were reported to exhibit superior chemical stability in methanol, acetonitrile and DMF [100, 101]. In addition, the fabricated membrane demonstrated high selectivity, with MWCO of less than 500 Da [100].

The list of solvent resistant polymers is non-exhaustive, and researchers are continuously finding new polymers for OSN applications. Admittedly, polymeric membranes are still plagued by the usual compromise between permeability and selectivity while also having the need to maintain stability in strong solvents for long periods of time. Over the past few decades, large number of literatures have been dedicated to the optimisation of a membrane's permeability and rejection. This can be done by replacing the polymer used, adding of nanoparticles into the matrix or modifying the fabrication process [21, 81]. Therefore, with plenty of modifications available in the literature, researchers can find the best combinations to optimise a membrane's performance. Overall, the polymer chosen for OSN application should exhibit excellent selectivity for the solute-solvent system and be able to maintain stability under long periods of filtration.

Table 2-1 Summary of polymers used in OSN membrane fabrication

Material	Structure
Polyimide (P84)	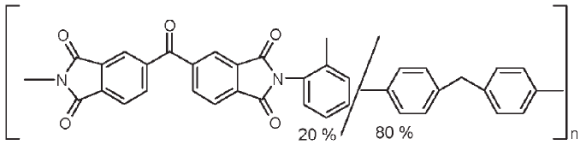
Polyimide (Matrimid)	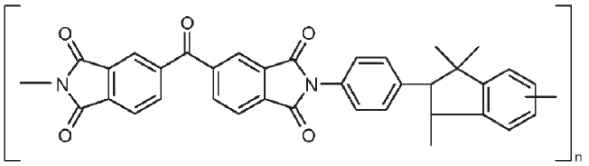
Polyimide (Torlon)	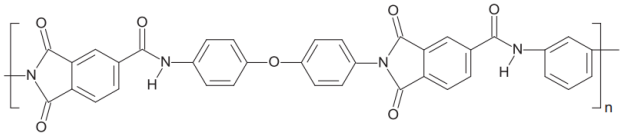
Poly(etherimide) (PEI)	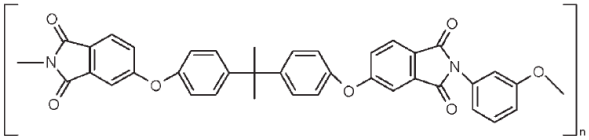

Polydimethylsiloxane (PDMS)	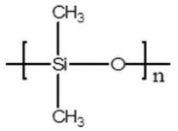
Polyamide (PA)	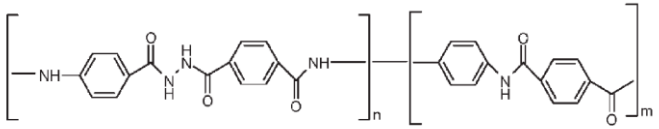
Poly (Ether Ketone) (PEEK)/Sulfonated PEEK R = H/ R = SO_3H	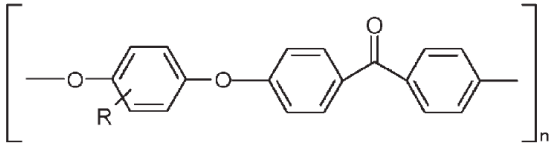
PBI (Polybenzimidazole)	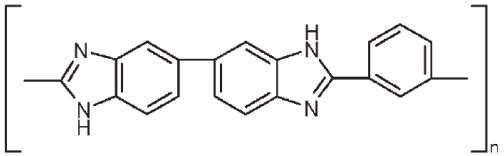
Polyacrylonitrile (PAN)	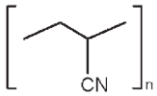
Poly (vinylidene fluoride) (PVDF)	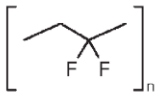

2.2.2 Crosslinking

The most direct way to fabricate OSN membranes is using chemically stable polymers like SPEEK and PDMS. However, such membranes are difficult to dissolve in many solvents and preparing their dope solution with suitable additives proves to be challenging. Another way of developing OSN membranes is to cross-link a polymeric membrane to make it resistant to organic solvents. The purpose of cross-linking is to form strong chemical bonds between the functional groups in the polymer such that it will not interact with the organic solvent. This process not only makes the polymer more chemically resistant, but it also changes the morphology of the membrane. The polymer typically becomes stronger but more brittle. Depending on the cross-link density, the free volume of the membrane can also be drastically reduced. Combined with the reduction in pore size, solvent permeability significantly decreases.

Several cross-linking methods are currently used for OSN membranes, including the use of radical initiated, chemical cross-link as well as thermal treatment [87, 102, 103]. The fabrication typically involves a two-step process, firstly by phase inversion and then followed by cross-linking. The polyimide membrane is dissolved in a suitable solvent such as n-methyl pyrrolidone (NMP) and a homogenous solution is achieved through mixing. The dope solution is then casted onto a non-woven support and introduced into a non-solvent such as deionised water to induce phase inversion. Thereafter, the membrane is then placed in a cross-linker solution, typically consisting of diamines dissolved in short-chain alcohols [101, 102]. The polar solvent swells the polymer chains of the membrane to ensure sufficient contact between the cross-linker and polymers to facilitate thorough cross-linking [81]. It should be noted that though cross-linking can improve its stability in harsh solvents, its permeability will be negatively affected. In one study, the permeability decreased significantly after just 5 mins of cross-linking time however, the opposite trend for rejection is observed [104]. The performance

of cross-linked polyimides has showed good performance in OSN application. It is stable in aprotic solvents such as DMF and NMP, having shown a permeability of 5.4 (l m^{-2} h^{-1} bar^{-1}, LMH/Bar) with a high rejection for rose bengal (>98%) and methyl orange (>95%) [105]. In a recent study, polyimide membranes has been reported to show ethanol permeance of more than 400% as compared to commercially available ones (Duramem 300) while maintaining similar rejection rates [84]. This was achieved by a simple method of solvent annealing, where the rearrangement of the polymer chain occurs after phase inversion. This increased the density of the top layer while maintaining a relatively porous sublayer for improved permeance. Thus, the permeance of solvent across the membrane layer becomes higher due to the higher porosity of the sublayer while the rejection of solute is not compromised.

2.3 Membrane fabrication

2.3.1 Phase inversion

Due to the wide range of possible applications of OSN, ceramic and polymeric membranes are currently being developed for specific applications. However, most commercial OSN membranes are polymeric due to their relatively low cost of manufacture and wide range of polymers to choose from. Polymeric membranes are generally fabricated via phase inversion, which was developed by Loeb and Sourirajan [4]. The thermodynamic behaviour of this process can be represented by the ternary phase diagram illustrated in Figure 2-2 and detailed explanation of the membrane formation process can be found elsewhere [106, 107]. Through processes such as gelation, vitrification or crystallisation, a thin film of solution is transformed into a solid piece of membrane [107]. The polymer-rich phase constitutes the solid membrane matrix while the polymer-lean phase will form the pores in the membrane. The phase inversion process can be induced through several methods, immersion precipitation, controlled

evaporation, thermal precipitation and vapor induced phase inversion. Among these methods, the immersion precipitation method is the most widely used due to its versatility and simplicity [17, 62, 108]. It is a membrane preparation method where a polymer solution is submerged into a coagulant (non-solvent) bath resulting in phase separation. The phase exchange between the coagulant and the solvent causes a distinct boundary layer known as the solvent front. This is also accompanied by a phenomenon called 'viscous fingering', where an instability is formed due to the difference in viscosity of the two fluids. This forces the polymer solution to form a structure that consist of a matrix (polymer) with voids, which affects the permeability of the membrane. The extent to which this phase exchange occurs is dependent on several factors and generally can lead to one of two microstructures as shown in Figure 2-3.

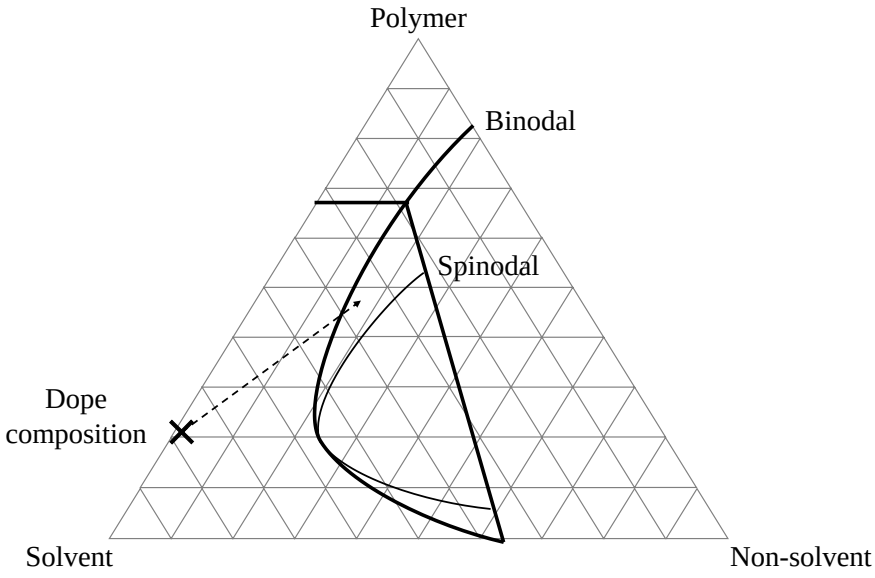

Figure 2-2: Ternary phase diagram. Mechanism of phase separation for membrane fabrication

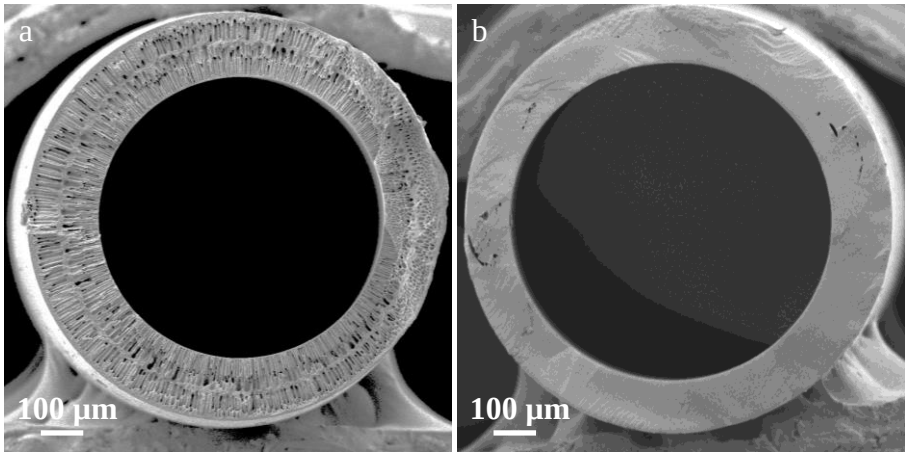

Figure 2-3 (a) Support layer with finger-like structures (macrovoids) (b) Support layer with sponge-like structures (interconnected pores)

The sponge-like structure exhibit excellent mechanical strength and good solvent permeability due to the presence of interconnected pore in the membrane. This structure is generally favoured for high pressure operations such as RO. On the other hand, macrovoids present in the membrane is generally unwanted due to the presence of weak spots that can result in severe membrane compaction under high pressure operations. However, these macrovoids provide less mass transport resistance which enables higher permeability, suitable for use in low pressure applications such as FO and NF [109]. The sponge-like structure can be obtained with dope solution of a lower osmotic pressure and higher viscosity. This impedes the viscous fingers from advancing into the dope solution at a faster rate than the solvent front. This results in a delayed demixing and a sponge-like structure with interconnected pores is formed in favour of finger-like structures [110]. The formation of such macrovoids can also be suppressed by lowering the temperature of the coagulation bath, adding inorganic salts into the coagulation bath to reduce its activity and replacing with a solvent that has lower affinity with the non-solvent.

Extensive research has been carried out to investigate the factors that influence the membrane microstructures and performance. The pore size, pore size distribution and porosity of the membrane depend on factors such as the polymer concentration, solvent system, initial temperature of the solution as well as the duration of immersion in the coagulation bath [81]. These factors affect the rate of diffusion of solvent out of and non-solvent into the dope solution, which in turn determines the membrane structure. There are also factors specific to certain membrane fabrication techniques that affects the membrane structure. For example, the dry-jet wet spinning method shown in Figure 2-4 has several factors that affect the phase inversion process. Parameters such as the viscosity of the dope, dimension of the spinneret, air gap, flow rates of bore and dope fluid, bore fluid composition as well as the uptake speed of the collecting drum have significant impact of the resultant structure of the hollow fibre membrane [50, 61, 107, 111-114].

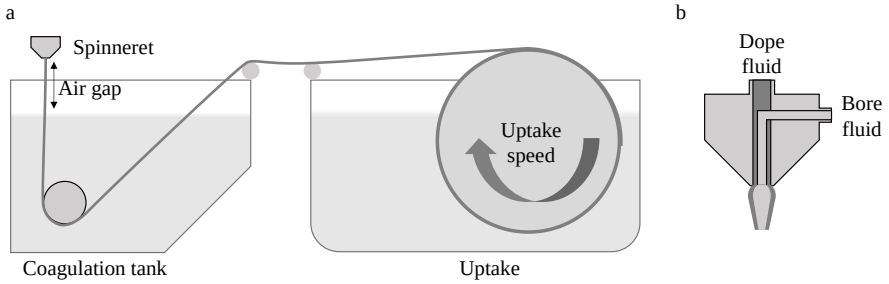

Figure 2-4: Schematic drawing of hollow fibre membrane fabrication using dry-jet wet spinning. (a) Spinning setup; (b) cross-section of spinneret

2.3.2 Fabrication of integrally skinned asymmetric membrane

The first integrally-skinned asymmetric (ISA) membrane was developed by Loeb and Sourirajan in 1960s for RO process [4]. Since then, their method has been modified and applied to develop many types of polymeric ISA membranes for other applications, such as microfiltration and nanofiltration processes. In essence, ISA membranes are typically formed through the phase inversion process, as discussed in Section 2.3.1. A binary solution, containing a polymer and solvent, was immersed into a coagulant, typically water, to form polymer-rich and polymer-lean phases. These phases form the polymer matrix and voids, respectively. Through the phase inversion process, a steep polymer concentration gradient can be observed throughout the membrane matrix, as shown in Figure 2-5. A dense skin layer is typically formed on the surface of the membrane, while the polymer matrix decreases in density across the depth of the membrane. There on, studies have been done to evaluate the key parameters that affect the formation of ISA membranes. Twos such parameters are the dope composition and the effects of various dope additives on ISA membrane performance.

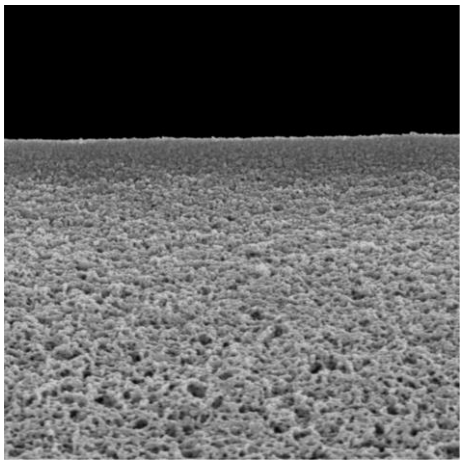

Figure 2-5: Integrally-skinned asymmetric membrane

Researchers have been altering the concentration of polymer in the dope solution to develop membranes for different applications. A higher polymer concentration leads to a more viscous dope solution, which reduces the rate of solvent and non-solvent exchange (delayed mixing)

within the solution [115-117]. This results in a membrane that has higher selectivity and lower permeability. The choice of solvent for preparing the dope solution can also affect the interaction with non-solvent in the coagulation bath. Usually, polar aprotic solvents such as N-methyl-2-pyrrolidinone (NMP) and DMF due to their high affinities with many polymers. The affinity between the solvent and non-solvent is also an important factor in the phase inversion process. A higher solvent and non-solvent affinity will result in faster demixing, which consequently produce more porous membranes [108]. Other than the polymer and solvent, additives that are added into the dope solution can also affect the phase inversion process.

The use of additives in dope preparation has been intensively studied since the advent of membrane fabrication [77, 118]. Additives can be loosely categorised into two branches, inorganic and organic additives. The former consists of inorganic salts such as metal halides, metal sulphates and hydrated salts. Inorganic salts such as LiCl, NaCl, KBr and KCl are generally pore formers that leeches out of the membrane after phase inversion [50, 116]. Other inorganic additives such as metal oxides and metal nanoparticles are also being studied to evaluate the improvement in performance of the membrane using these additives [92, 119]. Metal oxides such as TiO_2 contained in PI for OSN application have shown to improve the mechanical strength of the membrane [120]. In addition, they resist the formation of macrovoids when TiO_2 wt% increased to above 3%. This is attributed to the increased in viscosity of the dope solution, as well as lowering its thermodynamic stability.

Alternatively, organic additives can also be added into the dope solution to change the microstructure of the membrane. Low MW additives such as diethylene glycol (DG) and alcohols and higher MW additives like polyethylene glycol (PEG) are often used as pore formers in UF membranes [121]. Depending on their MW, they are either leeched out during the phase inversion process which result in pores or be retained in the membrane thereby

improving hydrophilicity. This has been demonstrated to improve water permeability in membranes [8, 121]. Addition of organic additives such as PEG also cause the dope solution to be thermodynamically less stable, resulting in faster demixing [8].

Another form of additives that are frequently used in the fabrication of OSN membranes are co-solvents. Typically, co-solvents such as tetrahydrofuran (THF) and ethanol are added into the dope solution to improve selectivity of asymmetric membranes. Since THF and ethanol are volatile, they rapidly evaporate during the phase inversion process. This increases the polymer concentration at the surface of the dope and forms a dense-skin layer, delaying the demixing process. As such, the asymmetric membranes formed using this method consist of a dense skin-layer on top of a highly porous sponge-like support.

2.3.3 Fabrication of OSN TFC membrane

Though the fabrication of integrally skinned asymmetric (ISA) membranes through phase inversion has proven to be economical and versatile for various polymeric membranes, the need for lower energy consumption and better performance have led to innovative processes such as thin film composites (TFCs). The permeability of a membrane is inversely proportional to its thickness thus, focus has been made to develop thinner membranes that exhibit higher permeability while at the same time, maintaining its mechanical strength and selectivity [29, 50, 122-124]. For a membrane to have such performance, membranes made of two distinct materials have been developed. The selective layer is made of a thin layer of material like PA via interfacial polymerisation. The reported thickness of such selective layer is usually less than a few hundred nanometres [29, 30, 122, 125-128]. This highly optimised layer ensures that the rejection of solutes remain high while thin enough to provide exceptional permeability. As this layer is very thin, it does not have the mechanical strength to withstand high pressure

operations thus, a substrate (sublayer) is required. The sublayer is made of a highly porous material that provides mechanical strength to the membrane with minimal resistance. To develop such selective layers, we must first understand the working principle of interfacial polymerisation. IP is achieved by an in-situ polymerisation reaction occurring at the interface between two immiscible solvents containing the two reactive monomers (Figure 2-6). The active layer in TFCs can be synthesized using several methods available in literatures.

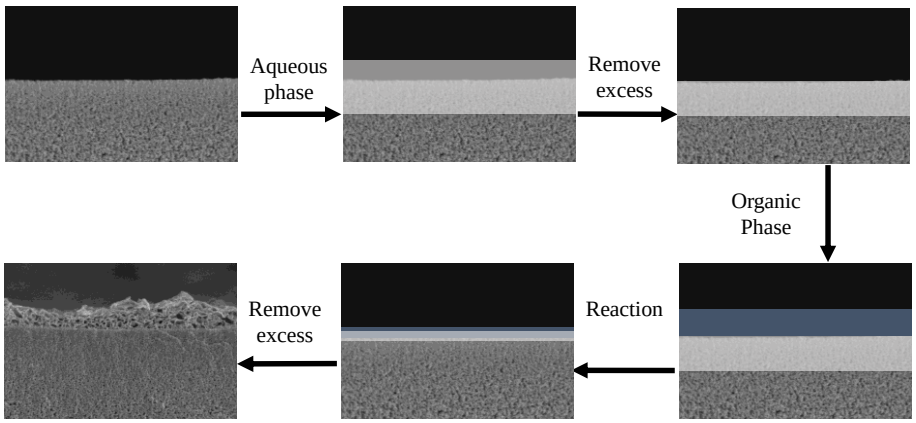

Figure 2-6: Interfacial Polymerisation

The supporting layer is first impregnated with the aqueous phase containing the hydrophilic monomer, followed by the removal of excess solution from the membrane. The organic phase containing the oleophilic monomer then meets the saturated support layer. The monomers react instantaneously, forming a dense selective layer on top of the substrate. This self-limiting reaction prevents further formation, thus forming a thin layer of only several hundred nanometres. The remaining solutions are then removed from the supporting membrane by means of flushing with DI water or inert gas, leaving behind a thin selective layer.

There are several types of polymers that are currently being synthesized using this method. From literature, a large portion of TFC membranes consist of polyamide (PA) active layer as

it is suitable to be used in a wide range of solvents when cross-linked. Cross-linked PA showed excellent solvent resistance in various organic solvents and since it can be easily synthesized using the IP method, it is commonly used for the selective layer of a composite membrane [19, 123, 128]. In general, the IP process involves the mixing of two monomers of PA in an aqueous and organic solvent on the surface of a support layer. There are several monomers that can be used to form PA, more commonly used ones are m-phenylenediamine (MPD) or piperazine (PIP) in aqueous media with trimesoyl chloride (TMC) in organic media. Low concentrations of monomers (<2% MPD and <0.5% TMC) are used to produce a selective layer with good permeability and rejection [123].

In addition, polyamide imide (PAI), poly ether amide (PEA) as well as poly urea amide (PUA) are also being developed as novel alternatives [19]. The performance, morphology as well as the composition of these active layer is also dependent on the same factors. The concentration of monomers and diffusion rate determines the thickness and density of the active layer formed [30]. Increase in both factors will result in higher rejections but lower permeability. Other parameters such as post treatments and overall kinetics can drastically change the morphology of the membrane. Thus, researchers have to understand the effects of these parameters prior to fabricating the membranes. Overall, this innovation has led to drastic improvement of the membrane performance. However, it should be noted that the added step of making the sublayer and selective layer increases the complexity and cost of the synthesis process and correspondingly, reducing the reproducibility of the membranes.

2.3.4 Fabrication of OSFO TFC membrane

The fabrication of TFC membrane for OSFO process follows similar methodology as that mentioned above. The selective layer should be thin to enhance solvent permeability, yet dense

for high solute rejection. However, the requirements for the substrate are different due to the issue of ICP in osmotically driven processes. The suitability of a substrate for FO process can be characterised by its structural parameter (S), as defined in equation 2.9, where Δx_s, τ and ε are substrate thickness, tortuosity, and porosity, respectively.

$$S = \frac{\Delta x_s \tau}{\varepsilon} \qquad (2.9)$$

The derivation of S has been discussed elsewhere [50, 65, 129-131] but generally, a lower S will improve mass transport, thereby lowering ICP [132-138]. Since FO processes do not have significant hydraulic pressure, the membrane can be made very thin and porous through control of the dope composition and spinning parameters. A lower polymer concentration can be used to increase porosity while additives can be included to modify the viscosity to maintain spinnability [121, 139, 140]. The drum uptake speed can be increased while the dope and bore fluid flow rates can be kept low to increase elongation of fibres, thereby reducing overall thickness [109, 117]. The porosity of the substrate can be further improved by inducing the formation of finger-like structures throughout the polymer matrix [50]. Combining these voids with interconnected pores throughout the membrane, the membrane resistance can be substantially reduced. Therefore, by adjusting the dope composition and spinning parameters, a suitable substrate can be fabricated for OSFO process.

2.3.5 Membrane configurations and module design

Other than choosing a suitable polymer for membrane fabrication, it is also important to choose the right membrane configuration for the intended application. Membrane configuration refers to geometry in which the flow of feed and permeate is to the relation of the membrane. As most

membrane applications are based on a modular design, the membrane configuration also determines the manner in which the membranes are packed into modules [141]. Over the years, several membrane configurations have been used to form the basis for membrane fabrication. Each of these configurations have their advantages and disadvantages which researchers and engineers can use to determine the optimal configuration for different materials and applications. The characteristics of each membrane configurations have been analysed previously and can be summarised as shown in Table 2-2. There are several aspects to be considered when determining which membrane configuration to use. In an industrial setting, the production cost, packing density, energy consumption, flow distribution as well as fouling control are key parameters that operators consider.

In the plate-and-frame configuration resembles that of a conventional filter press-concept. The semi-permeable membrane, along with a support spacer, are clamped together and stacked between plate housings as illustrated in Figure 2-7 (a). This membrane configuration offers the simplest design for packing flatsheet membranes and are often used in small-scale operations. However, it has low packing density and cannot withstand high pressures and thus are limited to MF and UF operations [142]. In addition, the often replacement of membrane is labour intensive and thus it is not suitable for large scale membrane separation operations.

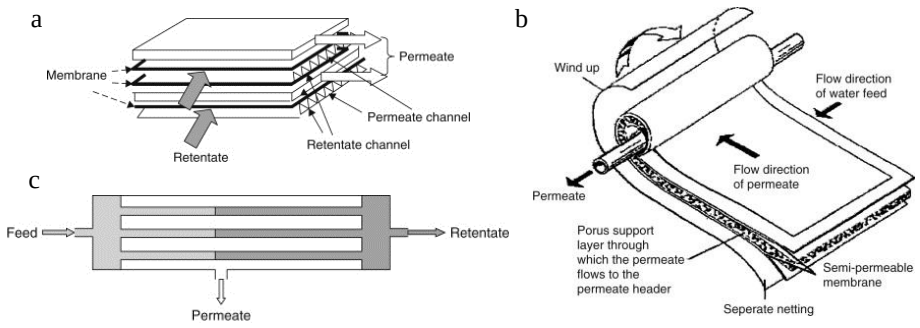

Figure 2-7: Schematic illustration of membrane configurations. (a) Plate-and-frame; (b) Spiral wound; (c) Tubular / Hollow fibre. Modified from [141]

Another type of membrane configuration that is often used to pack flatsheet membranes is the spiral wound module. The flatsheet membranes, feed flow spacers and membrane supports are sandwiched and rolled around a tube as shown in Figure 2-7 (b). The feed solution passes axially along the module while the permeate is collected centrally at the perforated tube. It is widely used in large scale RO, UF and GS processes due to several advantages. The packing density of spiral wound modules are relatively high compared to other configurations while being relatively easy to manufacture [143]. However, spiral wound modules are prone to fouling due to its small feed channel. In addition, the module size is limited due to significant pressure loss at the permeate [142]. As such, studies are currently being done on module geometry and spacer designs to improve mass transfer at the membrane surface [143].

One notable configuration that has always been touted as a potentially efficient configuration to be used in industries is hollow fibre. Fibres are packed into a tube and held at both ends by epoxy. The feed typically flows through the bore of the fibre and exits from the other end while the permeate is collected from the tube. Hollow fibre has one of the highest packing densities, which reduces the space needed for the system. In addition, it is relatively simple to manufacture, driving manufacturing cost down. Since hollow fibres can be potted into modules

of different sizes, it allows retrofitting onto existing separation infrastructures, saving on capital cost [142, 144]. In addition, hollow fibre membranes can withstand high pressure without support, widening the potential use for the technology that cannot be done by other configurations. However, hollow fibres do come with its disadvantages and challenges that prevents it from being widely used in industries. Given the small diameter (<1000 μm) of the fibres, it is extremely susceptible to concentration polarisation and fouling from macromolecules and particles. Thus, extensive pre-treatment is required to when hollow fibres are used in separation. With these challenges addressed through extensive research, hollow fibre will prove to be a better membrane configuration to be used in many other industrial applications.

Table 2-2: Summary of commercial membrane configurations and their advantages and disadvantages [40]

Membrane module	**Packing density (m^2 m^{-3})**	**Membrane costs**	**Control of concentration polarization**	**Application**
Filter cartridge module	800 -1000	low	Very poor	Dead-end MF
Plate-and-frame module	400 - 800	medium	good	MF, UF, RO, D, ED
Spiral-wound module	800 - 1200	low	good	UF, RO, GS
Tubular module	20 - 100	very high	very good	MF, UF, RO
Capillary module	600 - 1200	low	very good	UF, MF, D, SLM
Hollow fibre module	2000 - 5000	very low	very poor	RO, GS

2.4 Membrane application in pharmaceutical industry (include OSFO)

2.4.1 Solvent exchange

Over the years, industries such as food and beverage, petrochemical and pharmaceutical have begun exploring the use of OSN and OSFO membranes as greener alternatives to conventional processes. Table 2-3 lists commercial OSN membranes used in the industry. It can be observed that there is a wide variety of membranes being used by the industries. Due to the wide range of industrial applications, there is a broad array of membrane products available in the market. Each membrane product is only suitable for a range of organic solvents and companies have to choose appropriate membranes for each desired application.

In the pharmaceutical industry, it has been reported that more than 50% of capital investment is spent on the operation of separation processes [22, 145-147]. In addition, many processes utilized by the pharmaceutical industries are solvent and energy intensive [19, 22, 147, 148]. Figure 2-8 shows a flow diagram of a multi-step active pharmaceutical ingredient synthesis process. As various solvents are typically used in the multi-step synthesis process, a solvent-exchange unit is required in between each reaction step. A typical solvent-exchange unit consist of a distillation column. The first solvent is concentrated via distillation while a secondary solvent is added step-wise. This process is repeated until the original solvent is significantly reduced and the reactants are dissolved into the new solvent. Such processes are energy intensive and also requires a large amount of solvent.

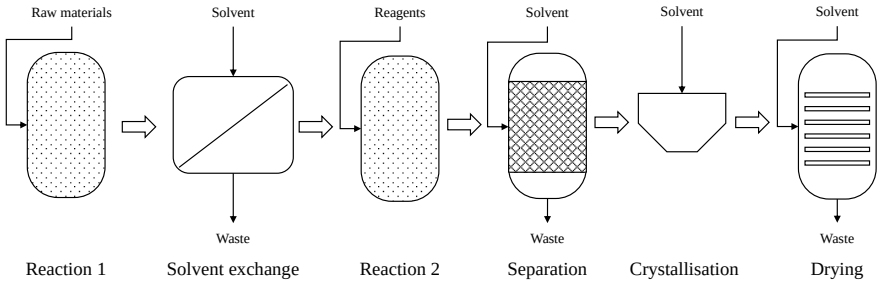

Figure 2-8: Flow diagram of active pharmaceutical ingredient synthesis process

As such, membrane separation processes have been suggested as greener alternatives to conventional solvent exchange processes [22, 145-147, 149]. The main benefit of using membrane separation processes is that it usually occurs at room temperature, which is particularly useful for handling thermally sensitive compounds. The athermal process also reduces the amount of energy required for the entire process [22, 145, 146, 149]. In addition, the amount of the compatible solvent used is significantly reduced. Studies have shown that membrane-based solvent exchange processes can achieve high solute rejections while minimising the amount of solvent waste produced [146, 149, 150]. To obtain higher purity of compound or higher percentage of solvent exchanged, multi-staged membrane processes can be employed. These cascading membrane stages can therefore increase the purity of the final product obtained, while minimizing the use of resources.

Table 2-3: Commercial OSN membranes

Membrane name	Manufacturer	Membrane type and material	Solvent stability	Applications
MPF-50	Koch Membrane Systems (USA)	TFC, comprising a dense silicone top layer on a porous cross-linked PAN-based support	Alcohols, ketones, esters, alkyl halides, alkanes	Recovery of organometallic complexes from DCM, THF, ethyl acetate; recovery of phase transfer catalysts from toluene, separation of triglycerides from hexane, solvent exchange in pharmaceutical manufacturing
MPF-44	Koch Membrane Systems (USA)	TFC, comprising a dense silicone top layer on a porous cross-linked PAN-based support	Aqueous mixtures of lower alcohols, hydrocarbons, chlorinated solvents (DCM, chloroform), aromatics (toluene, xylene), ketones (MEK),	Recovery of clindamycin from fermentation wastewater.

			diethyl ether, ethyl acetate, cyclohexane, propylene oxide, acetonitrile, THF, 1,4-dioxane.	
Starmem 120, 122, 228, 240	W.R. Grace-Davison (USA), distributed by Membrane Extraction Technology (MET) (UK)	Integrally skinned asymmetric membranes with active surfaces based on polyimide (pore size <5 nm)	Alcohols (e.g., butanol, ethanol, and iso-propanol); alkanes (e.g., hexane and heptane); aromatics (e.g., toluene and xylene); ethers (e.g., methyl-tert-butyl-ether); ketones (e.g., methyl-ethyl-ketone and methyl-isobutyl-ketone); and others (e.g., butyl acetate and ethyl acetate).	Solvent recovery in lube oil dewaxing and aromatics enrichments, pharmaceutical manufacturing for solvent exchange and microfluidic purification, biotransformation in membrane bioreactors (MBRs)
PuraMem S380	Evonik MET (UK)	TFC with cross-linked PDMS layer on	Heptane, hexane	Applications in apolar hydrocarbon-type solvents

		polyimide ultrafiltration support		
DuraMem, Puramem 280	Evonik MET (UK)	Integrally skinned asymmetric cross-linked polyimide-based membrane	Acetone, ethanol, methanol, tetrahydrofuran, dimethylformamide, dimethyl sulfoxide, dimethylacetamide, isopropanol, acetonitrile, methylethylketone, ethyl acetate.	Applications in most called aggressive solvents such as solvents of the polar aprotic solvent family
SolSep NF010206	SolSep (The Netherlands)	TFC	Alcohols, esters	Upgrading of solvent mixtures for reuse in industrial applications
SolSep NF010306	SolSep (The Netherlands)	TFC	Alcohols, esters, ketones, aromatics, chlorinated solvents, reducing atmospheres	Upgrading of solvent mixtures for reuse in industrial applications

SolSep NF030306	SolSep (The Netherlands)	TFC	Alcohols, esters, ketones, aromatics, chlorinated solvents, reducing atmospheres	Upgrading of solvent mixtures for reuse in industrial applications
SolSep NF030306F	SolSep (The Netherlands)	TFC	Alcohols, ketones, aromatics, chlorinated solvents	Upgrading of solvent mixtures for reuse in industrial applications
SolSep NF030105	SolSep (The Netherlands)	TFC	Alcohols, aromatics, ketones	Upgrading of solvent mixtures for reuse in industrial applications
GMT-oNF-2	GMT Membrantechnik GmbH (Germany)	TFC comprising a PDMS-based top layer on a PAN (Polyacrylonitrile)		

Desal-5	GE/Osmonics	TFC comprising a poly(piperazine amide) top layer with an intermediate sulfonated PSf layer	Toluene, ethyl acetate, methanol, dichloromethane	Separation of oleic acid from methanol; separation of Pd-BINAP and Wilkinson catalyst from dichloromethane
Desal-5-DK	GE/Osmonics	TFC comprising a PA-based top layer	Limited chemical stability in solvents such as ethyl acetate and toluene	
HITK-T1	HITK (Germany)	Silylated TiO_2-based ceramic membrane	Methanol, acetone; apolar solvents	Retain of transition-metal catalysts in apolar solvents
Inopor 0.9 nm TiO_2	Inopor GmbH	TiO_2	Methanol, 2-propanol, tetrahydrofuran (THF), n,n-dimethylformamide.	
Inopor 3 nm Zr PHOB	Inopor GmbH	ZrO_2 with a silane top layer	Apolar solvents	

2.4.2 Solvent recovery

The manufacturing of pharmaceuticals usually requires a large quantity of organic solvents and this leads to a large amount of waste solvents produced. In most cases, these solvents are disposed of and the economic and environmental cost are tremendous [22]. With increasing pressures imposed on the pharmaceutical industry for environmental sustainability, there is a growing need for more recovery of waste solvents. Conventionally, there are several methods to recovery these solvents, such as fractionation and azeotropic or extractive distillation [151]. However, these processes are typically energy intensive and take up a relatively large footprint. In addition, the recovered solvent have to be of very high purity as the quality of solvent used in the synthesis process is a critical parameter [22]. As such, the throughput of the recovery process will be reduced to achieve higher purity. Thus, the solvent recovery process can potentially be augmented by OSN membranes. When the solvent waste is collected, it can first be refined by OSN to reduce the concentration of impurities present. Further polishing can be accomplished by multi-stage diafiltration process and a final distillation process can be used to achieve the required purity. Not only does it increase the throughput of the distillation column of a given footprint, but it can potentially increase the number of waste solvent avenues that can be recovered [16, 146, 152, 153].

One study by Sereewatthanawut et al. integrated an OSN-based solvent recovery unit with existing API purification process to reduced waste solvent generated while maintaining the desired product quality [153]. Figure 2-9 shows the schematic diagram of the integrated solvent recovery unit. The feed that is purified with API is send into the solvent recovery feed with a single-stage OSN. A large portion of the solvent is recovered as the permeate and pumped back into the purification unit to reduce the amount of fresh solvents used in other manufacturing steps. Simultaneously, the concentration of API in the recovery tank increases and can be

discharged when the desired concentration is reached. Overall, the case-study demonstrated that a high purity of API (99.7%) can be obtained while more than 90% was recovered. In addition, the total amount of fresh solvents consumed during the purification process was also significantly reduce. This study also demonstrated the modularity of membrane-based separation process and allows the implementation of solvent recovery units into existing flow processes. This indicates promising potential for OSN membranes to be used in other recovery processes.

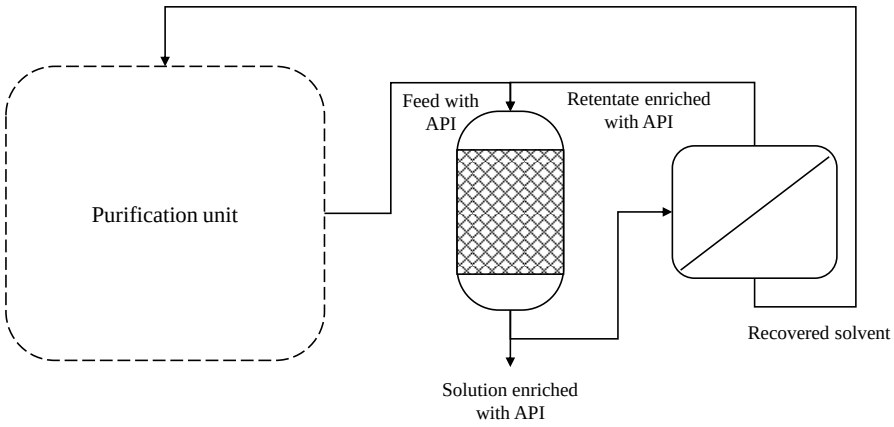

Figure 2-9: Schematic diagram of solvent recovery unit

2.4.3 Separation and purification of active pharmaceutical ingredients

Another potential application of membrane-based separation is the post-synthesis separation and purification of active pharmaceutical ingredients (APIs). After the reaction has taken place in the reactor, impurities such as by-products and unreacted materials need to be separated from the API. Crystallisation and chromatography are typically used in the purification process to obtain API of high purity. However, crystallisation is a complex process and difficult to scale-up, which requires a high degree of optimisation to achieve acceptable levels of purity [154]. Chromatography has been well-established as a purification process [151]. However, it usually

requires a large amount of solvents to achieve high purity, thereby producing large quantities of solvent waste in the process. In addition, some impurities may interact with the stationary phase of the chromatography column, affecting the separation factor [154]. Thus, OSN and OSFO membrane offers a viable alternative to these conventional processes.

Figure 2-10 shows the schematic illustration of a membrane-based concentration and purification process. In this illustration, the API is separated from the impurities based on its molecular size. However, as discussed in Chapter 2, section 2.1.2, the separation of solutes in the field of OSN is a complex process. This is especially relevant for smaller molecules of less than 300 Da, where the affinity and solubility constants play a major role in determining the selectivity of the membrane for particular solute-solvent systems [1, 16, 155]. Buonomenna et al. did a comprehensive review on the performance of current OSN applications for purification and concentration [145]. Notably, a 10-stage OSN process was proposed for the purification and recovery of an API from a number of impurities present in the feed stream. The multi-stage dead-end configuration achieved 80% recovery of API. Another case-study was on the purification of an aromatic amine (390 Da) from impurities (~781 Da) using DuraMem 200, a commercial OSN membrane from Evonik. Due to the relatively huge difference in molecular weights of the API and impurities, the OSN membrane showed excellent selectivity for the API and achieved purity that exceeds the specification limit.

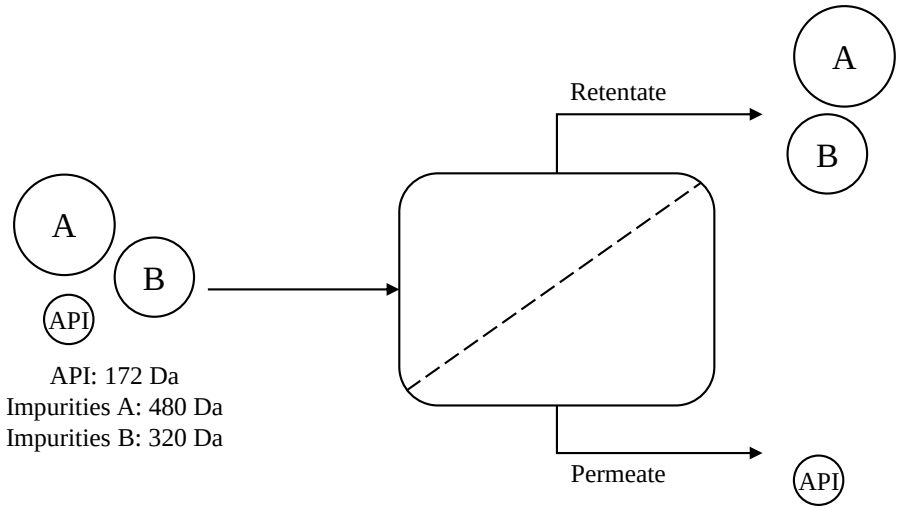

Figure 2-10: Schematic drawing of concentration and purification of active pharmaceutical ingredient

Chapter 3 Thin film composite hollow fibre membrane for low pressure organic solvent nanofiltration

3.1 Introduction

Organic solvent nanofiltration (OSN) has come a long way and has been successfully implemented in pharmaceutical and food industries where the recovery or purification of thermal sensitive substances is required [19, 146, 149, 156]. To embrace this paradigm shift towards the OSN technology, there has been an increasing interest in OSN research, especially on the fabrication of robust and high performance OSN membranes [1, 2, 6, 7]. However, due to the added complexity of fabricating OSN membranes with high solvent resistance, there are still limited choices of commercially available OSN membranes [19]. The challenge for a membrane to be thermally and chemically stable in various organic solvents and operating conditions narrows the number of polymers that can be used for making OSN membrane. Most commercial polymeric membranes such as polyethersulfone (PES) and polyvinylidene fluoride (PVDF) membranes cannot withstand aggressive organic solvents such as n,n-dimethylformamide (DMF) [17, 19]. Moreover, post-treatments are frequently required to enhance the stability of most polymeric membranes, which inevitably reduces permeability and increase manufacturing complexity [104]. Consequently, a high operating pressure of 5 to 30 bar is required to achieve desirable permeability. Not only are such high-pressure systems energy intensive but also potentially dangerous when separating highly flammable solvents such as acetone and methanol [82, 89, 96, 112, 157]. Therefore, there is a desire for OSN membranes that are capable of operating efficiently at lower pressure.

Thin film composite (TFC) membranes can potentially improve the performance of OSN membranes. The structure and properties of substrate and selective layer can be tuned

independently thereby achieving higher solvent permeability and solute rejection. Several materials have been used for making the separating layer of TFC membranes for nanofiltration (NF), such as polyamide, polymers of intrinsic microporosity and graphene oxide [23, 156, 158]. Polyamide is one of the most widely used polymer matrixes for TFC membranes and can be synthesized via interfacial polymerization, a promising approach to fabricate TFC membranes in large scale [159, 160]. With high cross-linking density, the polyamide thin film could exhibit excellent chemical resistance and mechanical robustness and show great separation performance.

The performance of polyamide is strongly dependent on the thin film morphology, structure and thickness. Various monomers, especially the aqueous phase reactants have been studied to achieve different polyamide cross-linking networks for desired membrane performance [127]. However, a typical dense polyamide layer was formed by employing trimesoyl chloride (TMC) as the organic phase monomer and m-phenylendiamine (MPD) as the aqueous phase monomer, resulting in a tight OSN selective layer with low permeability [161]. To achieve a higher solvent permeability, a looser polyamide layer with a lower degree of cross-linking can be synthesized using branched polyethyleneimine (PEI) as the aqueous phase monomer, which has previously been shown to have higher water permeability [125, 126]. A small amount of piperazine (PIP) could be added to fine-tune the cross-link density to yield enhanced selectivity with no significant decrease in solvent permeability [126]. However, this type of PEI-based polyamide layer has not been applied in OSN application yet.

The current work aims to develop high performance TFC hollow fibre membrane for low-pressure OSN applications. The first part of the study focused on the development of solvent resistant polymeric hollow fibre substrates that is suitable for polyamide thin film synthesis. Polyimide was chosen for the hollow fibre substrates due to its superior chemical and thermal

stability in a large range of organic solvents [17, 104]. Furthermore, the modification process used to improve the chemical resistance of polyimide against strong organic solvents was facile and scalable [104]. Polyamide thin film was then synthesized on the inner surface of the polyimide substrates via interfacial polymerization by circulating the monomer solutions consecutively. A combination of PEI and PIP was used as monomers in the aqueous phase to obtain loosely cross-linked polyamide selective layer for low pressure operation. The effects of PEI concentration on the formation of polyamide thin film on the hollow fibre substrates were investigated. The resultant TFC hollow fibre membranes were tested for OSN, permeating acetone and isopropanol, and retaining dyes in the solvents. A 72-h study was also carried out to study the stability of the TFC membranes. This study explored the possibility of fabricating polyamide TFC hollow fibre membranes for low-pressure organic solvent nanofiltration.

3.2 Materials and methods

3.2.1 Materials and chemicals

Polyimide (P84 Lenzing) was used to fabricate the substrate. 1-Methyl-2-pyrrolidinone (NMP, >99%) purchased from Merck, lithium chloride (LiCl, 99.98%) and diethylene glycol (DG, >99.5%) purchased from Sigma Aldrich were used in the phase inversion process. Isopropanol (IPA, >99.5%), polyethylene glycol 400 (PEG 400) and hexamethylene diamine (HDA, >98%) purchased from Sigma Aldrich were used for post-treatment and storage of membranes.

Branched polyethyleneimine (PEI) with molecular weight 50,000 Da was purchased from Sigma Aldrich, trimesoyl chloride (TMC, 98%, Sigma Aldrich), sodium dodecyl sulfate (SDS, >95%, Sigma Aldrich), piperazine (PIP, >99%, Sigma Aldrich) and cyclohexane (Merck)

were used for interfacial polymerization. To evaluate the rejection capability of the TFC membrane, rose bengal (RB, molecular weight (MW) of 1017 Da, >95%), acid fuchsin (AF, MW of 585, ~70%) and methyl orange (MO, MW of 327, >85%) purchased from Sigma Aldrich were used. Acetone (>95%), isopropanol (IPA, >99.5%) and n,n-dimethylformamide (DMF, >99.8%) purchased from Sigma Aldrich were used in the solute-solvent system.

3.2.2 Spinning of polyimide hollow fibre membranes and cross-linking

The polyimide hollow fibre substrates were fabricated via dry-jet wet spinning process. Polyimide was first dried in the oven at 50 ℃ overnight to remove the water content prior to dope preparation. NMP was selected as the solvent to dissolve polyimide, and LiCl and DG were added to adjust the dope composition. Table 3-1 summarises the dope compositions prepared for spinning polyimide hollow fibre membranes. The weight percentages of polyimide were kept at 20 wt% for all dope solutions. The bore fluid composition and percentage of polymer remained unchanged for all experiments.

Table 3-1 Dope composition for fabricating polyimide hollow fibre membranes

Dope code	Dope composition (wt%)
M1	polyimide/LiCl/NMP: 20/1/79
M2	polyimide/LiCl/NMP: 20/3/77
M3	polyimide/DG/NMP: 20/8/72
M4	polyimide/DG/NMP: 20/10/70
M5	polyimide/DG/NMP: 20/12/68

The dope solutions were continuously stirred in a water bath at 40 ℃ for 24 hours. They were subsequently transferred into the syringe pump and degassed in vacuum overnight before spinning. The dope and bore fluids were extruded through a spinneret (0.75 mm / 1.5 mm) at controlled rates using two syringe pumps. The fluids pass through an air gap before immersing into a coagulation bath containing tap water. The fibres were then collected onto a drum at free-falling take-up speed and subsequently rinsed with deionized (DI) water for 3 hours, to remove residual solvents. The air gap, dope and bore fluid flow rates were adjusted accordingly to obtain membranes with similar dimension and thickness. The details for the spinning parameters are shown in Table 3-2.

Table 3-2 Spinning parameters for polyimide hollow fibre membrane

Parameters	**M1**	**M2**	**M3**	**M4**	**M5**
Dope flow rate (ml/min)	8	10	3.5	5	4
Bore fluid, NMP/DI (wt%)	30/70				
Bore fluid flow rate (ml/min)	6	10	3	7	5
External coagulant	Tap water				
Coagulant temperature (˚C)	24				
Air gap (cm)	20	20	20	20	3

After fabrication, the membranes were placed in a bath of 20 g/l HDA in IPA to perform cross-linking for more than 18 hours at room temperature. The volume of cross-linker used was 0.01 l/g of membrane to ensure sufficient reactants in the cross-linking process. The bath was recirculated to induce mixing throughout the entire cross-linking process. After that, the membranes were soaked in IPA for 12 hours with circulation to remove any residual HDA

remaining in the membrane. The inner and outer diameters of the membrane before and after cross-linking were also recorded. The membranes were subsequently stored in PEG 400/IPA (40/60) wt% solution to preserve the microstructure. For additional testing and polyamide synthesis, the hollow fibre substrates were first air-dried for 24 hours and then potted into modules of 5 fibres each with an effective length of 24 cm.

3.2.3 Synthesis of TFC layer by interfacial polymerisation

Interfacial polymerization was performed on the modules to synthesize polyamide thin film layer, as described previously [126]. The lumen side of the hollow fibre membranes were first immersed in aqueous solution containing varied amounts of PEI (50 kDa) and PIP, and 0.1% SDS for 30 min. Prior to this, the pH of the solution was adjusted to 11 using sodium hydroxide (NaOH) and hydrochloric acid (HCl). Excess aqueous solution on the membrane surface was removed by pumping cyclohexane through the lumens for 2 min. The organic phase containing 0.13% of TMC in cyclohexane was then introduced in a similar manner for 2 min. Subsequently, the membrane was left to react for 20 min before rinsing the residual reactants with DI water.

3.2.4 Membrane characterisation

The cross-section, inner and outer surfaces of the polyimide substrates and composite NF hollow fibre membranes were examined by a Zeiss EVO 50 Scanning Electron Microscope (SEM). Hollow fibre samples were fractured in liquid nitrogen and coated with platinum using an EMITECH SC7620 sputter coater for the SEM preparation.

Fourier transform infrared spectroscopy (FTIR) was carried out using Prestige-21 spectrophotometer from Shimadzu to determine the degree of cross-linking in the substrate.

Typical polyimide bands at 1780 ad 1711 cm^{-1} (C=O) and 1361 cm^{-1} (C-N), and amide bands at 1634 cm^{-1} (C=O) and 1525 cm^{-1} (C-N) were identified to track changes to the polymer structure. To further confirm the presence of the polyamide selective layer after the interfacial polymerization reaction, X-ray photoelectron spectroscopy (XPS) was performed using a Kratos AXIS Ultra.

Mechanical properties of the substrate were characterised by the tensile strength test using Zwick 0.5 kN Universal Testing Machine. Hollow fibre samples were clamped on both ends and pulled at 50 mm/min until breakage. The tensile modulus, yield stress and yield strain of the fibres were measured along with the elongation process.

A number of characterisations were done to determine the organic resistance of the membrane. The weight loss of the membrane was analysed before and after immersion in acetone, IPA and DMF. Several pieces of membrane were dried in an oven at 50 ℃ for at least 24 hours and weighed. Thereafter the membrane was immersed in the respective solvents individually for 24 hours, dried and weighed. The weight loss was calculated using equation 3.1 with m_i and m_f (g) as the initial and final dry mass of the membrane, respectively.

$$Weight\ loss = \frac{m_i - m_f}{m_i} \times 100 \qquad (3.1)$$

The degree of swelling of the membrane was also evaluated by measuring the change in length of the membrane when immersed in an organic solvent. Several pieces of 10 cm long membranes were placed inside acetone, IPA and DMF for 24 hours before measuring the length. The degree of swelling can then be calculated using equation 3.2, where l_m and l_{m+s} are the length of dry membrane and solvent impregnated membrane, respectively.

$$Degree\ of\ swelling = \frac{l_m - l_{m+s}}{m_m} \times 100 \qquad (3.2)$$

3.2.5 Membrane separation properties

The membrane separation properties were evaluated using a crossflow setup. To prevent concentration polarization and excessive head-loss across the module, the flow rate of each setup was controlled.

The water, acetone and IPA permeability of the polyimide substrate and TFC membranes were evaluated by running the solvents from the lumen side at 1 – 2 bar for at least 1 hour before measurements were taken. The permeates were collected for at least 5 min and the performances were calculated using equation 3.3, where J_i (LMH/Bar) is the permeability of water, acetone or IPA, ΔP (bar) is the transmembrane pressure, A (m^2) is the effect area of the membrane, ρ_i (g cm^{-3}) is the density of water, acetone or IPA and t (h) is the time of permeate collected.

$$J_i = \frac{m_i}{\Delta P \times A \times \rho_i \times t} \qquad (3.3)$$

The molecular weight cut-offs (MWCOs) of the polyimide substrates were evaluated by running a 2000 ppm of dextran aqueous solution with molecular weight distribution ranging from 6k to 450k Da at 1 bar. Similarly, the permeate were collected after 1 hour of conditioning and measured using gel permeation chromatography (GPC) PL-GPC50 from Varian Inc. The rejection of each range of dextran molecules were calculated using equation 3.4, where R_i is the rejection coefficient for dextran molecule with certain molecular weight i, C_f and C_p (mV) are responses detected by the GPC for the feed and permeate solutions, respectively.

$$R_i = \frac{C_f - C_p}{C_f} \times 100 \qquad (3.4)$$

The rejection capability of the TFC membrane was measured by running acetone and IPA containing 35 µM of RB, AF and MO, respectively, at 2 bar. The permeates were collected after 1 hour of conditioning, and the dye concentrations were measured with a UV-1650 PC UV–Vis spectrophotometer from Shimadzu at 550 nm, 546 nm and 416 nm, respectively. The concentrations of dyes in acetone and IPA can then be calculated using Beer-Lambert's law. The calculated concentrations were then used to determine the membrane rejection for each dye using equation 3.4. In addition, 72-hour stability tests were also conducted to evaluate the performance of the membrane under prolonged filtration.

3.3 Results and discussion

3.3.1 Fabrication of solvent resistant polyimide hollow fibre substrates

As the solvent resistant polyimide hollow fibres were produced by cross-linking the as-spun fibres with HDA, a substrate with higher porosity was required to achieve high solvent permeability after cross-linking. Thus, two pore formers, LiCl and DG, were separately added into the dope solution to improve the porosity of the hollow fibres. The morphology of the cross-linked hollow fibre substrates is shown in Figure 3-1. When LiCl was used as the pore former (Figure 3-1 (a-d)) the membrane seemed to be dense and a thick skin layer was observed near the inner surface. The addition of LiCl was expected to increase the hydrophilicity of the dope composition and encourage a faster rate of phase inversion [162]. However, the rapid solvent exchange and high viscosity of the dope solution failed to generate porous microstructure and resulted in the formation of a dense structure as shown in the cross-section (Figure 3-1 (a)). On the contrary, when DG was used as the pore former (Figure 3-1 (A-D)), finger-like structure was observed in the cross-section (Figure 3-1 (A)). The pores near the surface also seemed to be more inter-connected (Figure 3-1 (D)) compared to those synthesized using LiCl as the additive (Figure 3-1 (d)). The finger-like structure could decrease the mass transfer resistance of the substrates though the mechanical strength may be compromised. However, the hollow fibres should have sufficient mechanical strength for low pressure OSN application and details of their mechanical properties will be discussed in the section 3.3.2.

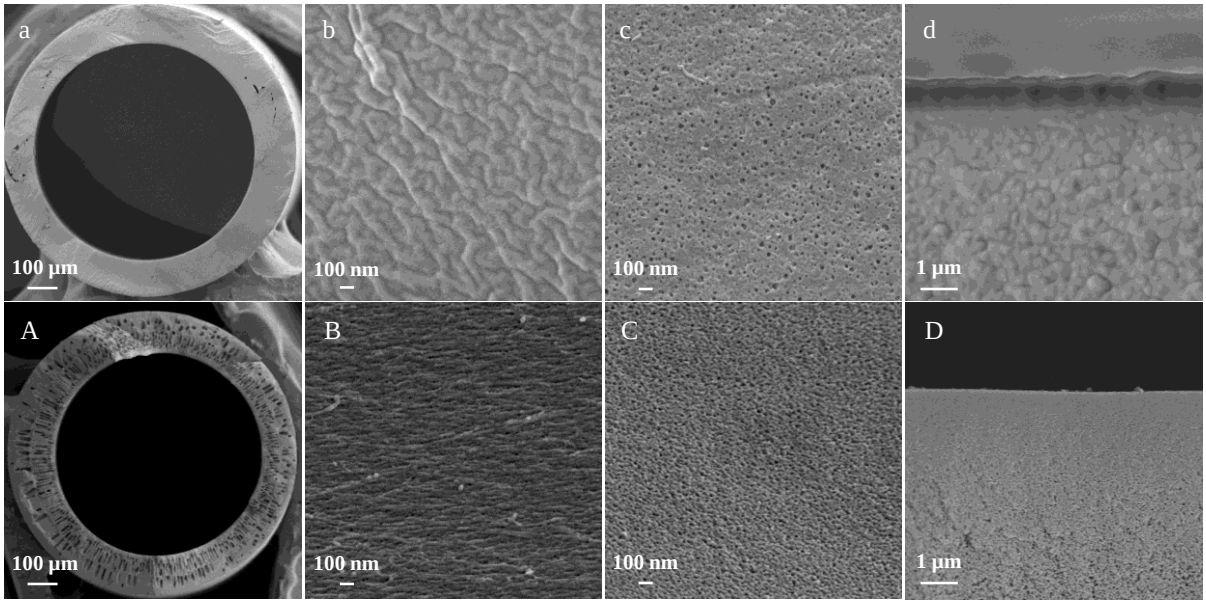

Figure 3-1 SEM images of hollow fibre substrate. (a-d) cross-section, inner surface, outer surface and enlarged cross-section of inner surface of the substrate with LiCl as pore former; (A-D) cross-section, inner surface, outer surface and enlarged cross-section of inner surface of the substrate with DG as pore former

The water permeability and MWCO of the hollow fibre substrates were tested, and the results are shown in Figure 3-2. Both hollow fibres M1 and M2 were synthesized using LiCl as the pore former. The water permeability of M1 was only 4.6 LMH/Bar and there was no water permeability for M2 when the concentration of the pore former was increased. As illustrated from the SEM images (Figure 3-1 (a-d)), the formation of the dense layer and low pore inter-connectivity resulted in the low water permeability of the hollow fibres. With such low water permeability, the hollow fibre membranes are not suitable as substrates for TFC membranes. Hollow fibres M3 to M5 were fabricated using DG as the pore formers and they showed much higher water permeability compared to M1 and M2. The water permeability of the hollow fibres increased with higher DG concentration in the dope solution and the use of DG successfully enhanced the porosity of the hollow fibre substrates. Meanwhile, the MWCO of the hollow

fibres also increased from 75 to 125 kDa as the trade-off for the higher water permeability when the concentration DG was increased from 8 to 12%. The MWCO of the substrates which reflects the pore size of the substrates is important for the subsequent interfacial polymerization and relatively small pore sizes are preferred for the formation of a defect-free polyamide thin film [50]. Therefore, hollow fibre M3 with a smaller MWCO but reasonable water permeability was selected as the substrate in this study. Besides, as the cross-linking has reduced the porosity of the hollow fibres considerably, the water permeability of the cross-linked polyimide substrates was relatively lower than that of the substrates used in aqueous nanofiltration in previous studies [85, 163].

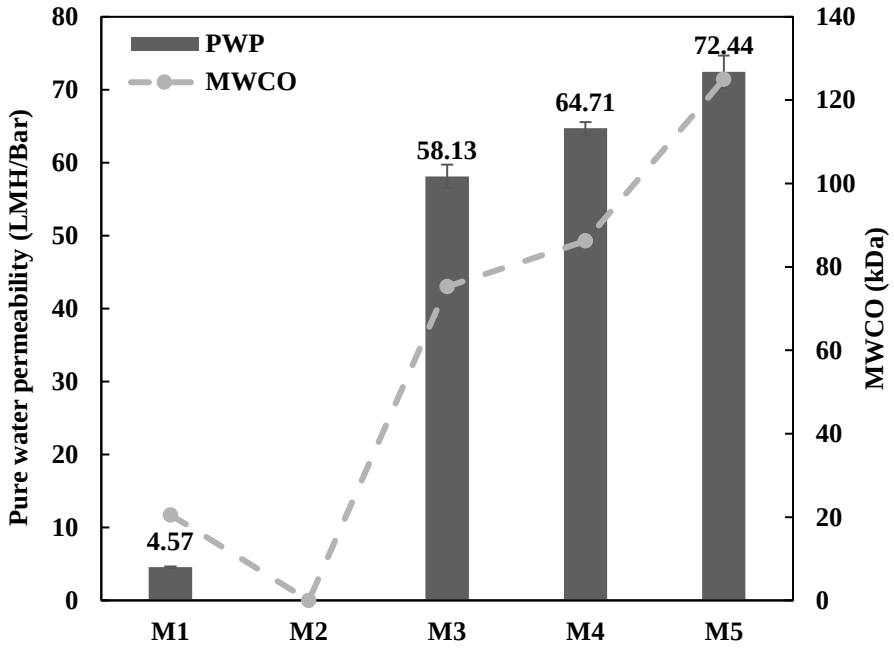

Figure 3-2 water permeability and MWCO for hollow fibre substrate

3.3.2 Solvent resistant properties of polyimide hollow fibre substrates

The physical changes of the M3 hollow fibres were observed after chemical cross-linking, as shown in Table 3-3. It is observed that the inner diameter of the substrate decreased from 864.0

μm to 851.3 μm after being cross-linked. Similarly, the outer diameter decreased and a thinner substrate was obtained after cross-linking. The effect of cross-linking could also be seen from the change in microstructure of the membrane, as shown in Figure 3-3. The microstructure near the membrane surface looked denser after cross-linking (Figure 3-3 (b)). The surface morphology also became slightly rougher as a result of the cross-linking (Figure 3-3 (B)). In addition, the membrane became slightly more brittle after the chemical cross-linking, as observed by the lower strain at break, from ~32.6% to ~22.4%. However, the tensile modulus and stress were higher after cross-linking due to extra intermolecular bonds. The mechanical strength was comparable to the hollow fibre substrates used in previous studies on low pressure nanofiltration processes [125, 164].

Table 3-3 Membrane properties of substrate before and after cross-linking

	Before cross-linking	**After cross-linking**
Inner diameter (μm)	864.0 ± 3.6	851.3 ± 8.1
Outer diameter (μm)	1185.7 ± 10.6	1167.0 ± 10.6
Thickness (μm)	160.8 ± 3.5	157.8 ± 3.6
Tensile modulus (MPa)	69.7 ± 4.9	78.4 ± 5.4
Stress (MPa)	6.08 ± 0.47	8.40 ± 0.42
Strain (%)	32.6 ± 9.1	22.4 ± 6.2

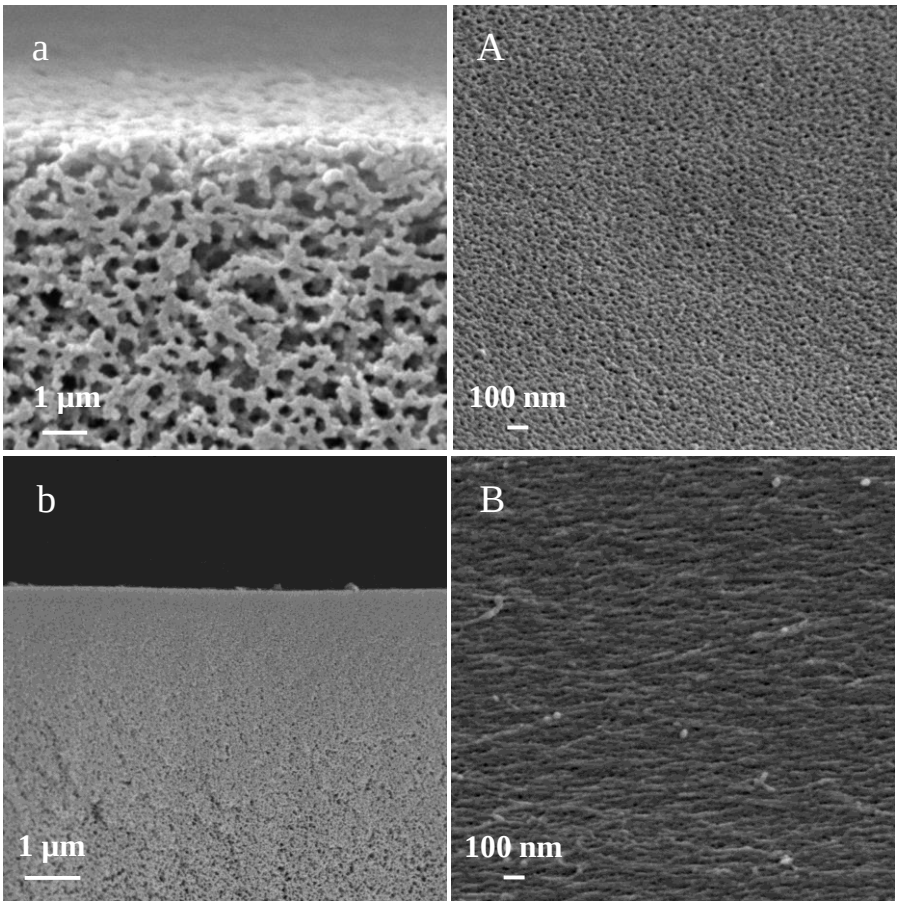

Figure 3-3 SEM images of hollow fibre substrate. (a) cross-section of uncross-linked; (A) inner surface of uncross-linked; (b) cross-section of cross-linked; (B) inner surface of cross-linked

The chemical compositions of the substrate before and after cross-linking were analysed by comparing their FTIR spectra as shown in Figure 3-4. The amide peaks, 1634 cm^{-1} and 1525 cm^{-1}, become stronger in intensity due to the formation of amide groups during cross-linking. On the other hand, the imide peaks at 1361 cm^{-1}, 1711 cm^{-1} and 1780 cm^{-1} diminished in intensity after cross-linking. These observations confirm that the substrate have been successfully cross-linked by HDA [104]. However, it should be noted that the minor peak at 1361 cm^{-1} after cross-linking indicates the presence of some unreacted imide groups after cross-linking. The cross-linking may not be complete in the entire membrane substrate due to

geometric and steric constraints [165]. The polyimide substrate may still be susceptible to swelling and weight loss over long period of time in strong solvents such as NMP and DMF. The chemical resistance of the cross-linked substrates should be significantly enhanced but further improvement may still be needed for applications in strong solvents.

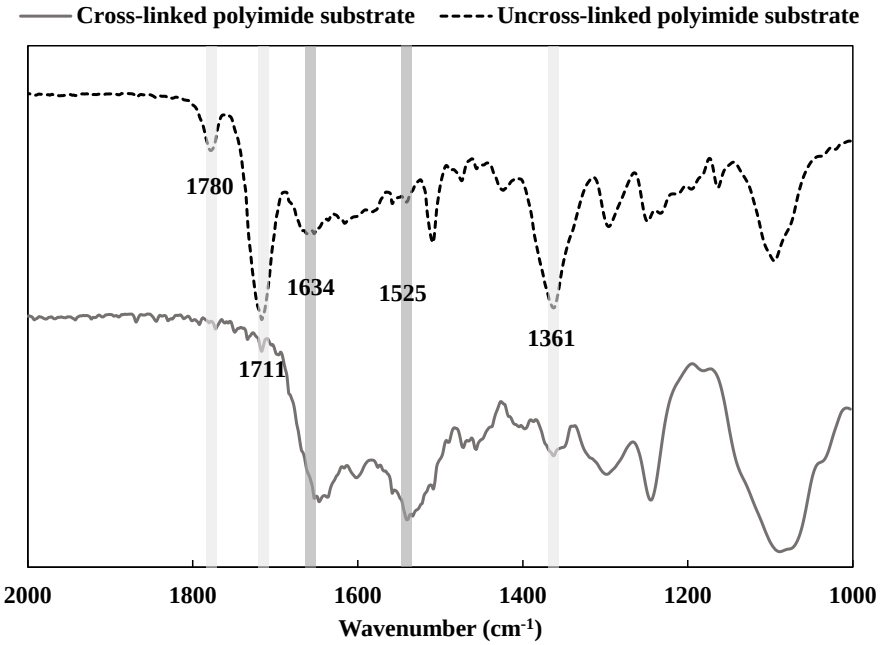

Figure 3-4 FTIR of uncross-linked and cross-linked polyimide substrate

To examine the chemical stability of the cross-linked hollow fibres, the weight changes before and after immersing in acetone, IPA and DMF for 24 hours were measured, and the results are shown in Table 3-4. The hollow fibres were highly stable and experienced negligible weight loss in all solvents, demonstrating great potential for OSN application. It is not surprising to see that uncross-linked polyimide is unstable in aprotic solvents such as DMF and tetrahydrofuran (THF), which dissolves the hollow fibre membranes [104]. Besides that, organic solvents could disrupt the packing of chains and induce polymer swelling and compromise their performances [20, 104, 166]. To use it as a substrate for TFC membranes, the hollow fibres are also required to have minimum swelling in organic solvent to avoid

delamination and excess stretching of the selective layer. The degree of swelling of the membrane was examined by monitoring the change in length of the hollow fibre membrane when immersed in organic solvents. There was no swelling observed in IPA while the degree of swelling in acetone and DMF were about 1% and 6% respectively, which was much lower than many reported solvent resistant hollow fibres [91]. The degree of swelling was also smaller than the uncross-linked polyimide membranes in other solvents [166]. With enhanced chemical stability, the cross-linked hollow fibres could be used as the substrates for TFC membranes in OSN application.

Table 3-4 Swelling factor and weight loss for the cross-linked membrane

	Solvent	**Before immersion**	**After immersion**	**Difference %**
Mass (mg)	DMF	74.4 ± 2.0	74.2 ± 3.6	0.3
	Acetone	74.1 ± 3.2	74.2 ± 2.5	0
	IPA	74.3 ± 2.6	74.3 ± 2.9	0
Length (cm)	DMF	10.0 ± 0.2	10.6 ± 0.1	6
	Acetone	10.0 ± 0.1	10.1 ± 0.2	1
	IPA	10.0 ± 0.1	10.0 ± 0.2	0

3.3.3 Polyamide synthesis on cross-linked polyimide hollow fibres

Polyamide thin film membrane was synthesized (Figure 3-5) on the inner surface of the hollow fibres by circulating the monomer reactants through the lumen of the hollow fibres. This method enabled the formation of a uniform thin film layer on the hollow fibre substrates and has been proven to be scalable [160]. Before the interfacial polymerization, the inner layer was smooth with uniformly distributed pores as shown in Figure 3-3 (B). After the thin film was formed, a rougher fibre inner surface was observed, and the rings of polyamide are shown in

Figure 3-5 (a). This observation suggests successful formation of the polyamide layer, with morphology similar to PEI-based TFC reported in literatures [123, 126, 167]. The thickness of the polyamide selective layer was estimated to be about 50-70 nm as indicated in Figure 3-5 (b).

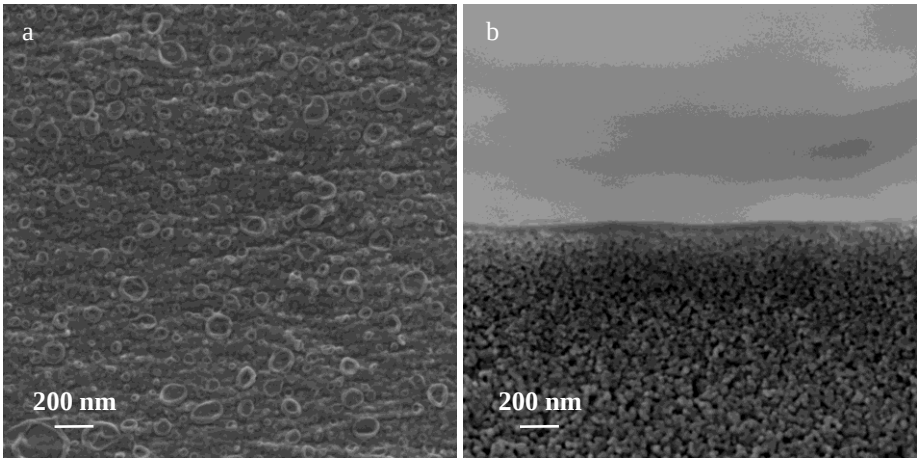

Figure 3-5 SEM images of TFC. (a) inner surface; (b) enlarged cross-section

The changes in surface chemistry of the polyimide substrate after interfacial polymerization were examined using XPS, as illustrated in Figure 3-6. Since polyamide and polyimide have similar C1s peaks, only the nitrogen and oxygen contents are discussed here. The N1s and O1s peaks were deconvoluted into their respective peaks to quantify the chemical species within the structure. For the N1s peaks, the deconvoluted peaks at 399.2 eV and 400.7 eV correspond to the amide groups and imide rings, respectively [83]. As observed, the peak of amide bonds increased after the polyamide layer was coated onto the substrate. The presence of a small imide peak was due to the small amount of PIP used in the polyamide layer synthesis. For the O1s peaks, the peak for the polyimide substrate can be deconvoluted to O=C-N (531.6 eV) and C=O (533.3 eV), while the peak for the polyamide thin film can be deconvoluted to O=C-N (531.6 eV) and O=C-O (533.5 eV) [24, 168]. The C=O peak observed in the polyimide

substrates was not present after the polyamide layer coating, but a new O=C-O peak was detected. Using the wide scan XPS on the substrate and the TFC membrane (Table 3-5), it is observed that there is an increase in atomic ratio of nitrogen (9.33% to 11.29%) after the substrate was coated with the polyamide layer. This can be explained by the presence of more nitrogen content in polyamide compared to cross-linked polyimide thus indicating the successful formation of polyamide layer on the substrate [169].

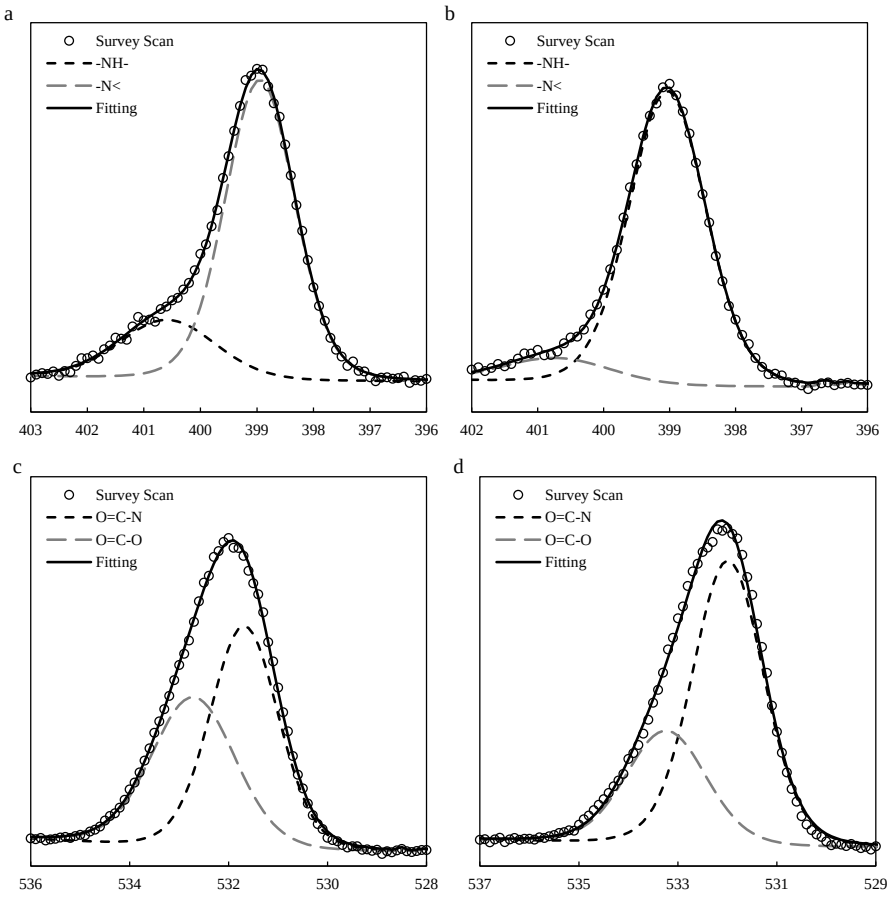

Figure 3-6 XPS narrow scan spectra on the surface of (a): N1s cross-linked polyimide substrate, (b) N1s polyamide thin film composite, (c) O1s cross-linked polyimide substrate, (d) O1s polyamide thin film composite

Table 3-5 Surface chemical composition of cross-linked polyimide substrate and polyamide TFC membrane by XPS wide-scan analysis

Sample	C (%)	N (%)	O (%)
Polyimide substrate	60.07	9.33	30.6
Polyamide TFC	57.82	11.29	30.89

The PEI-PIP type of polyamide was first studied in the OSN application, and the effect of PEI concentration on the formation of polyamide layer was analysed. From Figure 3-7, the acetone permeability decreased with increasing PEI concentration in the aqueous phase and there was a significant drop of 33% in acetone permeability when the PEI concentration increased from 0.1 to 0.2 wt%. The higher monomer concentration led to a more complete interfacial polymerization reaction resulting in a denser and less defective selective layer [170]. However, the subsequent increase in PEI concentration from 0.2 wt% to 0.4 wt% had lesser effect on the acetone permeability. This is probably due to the relatively higher concentration of PEI than PIP added as the aqueous monomer. The longer chained PEI monomer formed a looser selective layer, thereby being able to maintain its acetone permeability when varying PEI concentration from 0.2 wt% to 0.4 wt%.

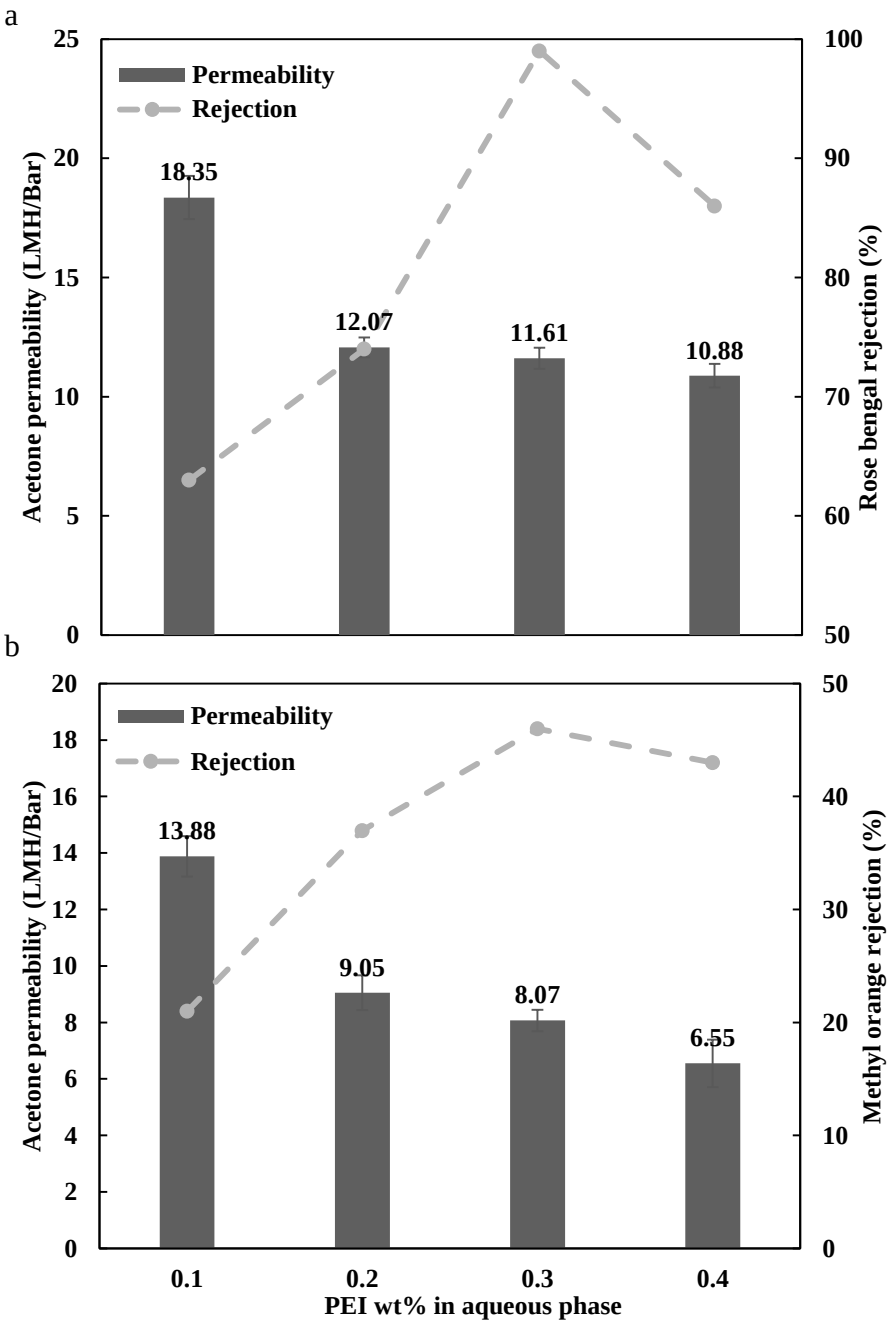

Figure 3-7: Effect of PEI concentration on acetone permeability and dye rejection. (a) RB; (b) MO (amine solution pH=11; rejection of 35 µM dyes at pressure of 2 bar)

On the other hand, it seems that PEI concentration below 0.3 wt% was not sufficient to form a continuous film with minimum defects, probably due to slower reaction at the interface, though an increase of PEI concentration from 0.1 wt% to 0.3 wt% led to an increase in overall rejection of RB dyes. However, further increase in PEI concentration to 0.4 wt% brought a slight drop in the rejection. This may be caused by competing effect between the two aqueous monomers, PIP and PEI, during the interfacial polymerization process that stifled the cross-linking reaction between TMC and the amines, as pointed out by previous studies [126, 167]. In addition, an increase in long chain PEI monomers as compared to PIP may result in a looser selective layer that lowers the rejection. From these observations, a PEI concentration of 0.3 wt% and 0.1 wt% PIP can be said to achieve the optimal balance between dye rejection and acetone permeability.

3.3.4 Performance of TFC hollow fibre membranes

The acetone, IPA and water permeabilities of the TFC hollow fibre membranes were tested in a crossflow filtration setup as shown in Figure 3-8. The TFC hollow fibre membranes showed a high acetone permeability of 11.6 LMH/Bar, which was one of the highest so far compared to other OSN hollow fibre membranes published in recent years [16]. The membranes also showed a moderately high IPA permeability of 4.5 LMH/Bar. Though this study focuses on OSN application, the water permeability was also measured to compare the membrane performance with previous studies on PEI-based polyamide membranes used for water application. It could also shed light about the transport mechanism of the membrane. The water permeability of the membrane was 6.8 LMH/Bar, which was lower than our previous work [125]. This could be attributed to the nature of cross-linking process of the hollow fibre substrate, which increased the overall transport resistance of the membrane [20, 104]. The higher acetone permeability compared to both water and IPA could be due to the relatively lower viscosity of acetone [61]. Besides that, solvent permeability is often affected by solubility

and acetone could also have a Hansen solubility parameter closer to the PEI-base polyamide membranes [171].

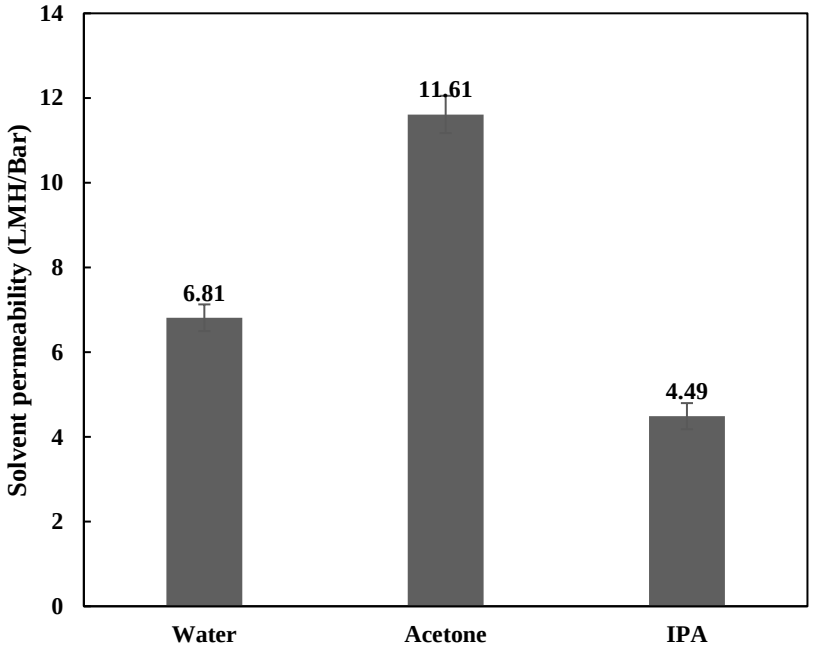

Figure 3-8: Solvent permeability of thin film composite membrane

In addition, the selectivity of the TFC membrane was evaluated by measuring the rejection of dyes with different molecular weights and the results are summarised in Figure 3-9. The membrane achieved high rejections for both rose bengal (>99%) and acid fuchsin (~92%) in acetone and IPA. However, the rejections of acid fuchsin and methyl orange were much higher in water (>95%). This could be due to minor swelling of both polyamide selective layer and polyimide hollow fibre substrate when exposed to organic solvents [17]. In addition, the hydrodynamic radius of the solutes in different solvents could result in different rejections obtained for both cases [68].

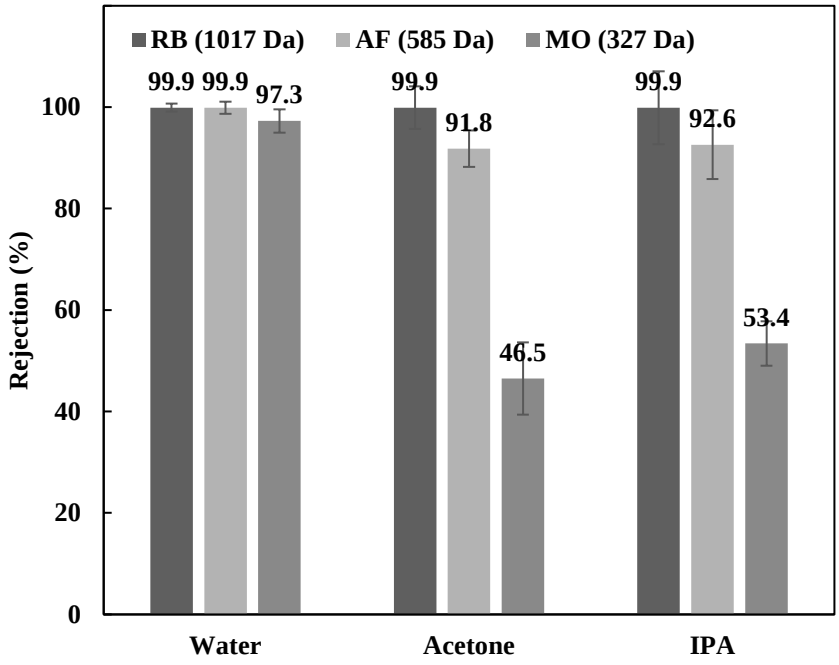

Figure 3-9 Comparison of rejection and with different molecular weights

To preliminarily evaluate the stability of the membrane, a 72-h stability test was conducted with a feed solution of 35 μM acid fuchsin in acetone under 2 bar and the results are shown in Figure 3-10. Due to safety reasons, the test was stopped at night and resumed the follow day. The membrane was stored in the solvent and the membrane was conditioned for 1 h after each resumption of experiment. As observed, the permeability and rejection fluctuated in a narrow range over the period of test with initial permeability and rejection at 10.8 LMH/Bar and 90.3% respectively. This suggests that the performance of the membrane can potentially be maintain over a long period of time.

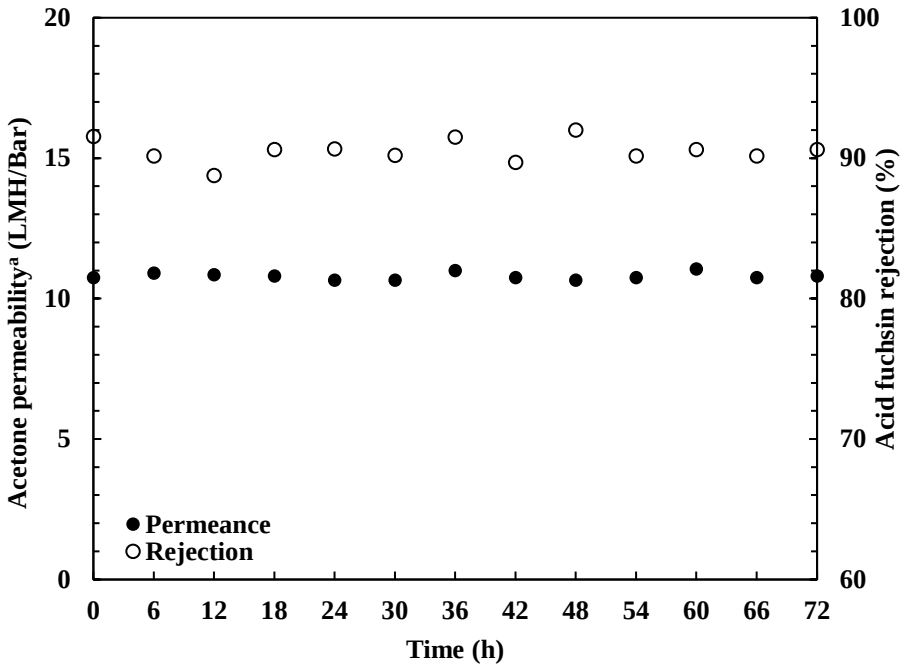

Figure 3-10 72-h filtration test (35 μM acid fuchsin in acetone at 2 bar for 72 hours)[a]: The permeabilities are obtained from acetone feed with acid fuchsin rather than pure acetone.

A summary of OSN hollow fibre membranes recently developed is shown in Table 3-6. It can be seen that several TFC membranes are able to outperform ISA membranes, which faces the limitation of a one-step phase inversion process [16]. Additionally, there are not many studies on OSN hollow fibre TFC membranes. The membrane developed in this work exhibits comparable or superior OSN performance to many other TFC membranes reported in literature. The higher permeability could be attributed to several modifications done in this work. The narrow finger-like structures present in the substrates could have increased the porosity and thereby increasing permeability of the solvent [50]. These finger-like structures are beneficial in membrane systems that operating at low pressure as they will not be subjected to compaction. The PIP/PEI combination used to synthesize the selective layer also improved the permeability of the TFC membrane. The relatively loose polyamide structure allows for higher solvent permeability while maintaining selectivity in NF range. Overall, in terms of permeability and rejection, the mixed polyamide based TFC membrane shows significant improvements compared to many other recently developed TFC membranes.

Table 3-6 OSN performance of polymeric hollow fibre membranes reported in literature

Material (Type)	Solvent permeability (LMH/Bar)	Solute (M_w, Da)	Rejection (%)	Pressure (bar)	[Ref] Year
PBI-H_2SO_4 (ISA)	3.5 (MeOH)	TC (444)	98	5	[100] 2019
Cross-linked PAN (ISA)	2.32 (EtOH)	RBB (626) MB (320)	99.9 15.8	2	[172] 2017
Polyamide-imide (ISA)	6.4 (IPA)	RB (1017)	97.3	2	[164] 2016
Cellulose (ISA)	6 (EtOH) 7 (DMF)	CR (696) RBB (626)	~99 ~50	0.2	[173] 2019
Polyamide with PEG 300 (ISA)	0.32 (MeOH)	VB_{12} (1355)	97.7	3	[174] 2018
PBI on P84 polyimide (TFC)	1.58 (Acetonitrile) 2.6 (MeOH)	MB (320)	99	1	[175] 2015

	4.31 (Acetone)	BBR (826)	99.9		
P84 polyimide with NH_2-MWCNT (TFC)	1.17 (EtOH)	TC (444)	97.4	5	[82] 2018
	0.53 (IPA)	MB (320)	99.8		
SFPS dual-layer Matrimid polyimide (TFC)	0.83 (MeOH)	RBB (626)	99.3	16	[176] 2015
		RB (1017)	99.9		
Polyamide on P84 polyimide substrate (TFC)	11.6 (Acetone)	AF (585)	91.8	2	This work
	4.5 (IPA)	MO (327)	46.5		

PS: polystyrene, RB: Rose bengal, MB: Methylene Blue, RBB: Remazol Brilliant Blue R, TC: Tetracycline, AF: Acid fuchsin, MO: Methyl orange, CR: Congo Red

3.4 Conclusions

Low-pressure hollow fibre TFC membranes were successfully fabricated for OSN application using dry-jet wet spinning method. The polyimide substrate was chemically cross-linked to enhance its solvent resistance, followed by interfacial polymerization to form a mixed-polyamide selective layer. LiCl and DG were used as additives in dope preparation and a substrate with narrow finger-like structure was fabricated with DG, showing higher pure acetone permeability as compared to the sponge-like structures (LiCl), due to reduced transport resistance of the membrane. The cross-linking process enabled the substrates to possess excellent resistance to acetone and IPA with minimal weight loss and swelling. However, strong solvent such as DMF still caused significant swelling to the membrane which might affect the filtration performance of the TFC over long period of time.

The effects of PEI monomer concentration on the performance of the selective layer were studied. Results showed that a 0.3 wt% of PEI with 0.1 wt% PIP delivered an optimal balance between solvent permeability and solute selectivity. The TFC hollow fibre membranes achieved high acetone and IPA permeabilities of 11.6 and 4.5 LMH/Bar, respectively, while having more than 90% rejection for acid fuchsin, a dye with 585 Da molecular weight. This shows that the TFC membrane can achieve relatively high selectivity in the nanofiltration range. In addition, the prolonged filtration test demonstrated that the performance of the TFC membrane is stable. Given the scalability and simplicity of the fabrication processes of the substrate and selective layer, this work proves to be a promising technique, which has potential to be further developed for low pressure commercial OSN hollow fibre membranes.

Chapter 4 Thin film composite hollow fibre membrane for pharmaceutical concentration and solvent recovery

4.1 Introduction

During the manufacturing of pharmaceuticals, active pharmaceuticals ingredients (APIs) and intermediates are often separated and concentrated throughout different reaction stages [147, 149]. The molecular weights of these solutes are typically in the range of 200 – 1000 Da [33, 177]. By using appropriate membranes, these APIs and intermediates can be separated via the differences in their molecular weights and affinity to the targeted organic solvents. In addition, these solutes are dissolved in commonly used organic solvents such as IPA and acetone, which can potentially be recycled after each reaction step. Currently, solvents are either treated and discharged, or recycled using energy consuming distillation techniques, leading to greater operating cost of the manufacturing plant [22, 54]. In this case, the use of membrane separation for solvent recovery can potentially reduce the overall operating cost. To achieve high production yield and reduce material wastage, the separation, concentration and recovery of these materials requires a solvent resistant membrane with superior selectivity in the nanofiltration range, given the small molecular sizes of the solutes.

In Chapter 3, an OSN hollow fibre TFC membrane for low pressure application was developed. Although the TFC membrane achieved over 90% rejection of acid fuchsin (585 Da), it is still inadequate for pharmaceutical applications due to high purity requirements. In this work, a significantly more selective TFC hollow fibre membrane was developed to concentrate an API while recovering the organic solvent to a relatively high purity. P84 polyimide substrate was used as the substrate as it has been proven to be solvent resistant in several commonly used organic solvents [29]. In addition, the chemical cross-linking process used was easily scalable

and facile [164]. The substrate fabricated in previous work was further improved to increase the performance of the overall TFC membrane by adjusting its spinning parameters. To increase the selectivity of the TFC membrane for smaller (<300 Da) solutes, the monomers used in the interfacial polymerisation (IP) step was changed from a combination of piperazine/polyetherimide (PIP)/ (PEI) to m-phenylenediamine (MPD), and the IP process was carefully adjusted to obtain a denser selective layer for higher selectivity. This is expected to reduce the loss of valuable APIs during the concentration process and improve the purity of the recovered solvent. The permeability of the membrane was enhanced through solvent activation by n,n-dimethylformamide (DMF), opening up the pores of the selective layer and substrate while maintaining excellent rejection of solutes. To determine the scalability of the TFC fabrication process, the performance of a 5-piece module was compared with a 100-piece module. In addition, 7-day filtration experiment of the 100-piece module was also carried out to study the stability of the solvent-activated TFC membrane under operating conditions. Lastly, an API with a relatively small molecular weight was concentrated in a batch process and the organic solvent was recovered simultaneously. Overall, this study explored the scalability and stability of the TFC OSN membrane and its potential use in pharmaceutical industry.

4.2 Materials and methods

4.2.1 Materials and chemicals

The materials used for the fabrication of the substrate have been listed in Chapter 3, section 3.2.1. For the IP process, m-phenylenediamine (MPD, >99%, Sigma Aldrich), cyclohexane (>99%, VWR) and benzene tricarbonyl trichloride (TMC, >98%, Sigma Aldrich) were used.

To evaluate the rejection capability of the TFC membranes, rose bengal (1017 Da in molecular weight (MW), >95%, Sigma Aldrich), acid fuchsin (585 Da in MW, ~70%, Sigma Aldrich), methyl orange (327 Da in MW, >85%, Sigma Aldrich), methyl red (269 Da in MW, ACS reagent) and levofloxacin (361 Da in MV, >98%, Sigma Aldrich) purchased from Sigma Aldrich were used. Acetone (>95%, Sigma Aldrich), acetonitrile (>99.5%, Sigma Aldrich), isopropanol (IPA, >99.5%, Sigma Aldrich), ethanol (>99.5%, Sigma Aldrich) and n,n-dimethylformamide (DMF, >99.8%, Sigma Aldrich) were used in the solute-solvent system.

4.2.2 Fabrication of hollow fibre membrane module

The preparation of dope is similar to that mentioned in Chapter 3, section 3.2.2. Incidentally, a dope mixture of 20/8/72 wt% P84/DG/NMP, respectively, was used. The P84 polyimide hollow fibre substrate was spun using the dry-jet wet spinning process according to the following conditions (Table 4-1). The spinning parameters from the previous work were further improved in this study to increase the performance of the substrate. For example, a smaller spinneret (0.5 mm / 1.0 mm) was used to increase its packing density for future scale-up works. In addition, a harder bore fluid and lower air gap were used to increase the extent of finger-like structures from the inner and outer surfaces of the membrane. This further reduces the

resistance of the membrane, thereby improving permeability. A detailed procedure for spinning and cross-linking post treatment can be found in Chapter 3, section 3.2.2.

Table 4-1 Spinning condition for P84 hollow fibre

Parameters	**This work**	**Previous work [29]**
Spinneret (mm/mm)	0.5/1.0	0.75/1.5
Dope flow rate (ml/min)	3	3.5
Bore fluid	de-ionised water (DI)	NMP/DI (30/70) wt%
Bore fluid flow rate (ml/min)	3	3
External coagulant	Tap water	Tap water
Coagulant temperature (°C)	24	24
Air gap (cm)	5	20

The organic solvent resistant substrates were then potted into two different sets of modules and sealed at both ends with solvent resistant epoxy resin. The two sets of modules have an effective length of 0.22 m and 0.36 m, respectively. In addition, the first set of modules contain 5 fibres each while the longer module contains 100 fibres each.

After the hollow fibre substrates were potted into modules, IP was carried out to produce a polyamide selective layer. This was done by soaking the modules in MPD solution and then purged with cyclohexane to remove excess MPD. A TMC solution was then pumped through the lumen to form a thin polyamide layer on the substrate. As the 100-piece module is longer and contains more fibres, a slightly higher crossflow rate of the solutions was used to reduce the dilution effect of reactants at the outlet. The modules were kept in DI for storage before use. A detailed explanation of the IP process can be found in Chapter 3, section 3.2.3.

4.2.3 Membrane characterisation and performance evaluation

The physicochemical characteristics of the hollow fibre substrate and selective layer were comprehensively examined through a series of standard scientific characterisation techniques as described in Chapter 3, section 3.2.4. Concisely, the morphology of the polyimide substrate and TFC membrane were examined under a Zeiss EVO 50 Scanning Electron Microscope (SEM). Fourier Transform Infrared Spectroscopy (FTIR) was carried out using Prestige-21 spectrophotometer from Shimadzu to examine the cross-linking of the polyimide substrate and presence of polyamide layer. To further confirm the presence of the polyamide TFC after the IP reaction, X-ray photoelectron spectroscopy (XPS) was performed using a Kratos AXIS Ultra. Mechanical properties of the substrate were characterised by the tensile strength test using Zwick 0.5 kN Universal Testing Machine. The organic solvent resistant of the substrate was also determined by measuring its weight loss and degree of swelling in the organic solvents, using methods discussed in Section 3.2.4.

A crossflow setup was used to carry out membrane performance tests to reduce concentration polarisation and excessive head-loss across membrane modules. The permeabilities of water, acetone, acetonitrile and ethanol for the polyimide substrate and TFC membranes were evaluated using similar methods described in Chapter 3, section 3.2.5. The selectivity of the substrate and TFC membranes were evaluated using dextran aqueous solution and dye organic solutions, respectively. 50 ppm of rose bengal, acid fuchsin, methyl orange and methyl red were used as solutes for the organic solvent systems to provide solutes of a wide range of molecular weights.

4.2.4 Effect of solvent activation on membrane separation properties

Solvent activation was performed on the 100-piece TFC module to examine its effect on selectivity and permeability. DMF was pumped at 1 bar from the lumen side for 5 min to activate the membranes. Subsequently, distilled water was pumped, without recirculation, at 1 bar from the lumen side for 10 min to flush out any remaining DMF in the membrane pores. The selectivity and permeability tests described in Chapter 4, section 4.2.3 were then carried out immediately after solvent activation.

4.2.5 7-day stability test and concentration of active pharmaceutical ingredients

A 7-day stability tests of the pristine and solvent-activated TFC membranes were conducted to study the performance of the 100-piece TFC module under prolonged organic solvent filtration. The selectivity and permeability were determined using 50 ppm of methyl red in acetone. Levofloxacin was concentrated using the pristine and solvent-activated TFC membranes to simulate their performance on pharmaceutical purification process. For the pristine TFC membrane, 50 ppm of levofloxacin was dissolved in acetone and concentrated to 20,000 ppm to replicate the API recovery process. Likewise, the solvent-activated TFC membrane was used to concentrate levofloxacin from 5000 ppm to 20,000 ppm. The concentration of levofloxacin in the solutions was determined by HPLC analysis. It was carried out by Agilent HPLC system equipped with UV–Vis detector set at a wavelength of 220 nm and a Discovery HS C18, 150 x 46 mm column. 25 mM potassium phosphate (pH 3.0) and acetonitrile were used as the mobile phase with 9:1 volumetric flow ratio. The solutions were pre-diluted to ensure that the concentration of levofloxacin is within the accurate range of the calibration curve.

4.3 Results and discussion

4.3.1 Characterisation of P84 hollow fibre substrate

P84 polyimide hollow fibre substrate was spun in-house using the method described in Chapter 3, section 3.2.2 and cross-linked with HDA to achieve organic solvent resistance. The MWCO of the cross-linked substrate was measured to be about 100 kDa, well within the range of pore size suitable for a defect-free polyamide synthesis onto the substrate [50]. The changes in physical properties of the membrane were observed as shown in Table 4-2. Compared to our previous work, the inner diameter of the membrane was reduced using a smaller spinneret [29], aiming at achieving a higher packing density, which is beneficial to future scaling-up of the membrane. The SEM images of the cross-linked substrate were also taken to examine its morphology (Figure 4-1). As shown in Figure 4-1 (a), the low air gap and hard bore fluid used in the spinning process resulted in the formation of finger-like macrovoids, extending from both the inner and outer surfaces of the hollow fibre membrane [109]. These finger-like structures are understood to weaken the mechanical strength of the membrane and render it unsuitable for use in various applications such as gas separation and reverse osmosis. However, it improves the low-pressure performance of the membrane by lowering its tortuosity and increasing its porosity [137]. In addition, the hard bore fluid also enabled the formation of a thin dense layer on the inner surface which facilitates the formation of a defect-free selective layer through IP (Figure 4-1 (b and c)) [137, 178].

Table 4-2 Properties of membrane substrate before and after cross-linking

	Before cross-linking	**After cross-linking**
Inner diameter (μm)	677.2 ± 7.1	640.5 ± 5.2
Outer diameter (μm)	978.1 ± 9.6	920.4 ± 12.3
Thickness (μm)	150.5 ± 5.2	139.9 ± 7.7
Tensile modulus (MPa)	69.9 ± 5.0	79.7 ± 5.6
Stress (MPa)	6.30 ± 0.46	8.96 ± 0.70
Strain (%)	34.0 ± 1.4	22.4 ± 0.9

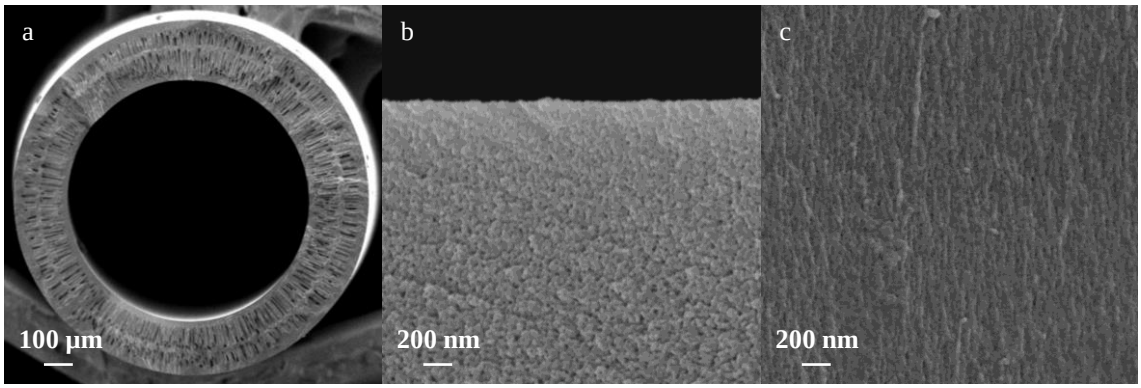

Figure 4-1: SEM images of hollow fibre substrate. (a) cross-section; (b) enlarged cross-section near lumen; (c) inner surface

The chemical compositions of the substrate before and after cross-linking were analysed by comparing their FTIR spectra as shown in Figure 4-2. The amide peaks, 1634 cm^{-1} and 1525 cm^{-1}, became more intense through the formation of amide groups while imide peaks at 1361 cm^{-1}, 1711 cm^{-1} and 1780 cm^{-1} diminished in intensity after cross-linking. These observations are consistent with previous work and thus, the solvent resistance of the fabricated substrate should perform similarly [29, 104].

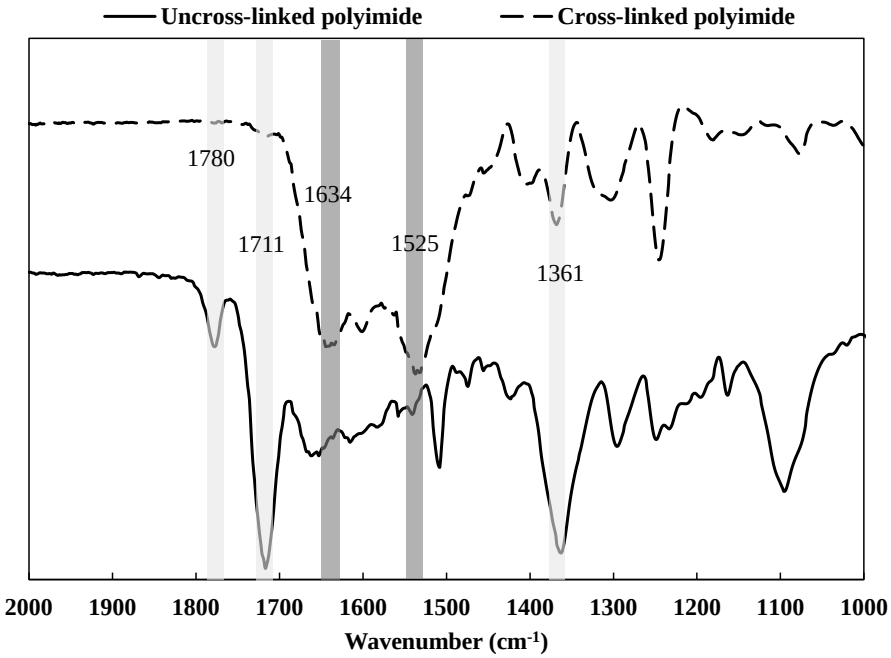

Figure 4-2 FTIR spectrum of uncross-linked and cross-linked polyimide substrate

The substrate was also tested for organic solvent resistance by immersing it in various organic solvents and measuring the change in mass and length. Table 4-3 shows the mass and length changes after immersing the cross-linked membrane in acetone, acetonitrile, IPA and DMF for 7 days. The cross-linked fibres showed negligible loss of mass for all solvents tested. On the other hand, swelling was observed in acetone and DMF at 1% and 6%, respectively. This observation was similar to that discussed in Chapter 3, section 3.3.2. Thus, the performance of the hollow fibre substrate was subsequently tested in solvents that did not have much swelling impact.

Subsequently, solvent permeabilities of the substrate were evaluated and illustrated in Figure 4-3. The substrate achieved relatively high water, ethanol and acetone permeabilities at 125.5, 50.6 and 195.9 LMH/Bar, respectively. As observed, a lower ethanol permeability compared to water might be due to the higher viscosity of ethanol (1.095 mPa.s) than water (0.89 mPa.s).

The increase in viscous resistance has been reported to significantly affect solvent permeation in nanofiltration membranes [179]. Similarly, the lower viscosity of acetone (0.302 mPa.s) might have attributed to its higher permeability across the substrate. In addition, the swelling of the substrate is most pronounced in acetone, which is another factor that contributed to the increase in acetone permeability [69].

Table 4-3 Swelling degree and weight loss for cross-linked membranes in organic solvents for 7 days

Parameter	Solvent	Before immersion (mg)	After immersion (mg)	%
Mass	**Acetone**	74.6 ± 2.4	74.2 ± 2.5	0
	Acetonitrile	74.3 ± 3.3	74.3 ± 3.1	0
	IPA	74.2 ± 1.7	74.3 ± 2.9	0
	DMF	74.4 ± 3.1	74.1 ± 3.6	0.4
Length	**Acetone**	10.0 ± 0.1	10.1 ± 0.2	1
	Acetonitrile	10.0 ± 0.1	10.0 ± 0.1	0
	IPA	10.0 ± 0.1	10.0 ± 0.2	0
	DMF	10.0 ± 0.2	10.6 ± 0.1	6

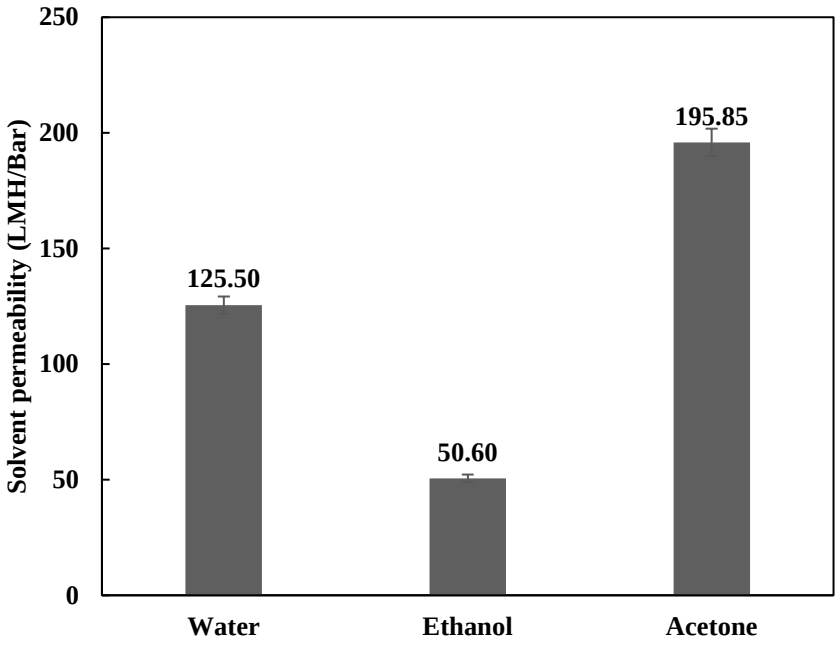

Figure 4-3: Solvent permeability of substrate

4.3.2 Characterisation of polyamide thin-film composite membrane

Polyamide selective layer was synthesized on the inner surface of the hollow fibres through in-house interfacial polymerisation process described in our previous work [29]. PEI/PIP aqueous monomers were replaced with MPD to achieve higher selectivity. The SEM images in Figure 4-4 show the change in morphology on the inner and cross-section of the hollow fibre membrane after IP reaction. From Figure 4-4 (a), the inner surface of the membrane became rougher and was covered by a ridge and valley-like layer, which is characteristic of an MPD-based polyamide layer [180]. Comparing with our previous work, the MPD-based polyamide layer is thicker than that made from a PEI/PIP-based polyamide layer. Like other polymeric amines, the long-chained PEI yielded a polyamide layer with a lower degree of cross-linking and thus reduced the overall thickness of the selective layer [126]. However, in the case of pharmaceutical concentration and solvent recovery process, selectivity is much more critical than permeability of the membrane. Thus, more emphasis was placed on controlling the IP

reaction to ensure a defect-free selective layer. As a result, a thicker selective layer was formed to achieve high separation of these expensive pharmaceutical products and higher purity of recovered solvent. The enlarged cross-section of the membrane (Figure 4-4 (B)) shows voluminous voids in the selective layer that is not typically seen in MPD-based membranes for reverse osmosis applications. This might be explained by the lack of high pressure during the testing process, which does not compact the selective layer prior to SEM imaging [181]. Nonetheless, the control of the IP reaction was able to prepare a selective layer onto the 5-piece and 100-piece modules with no noticeable defects.

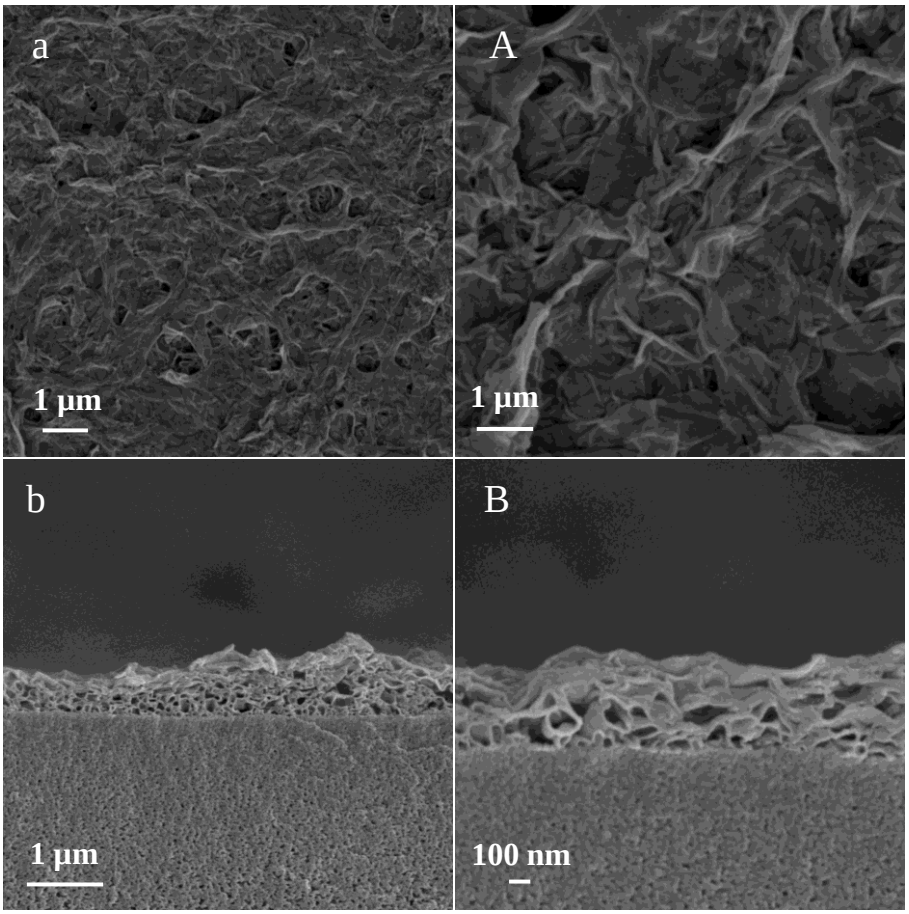

Figure 4-4 SEM images of TFC membranes, (a) inner surface; (A) enlarged inner surface; (b) cross-section; (B) enlarged cross-section

The changes in surface elemental composition of the substrate and TFC were analysed using XPS as illustrated in Figure 4-5. From the wide scan XPS spectra in Figure 4-5 (a), it is observed that there is a larger elemental N peak for the TFC membrane compared to the substrate. This can be attributed to the higher concentration of N in polyamide compared to polyimide [29]. The N1s and O1s peaks were deconvoluted into their respective peaks to quantify the chemical bonding present on the surface. From Figure 4-5 (b) and Figure 4-5 (c), the O1s peak for the polyimide substrate can be deconvoluted to O=C-N (531.6 eV) and C=O (532.6 eV), while the peak for the polyamide thin film can be deconvoluted to O=C-N (531.6 eV) and O=C-O (533.6 eV) [24, 168]. The C=O peak observed in the polyimide substrates was not present after the polyamide layer coating, but a new O=C-O peak was detected. For the N1s peaks, the deconvoluted peaks at 399.1 eV and 400.6 eV correspond to the amide groups and imide rings, respectively [83]. As observed, the amide peak increased after the polyamide layer was applied onto the polyimide substrate. From Table 4-4, it is observed that the percentage composition of N on the surface increased from 3.96% to 9.02% after the IP reaction. This change was also reported in the previous work where a polyamide selective layer was applied onto P84 substrate [29]. The final elemental composition of the TFC membrane is very similar to those reported in literature of MPD-based polyamide, thus, it indicates that a polyamide layer was successfully applied onto the substrate [30, 31, 160].

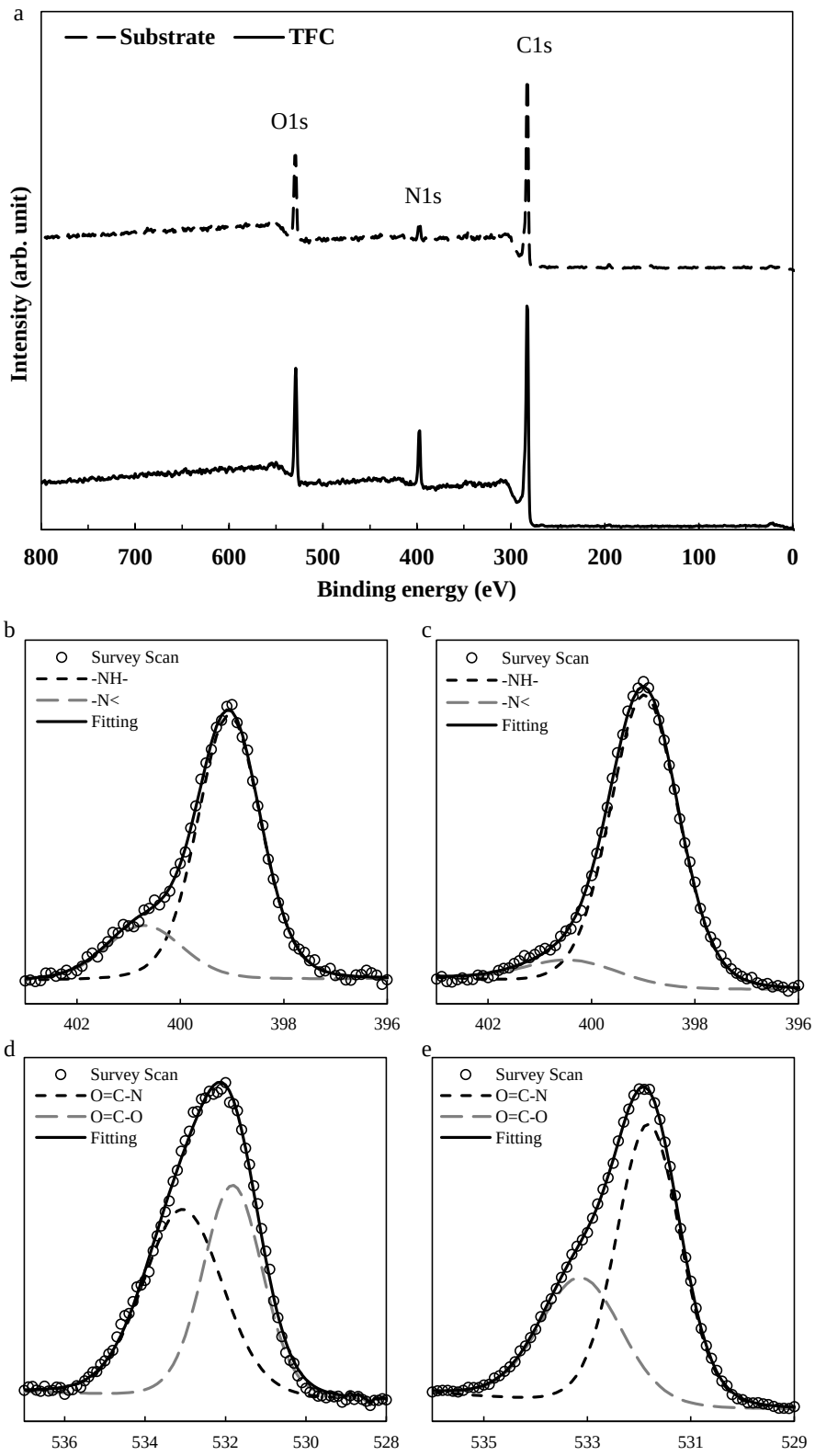

Figure 4-5 (a) XPS wide scan of polyimide substrate and polyamide TFC membrane, XPS spectra of (b) substrate N1s, (c) TFC N1s, (d) substrate O1s and (e) TFC O1s

Table 4-4 Elemental composition of substrate and thin-film composite surface by XPS wide scan

Element	Composition (%)	
	Substrate	TFC
O1s	13.66	11.62
C1s	82.38	79.37
N1s	3.96	9.02

4.3.3 Scalability of hollow fibre membrane

Figure 4-6 shows the photos of the cross-sections and outside views of the hollow fibre modules. The 5-piece and 100-piece modules have an effective surface area 22 cm^2 and 724 cm^2, respectively. The permeabilities and solute rejections of the modules were compared in Figure 4-7 and Figure 4-8, respectively. From Figure 4-7, it is observed that the pure solvent permeability was reduced when the selective layer was synthesized onto the 100-piece module. To ensure a defect-free selective layer for the large module, the crossflow rate for the IP reaction was tweaked slightly and this may have resulted in lower permeability [160]. However, more emphasis should be placed on the selectivity of the membrane when performing IP reaction section in the context of pharmaceutical separation and purification processes. In addition, the permeability can be enhanced through solvent activation, which will be discussed in the next section. A more comprehensive study should be done on the effects of scaling up on the performance of hollow fibre membranes to further understand these factors.

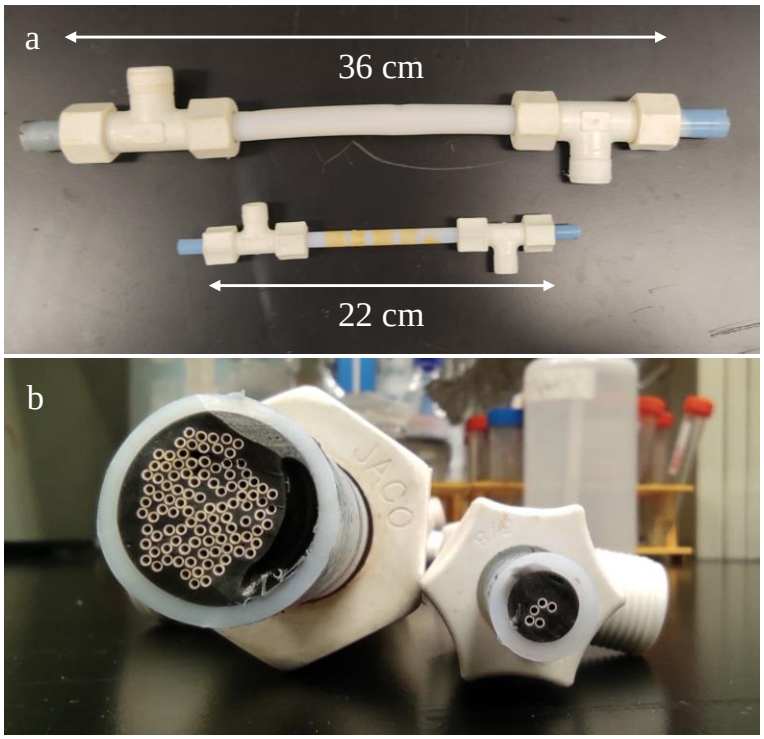

Figure 4-6: Outside view and cross-section of hollow fibre membrane modules; (a) Outside view of 5-piece and 100-piece modules; (b) Cross-section of 5-piece and 100-piece modules

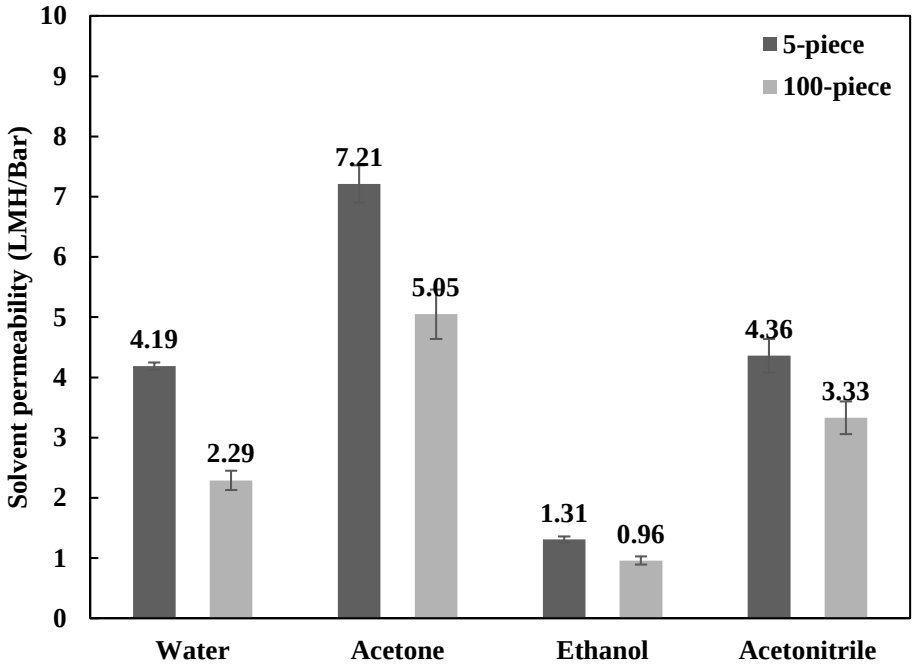

Figure 4-7 Solvent permeability comparisons for 5-piece and 100-piece modules

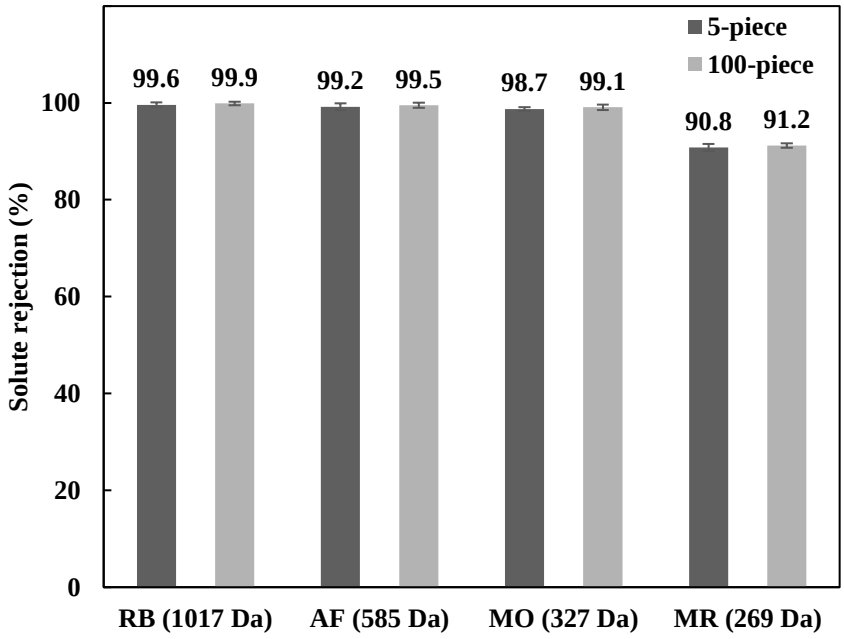

Figure 4-8 Solute rejections comparisons for 5-piece and 100-piece modules in acetone

It is also observed that there is a trend for solvent permeability, where acetone exhibited the highest permeability while ethanol being the lowest. These observations can be explained by the solvents' kinetic diameter, molar volume, viscosity as well as affinity towards the membrane [29, 69, 182, 183]. Solvents such as acetone and acetonitrile with lower viscosity and higher affinity to the substrate and selective layer can therefore pass through the membrane easily compared to ethanol. From Figure 4-8, it is observed that the rejections of solutes for the 5-piece and 100-piece modules were relatively similar. Both modules were able to achieve more than 90% rejection to methyl red, indicating a MWCO of less than 269 Da. Compared to the selective layer synthesized using a combination of PEI/PIP monomers in Chapter 3, the new highly selective layer shows promising potential for pharmaceutical concentration and solvent recovery applications. Upon closer inspection using SEM (Figure 4-9), it is revealed that a defect-free selective layer was successfully synthesized on the 100-piece module. Thus, the method for synthesizing the polyamide selective layer show promising scalability.

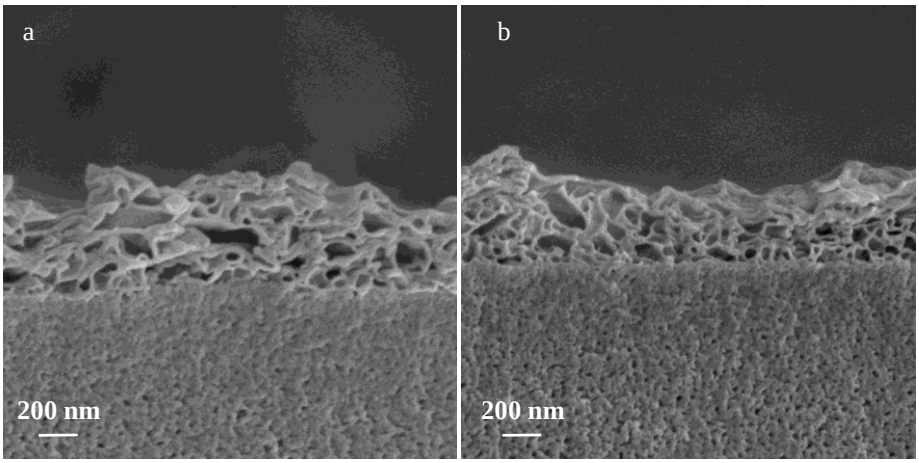

Figure 4-9 SEM images of the inner surface of the 100-piece module. (a) inlet of the module; (b) outlet of the module

4.3.4 Extended filtration test for pristine 100-piece module

A 7-day OSN filtration experiment was done on the pristine 100-piece module to evaluate its stability in OSN application. As observed from Figure 4-10, the acetone permeability remained stable at about 5.1 LMH/Bar while methyl red rejection kept constant at about 91.2%. This suggests that the performance of the membrane can be maintained for an extended period. However, given the low concentration of solute used in the test, the potential fouling issue should be further studied to understand the impact of fouling on its performance.

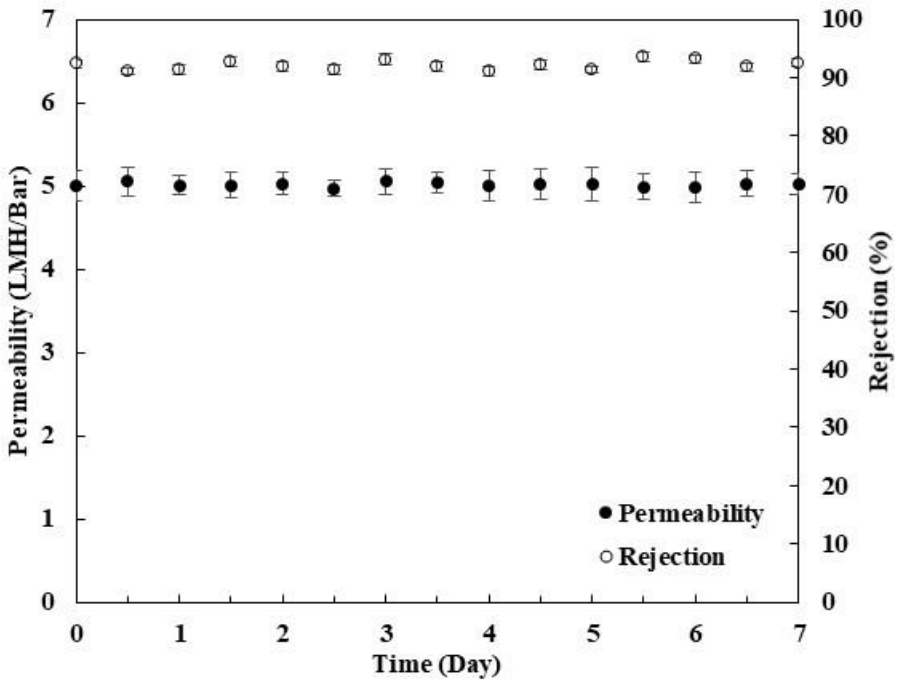

Figure 4-10 7-day filtration test for 100-piece module (50 ppm of methyl red in acetone at 2 bar)

4.3.5 Solvent activation of 100-piece module

To increase the permeability of the 100-piece module, it was subsequently activated by DMF. Figure 4-11 shows the SEM images of the pristine and solvent-activated membrane. The surface morphology of the selective layer did not show much noticeable change after activation as shown by Figure 4-11 (a) and Figure 4-11 (A). However, there is a noticeable increase in voids in the polyamide layer as shown in the cross-sections after solvent activation Figure 4-11 (b) and Figure 4-11 (B). As DMF is one of the top swelling solvents for aromatic polyamides, the polyamide layer might have been swollen and those smaller and uncross-linked molecular fragments were washed away by the entry of DMF into the membrane matrix [27, 184]. It can also be observed that there is a visible increase in porosity of the substrate, which can be explained by the slight loss of mass during the weight-loss experiment. Some uncross-linked polyimide polymers in the substrate may have also been dissolved by DMF, unblocking the

membrane pores and potentially increasing the overall permeability of the TFC membrane [27, 184].

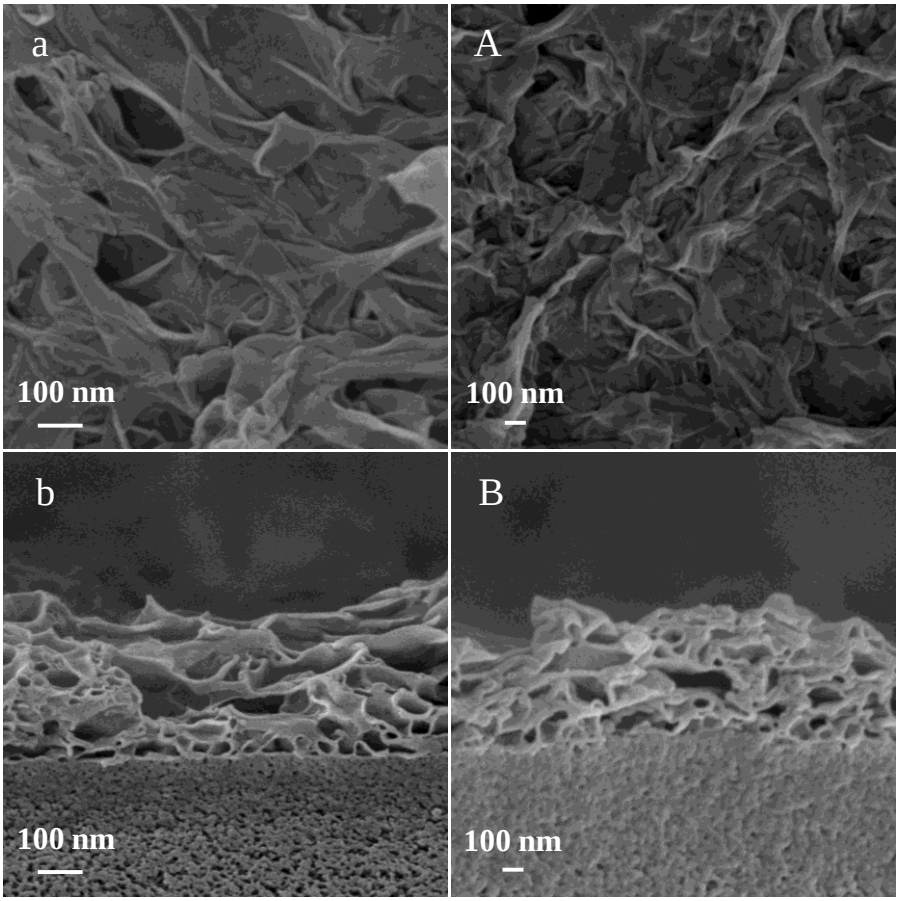

Figure 4-11: SEM images of pristine and solvent-activated membrane. (a) and (A) Inner surfaces of solvent-activated and pristine membranes; and (b) and (B) cross-sections of solvent-activated and pristine membranes

The permeability and solute rejection of the pristine and solvent-activated membranes were compared, and the results are shown in Figure 4-12 and Figure 4-13. As predicted, there is a significant increase in solvent permeability after solvent activation. Notably, acetone permeability increased dramatically by about 4.8 times from 5.1 LMH/Bar to 24.3 LMH/Bar. On the other hand, the collapsing of the pores on the surface due to lower polymer matrix modulus were able to maintain the rejections of the solutes [27]. This shows potential for scale-

up modules to use solvent activation as an effective approach to enhance permeability without the trade-off of much lower selectivity. However, a thorough analysis of solvent-activated membranes should be performed to ensure stable OSN performance over a long period of operation.

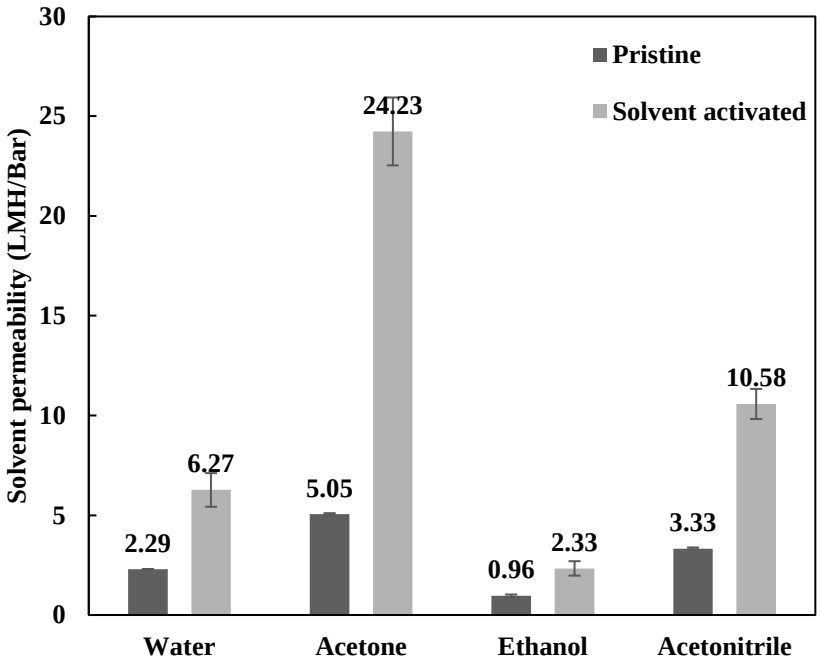

Figure 4-12 Solvent permeability of pristine and solvent-activated membranes

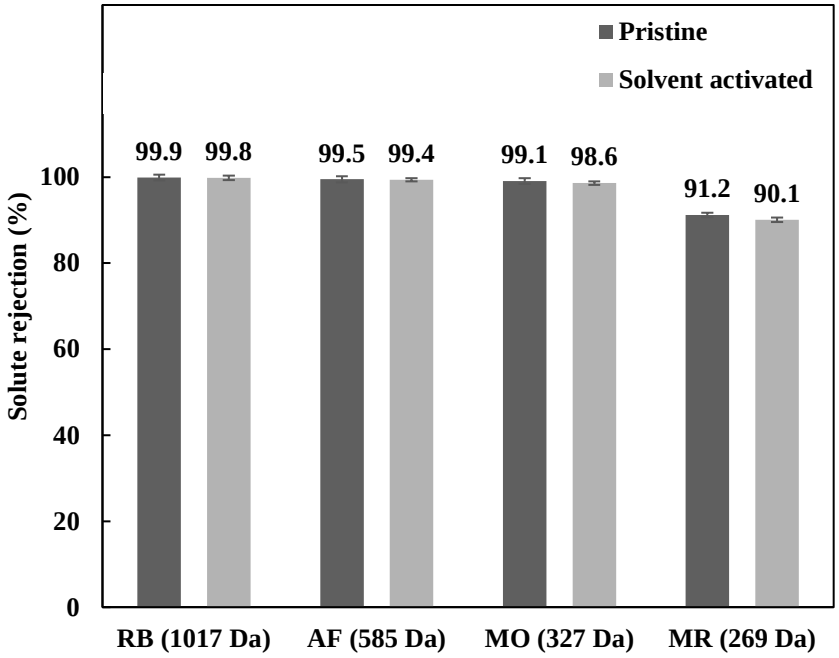

Figure 4-13 Solute rejection of pristine and solvent-activated membranes

A 7-day organic solvent filtration experiment was also performed on the solvent-activated membrane and the performance is shown in Figure 4-14. As observed, the membrane was able to maintain about 90% of methyl red rejection throughout the 7-day period. However, this is slightly lower than that attained by the non-activated membrane (~91.2%). This might be caused by the slight dissolution of the selective layer during the solvent activation process, negatively affecting its selectivity. On the other hand, the membrane maintained a high permeability of 23.5 LMH/Bar throughout the experiment. This demonstrates that solvent activation is an effective way to improve membrane performance, but the degree of the solvent activation needs to be controlled carefully. After all, the selectivity of a membrane plays a more important role in pharmaceutical industries due to the high value of key output materials (KOMs) [33], especially when industries seek for high purity in its products.

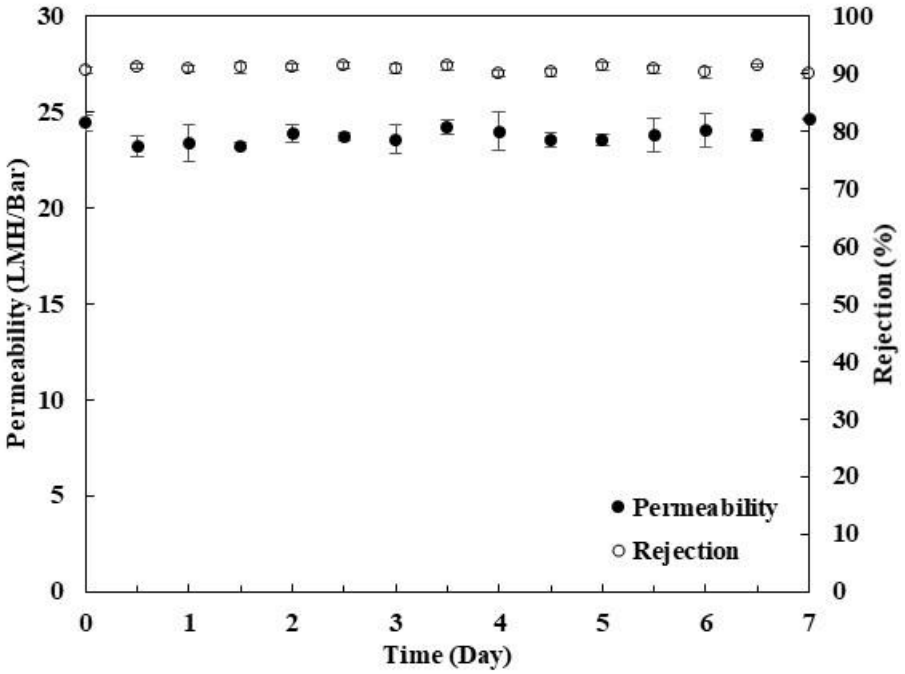

Figure 4-14 7-day filtration test for solvent-activated 100-piece module (50 ppm of methyl red in acetone at 2 bar)

4.3.6 Concentration of levofloxacin and solvent recovery

The capability of the 100-piece modules for concentrating API was demonstrated by performing a single-pass batch process using levofloxacin as a model API. The permeate was collected and stored in a separate tank while the retentate was recirculated back into the feed tank. Consequently, the volume of feed reduces, thereby increasing the concentration of API in the feed. Levofloxacin (361 Da), an antibiotic, was dissolved in acetone as feed for the experiment. Acetone was used as the solvent for this experiment as it is one of the commonly used solvents in manufacturing and pharmaceutical industries [22, 185]. In addition, levofloxacin is highly soluble in acetone. The permeability of acetone and rejection of levofloxacin were measured periodically, and the data obtained for the pristine and solvent-activated 100-piece module were plotted against time as shown in Figure 4-15. As observed, the initial rejection for the pristine membrane was maintained at about 99.2% for more than 9 hours of operations. Subsequently, there was a decrease in rejection to about 95% when the feed concentration was increased from about 5000 ppm to 20,000 ppm. This might be caused by concentration polarisation at the membrane boundary due to higher API concentrations. The rejection of the pristine membrane gradually decreases towards the end of the experiment when the concentration reaches 20,000 ppm. Similarly, the solvent-activated membrane also suffered a drop in rejection as the concentration of feed increased. An initial rejection of about 98.2% for the solvent-activated membrane gradually decreased to 94.1% at the end of the experiment, indicating that concentration polarisation is affecting its performance. On the other hand, the solvent permeability of the pristine membrane also dropped drastically from 5.1 LMH/Bar to 1.5 LMH/Bar over the course of the experiment. This further implies that fouling might have occurred on the membrane surfaces, reducing its permeability. Similar observation was also made on the solvent-activated membranes. An initial permeability of 16.2 LMH/Bar was gradually reduced to 6.21 LMH/Bar within 6 hours of operation. Evidently, the higher

permeability of the solvent-activated membrane resulted in a faster rate of concentration of the same amount of feed. This reduces the time taken for a batch process to complete. As demonstrated, the membrane was able to concentrate the API to 20,000 ppm from a low concentration. An even higher concentration of API can then be obtained by using energy intensive conventional methods of purification. In addition, more than 95% of acetone was recovered in each of the experiment. To reuse the recovered solvent, further polishing steps are required to remove trace amount of levofloxacin, but it is beyond the scope of current study.

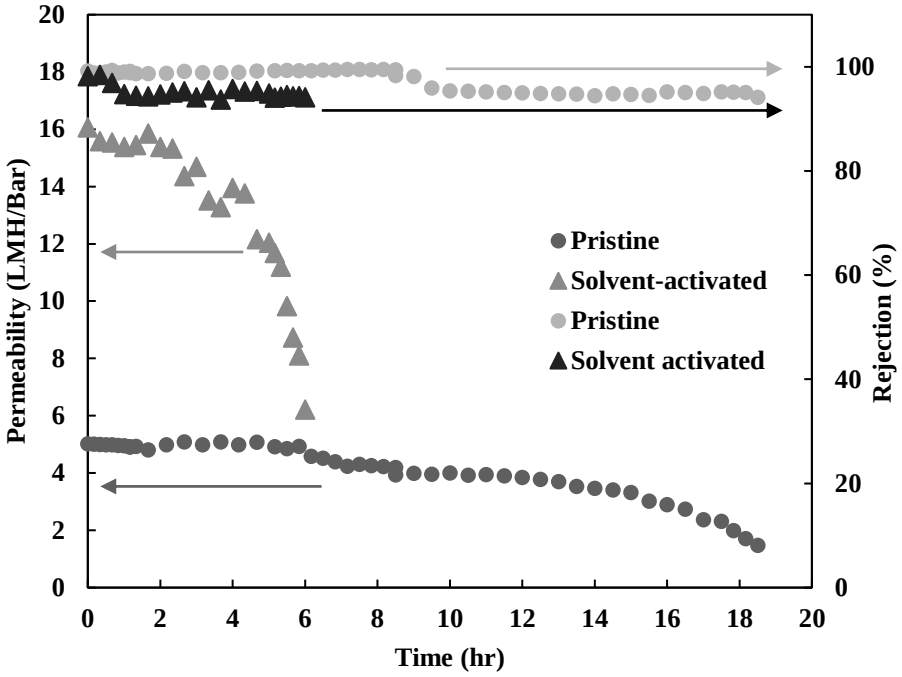

Figure 4-15: Levofloxacin concentration and solvent recovery - rejection and permeability for pristine and solvent-activated 100-piece module

To determine if the fouling was reversible, the modules were flushed with pure acetone at 2 bar for 1 hour at the end of the concentration experiment before measuring their performances again. It turns out that the modules were able to maintain 91% methyl red rejection and recovered more than 95% of their initial acetone permeability. This suggests that the fouling of the 100-piece modules by levofloxacin during the concentration experiment did not have

much permanent impact on their performances. It demonstrates that the OSN membrane can potentially be used to recover solvents from process streams in the pharmaceutical industries. Its high selectivity would also allow it to be used as a polishing step to remove trace amount of contaminants in the recovered solvent through multi-step filtration process. In addition, it can also be employed as a pre-treatment for distillation during API purification processes. The membrane filtration process removes the main bulk of the organic solvent, leaving a more concentrated pharmaceutical intermediate stream with a much lower volume, thereby reducing the energy required to heat the organic solvent during the final purification process. However, similar to any membrane–based processes, fouling is still a prevalent issue that needs to be addressed but this issue is not the focus of current study.

4.3.7 Performance comparison of solvent-activated membrane and commercial membranes

The performance of the solvent-activated 100-piece module was compared with several OSN membranes in Table 4-5. Most of the membranes shown in the table are in flatsheet configuration. On the other hand, the membrane fabricated in this work is of hollow fibre configuration, which offers higher packing density and self-supporting capability. For the solvent-activated membrane, the ethanol permeability was able to match most OSN membranes reported in literature at 2.33 LMH/Bar. The acetone permeability also increased significantly compared with our previous study (24.2 vs 11.6 LMH/Bar). In addition, the selectivity of the solvent-activated membrane performed much better than most of the other membranes mentioned in the table, with a MWCO of about 269 Da. For example, the solvent-activated membrane achieved comparable rejection to NH_2-MWCNT/PI membrane while having a significantly higher acetone permeability. The prolonged testing of the 100-piece module in this study also suggests that the solvent activation step is a promising approach. In addition,

the polyamide selective layer was successfully synthesized for the 5-piece and 100-piece membrane module, demonstrating the feasibility of scaling up the technology. Overall, the facile and scalable membrane fabricated in this work was able to match, if not outperform, many of the state-of-the-art OSN membranes.

Table 4-5 OSN membrane performance of recent works and 100-piece module developed in this work

Membrane	**Membrane size (cm^2)**	**Configuration**	**Solvent**	**Permeability (LMH/Bar)**	**Solute**	**Molecular weight (Da)**	**Rejection (%)**	**[Ref] Year**
(Catechol/POSS)/PI	21.2	Flatsheet	Ethanol	1.26	Rose bengal	1017	99	[186] 2017
PAN	19	Hollow fibre	Ethanol	2.32	Remazol brilliant blue R	626	99.9	[98] 2017
Pebax/PAN	12.6	Flatsheet	Ethanol	1.9	Brilliant blue R	826	95	[187] 2017
Cellulose	6	Flatsheet	Ethanol	0.3	Brilliant blue R	826	94.0	[188] 2018
Kevlar	14.6	Flatsheet	Ethanol	2.9	Rose bengal	1017	95	[189] 2019
sPPSU-ECH	9.62	Flatsheet	Ethanol	11.9	Brilliant blue R Eosin Y Tetracycline	826 645 444	96 95 76.8	[190] 2019
mZIF-8 TFC/PI	28.26	Flatsheet	Ethanol	2.8	Rhodamine B	479	99.1	[191] 2020

NH_2-MWCNT/PI	-	Hollow fibre	Acetone	4.31	Brilliant blue R	826	99.9	[82] 2018
PEI/PIP-based TFC/PI	32	Hollow fibre	Acetone	11.6	Acid fuchsin Methyl orange	585 327	91.8 46.5	[29] 2020
MPD-based TFC/PI (Solvent-activated)	724	Hollow fibre	Acetone Ethanol Acetonitrile	24.2 ± 1.7 2.33 ± 0.36 10.58 ± 0.75	Acid fuchsin Methyl orange Methyl red Levofloxacin	585 327 269 361	99.4 98.6 90.1 98.2	This work

4.4 Conclusions

In this study, a hollow fibre thin-film composite membrane was developed and scaled up by increasing the packing density through changes in spinning parameters. An RO-like selective layer was synthesized to achieve higher selectivity for pharmaceutical applications. Subsequently, solvent activation was applied to enhance permeability while maintaining high solute selectivity. Consequently, the solvent-activated membrane was able to achieve significantly higher permeability of various organic solvents than the pristine membrane, without compromising on its selectivity. In addition, it also demonstrated excellent stability in acetone under operating conditions over a period of 7 days. This demonstrates the scalability of thin-film composite fabrication and uses of solvent activation for improved performance. The fabricated membrane also exhibited promising results in the batch-processed concentration experiment of levofloxacin in acetone, reaffirming its potential for use in pharmaceutical OSN application.

Chapter 5 Thin film composite hollow fibre membrane: Upscaling

5.1 Introduction

In Chapter 4, we demonstrated the recovery of organic solvent and concentration of pharmaceutical product using a TFC hollow fibre membrane. An MPD-based polyamide selective layer was applied onto a polyimide substrate for high selectivity of low molecular weight (<300 Da) solutes. Furthermore, we demonstrated that the selectivity of the membrane was maintained when a 100-piece fibre membrane module was tested, showing upscaling potential for this fabrication method. However, the 100-piece module was not comparable to that of a commercially available membrane.

As such, the methods for fabricating a membrane module of commercial size were developed in this chapter. The effects of scaling up to commercial sizes were discussed and the performances of the scaled-up modules were compared with the lab-scale module. Comparisons were also made on properties such as packing density and surface area of the scaled-up modules with commercial membranes of similar sizes. Through these comparisons, the advantages and disadvantages of thin-film composite hollow fibre membranes for OSN applications were discussed. Lastly, a pharmaceutical product was concentrated to demonstrate the potential of the scaled-up module for OSN applications.

5.2 Materials and methods

5.2.1 Fabrication of hollow fibre membranes and modules

The materials and methodologies described in Chapter 4, section 4.2.2 for the preparation, fabrication and storage of the hollow fibre membrane will be used in this chapter. As such, the physiochemical characteristics of the substrate will be identical to that discussed in Chapter 4. The selective layer synthesized for this study was also based on that described in Chapter 4, section 4.2.2. However, factors such as crossflow velocities, purging and reaction times during the IP reaction were tweaked to accommodate for the increase in fibre and module length.

Typically, in a lab-scale module, the epoxy resin is potted into both ends of the module using a spatula. The potting method used in the lab-scale was not suitable for scaling up as it will take a longer time to pot a larger module and the epoxy resin volume used cannot be controlled easily. In addition, it is challenging to ensure that all the fibres are evenly spread and coated with epoxy resin to prevent leakage in the module. Instead, vertical potting was preferred due to its scalability and simplicity. Figure 5-1 shows the vertical potting method for a 2-in membrane module of 50 cm long. 2-in stainless steel modules were used for scaling up due to its availability as a size for commercial membranes as well as workability for a small study. The fibres were first aligned and bundled together using Teflon tapes to maintain its packing structure. For the module with 1500 fibres, 3D-printed spacers were slotted at both ends to separate the fibres evenly (Figure 5-2). This ensures that the fibres were evenly spread to allow the epoxy resin to flow. The ends of the fibres were cut cleanly and subsequently sealed with small amount of fast-setting epoxy resin. This is to prevent additional epoxy resin from seeping into the lumen of the membrane via capillary action during vertical potting. Solvent resistant epoxy resin was then introduced into one end of the module and left to cure. Excess epoxy resin on the module was subsequently removed. The steps described were then repeated on the

other side of the module. Overall, 3 types of modules were made and their dimensions are shown in Table 5-1.

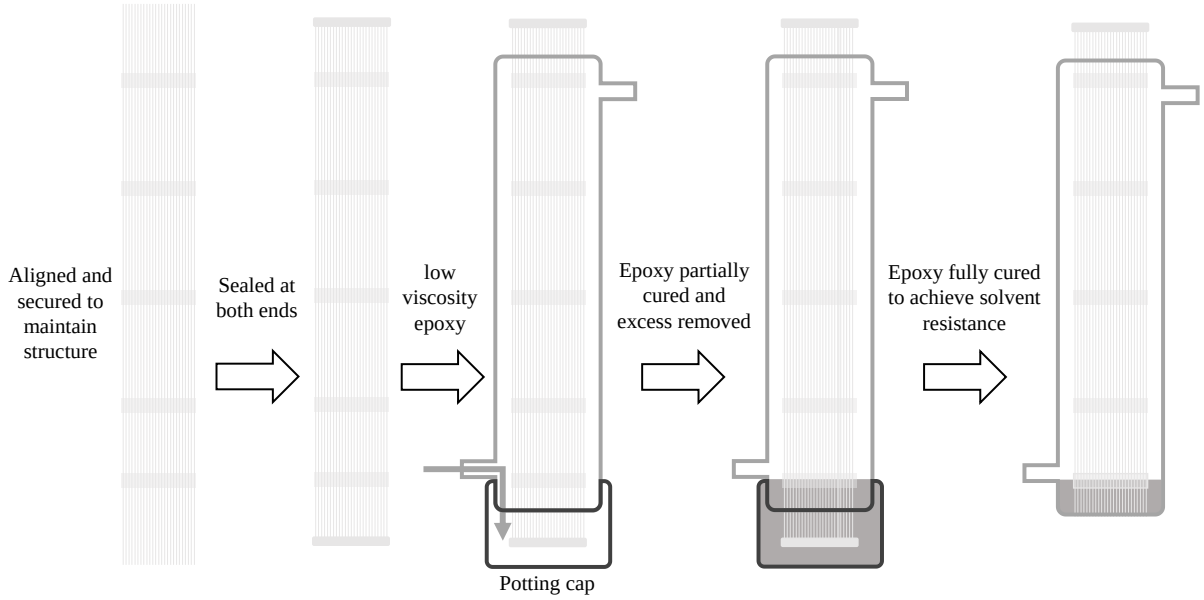

Figure 5-1: Potting of 2-inch module

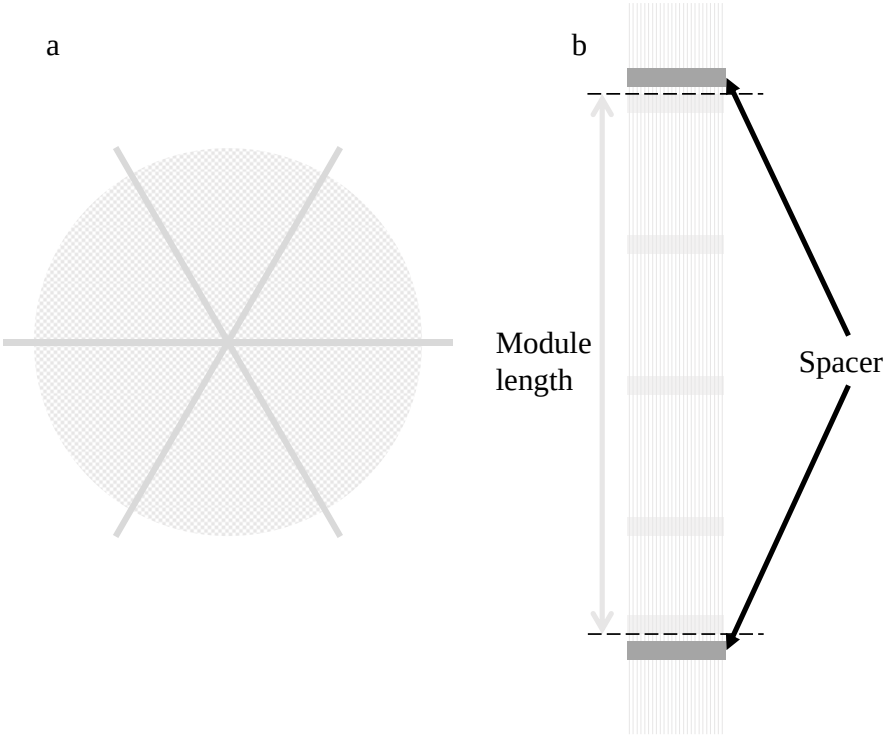

Figure 5-2: Spacer configuration for 2-in module. (a) cross-section of spacer; (b) location of space along fibre bundle

Table 5-1: Dimensions of hollow fibre modules

Module	**# of fibres**	**Effective membrane length (cm)**
P5	5	24
P500	500	46
P1500	1500	46

5.2.2 Defect identification and repair

Defective fibres can develop throughout the membrane fabrication process and this can severely affect the performance of the module. During the fibre fabrication process, defective fibres can form and remain unnoticed during the potting process. Rough handling of the fibres can also potentially result in forming defects. It is also possible that the selective layer was not applied uniformly onto all fibres, resulting in poor selectivity. As such, a method for identifying and repairing these fibres is paramount to ensure continual use of the membrane module.

Figure 5-3 shows the schematic drawing for defect identification and repair of a 2-in hollow fibre module. The permeate side (shell side) of the membrane is first purged of any residual solvent and filled with nitrogen gas. One end of the permeate outlet is capped while pressurised nitrogen gas is introduced from another permeate outlet. Bubbles can then be observed from defective fibres as the module is submerged in water. Subsequently, a nylon thread coated with solvent resistant epoxy resin was inserted into each defective fibre. The epoxy resin was left to cure fully before the module was used.

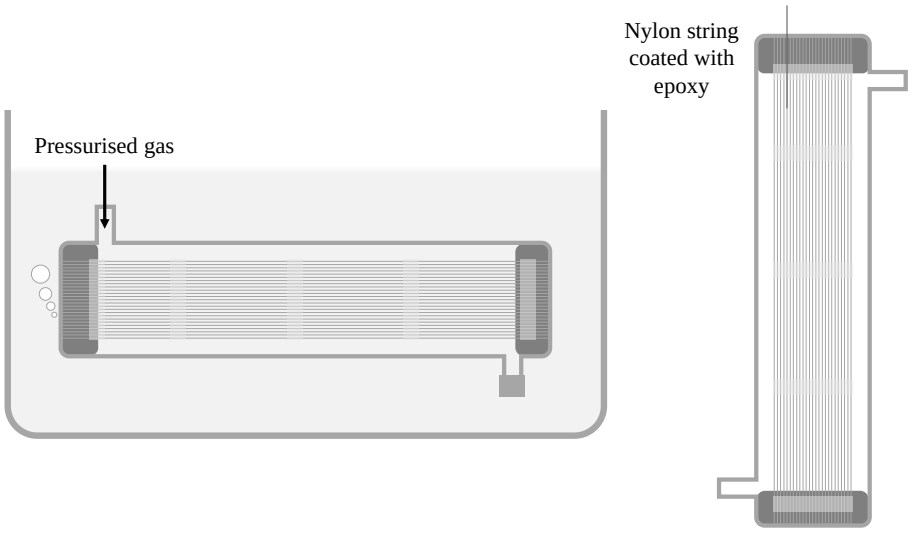

Figure 5-3: Schematic drawing of defect identification and repair

5.2.3 Membrane characterisation and performance evaluation

The hollow fibre substrates and selective layers were characterised using similar methods described in previous chapters. Solvent permeabilities and solute rejections of the selective layers were also examined accordingly to form a basis of comparison with the lab-scale module. Essentially, the morphologies of the selective layers were analysed using a Zeiss EVO 50 Scanning Electron Microscope (SEM). The presence of the polyamide selective layers after the IP reaction were verified with X-ray photoelectron spectroscopy (XPS) using a Kratos AXIS Ultra. A crossflow setup was used to carry out membrane performance tests to reduce concentration polarisation and excessive head-loss across membrane modules. The permeabilities of water, acetone, acetonitrile and IPA for the TFC membrane were evaluated using similar methods described in Chapter 3, section 3.2.5. The selectivity of the TFC membranes were evaluated at 2 bar, using dye dissolved in organic solvents. 50 ppm of rose bengal, acid fuchsin, methyl orange and methyl red were used as solutes for the organic solvent systems to provide solutes of a wide range of molecular weights. The concentrations of the dyes were measured using the same method mentioned in Chapter 3, section 3.2.5. An extended filtration experiment was also conducted to investigate the stability of the scaled-up module.

5.2.4 Simultaneous pharmaceutical concentration and solvent recovery

To evaluate the suitability of the scaled-up module for OSN application, P500 was used to concentrate levofloxacin and simultaneously recover acetone in a single-pass batch process. The rationale for choosing the solute-solvent system for this study has been mentioned in Chapter 4, section 4.2.5. Figure 5-4 illustrates the experimental setup. The permeability of acetone, concentrations of levofloxacin in the feed and permeate were collected and measured

periodically to evaluate the performance of the membrane. The performances obtained from this experiment were then compared with the membrane made in (P5 module) Chapter 4.

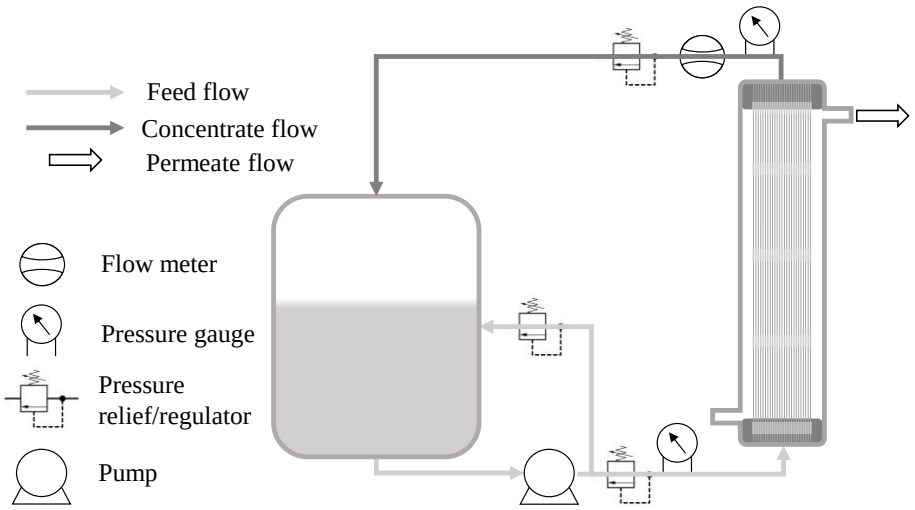

Figure 5-4: Schematic drawing of pharmaceutical concentration and solvent recovery system

5.3 Results and discussion

5.3.1 Characterisation of polyamide thin-film composite membrane

Hollow fibre substrate fabricated from Chapter 4 were potted into modules of various sizes and polyamide selective layers were synthesized on the lumen side of the membranes. The SEM images of the selective layers were shown in Figure 5-5. It can be observed that the thicknesses of the polyamide layer were different for each module. P5 had a polyamide layer thickness of about 100 nm while P500 and P1500 had thicknesses of between 300 – 500 nm. In addition, the selective layers formed in P500 and P1500 were of ridge-and-valleys structure [124, 192]. This observation is similar to that examined in Chapter 4, where the 100-piece module had a thicker selective layer with such characteristic. The difference in thicknesses between the lab-scale module and scaled-up modules might be caused by different parameters used during the IP reactions. A higher crossflow velocity was used for the scaled-up modules to enhance

purging of aqueous phase and maintaining concentration of TMC during the reaction phase. In addition, a longer time was preferred for the reaction phase to ensure complete polymerisation along the entire fibre. As such, these changes in parameters potentially resulted in forming a selective layer that is thicker with voluminous voids.

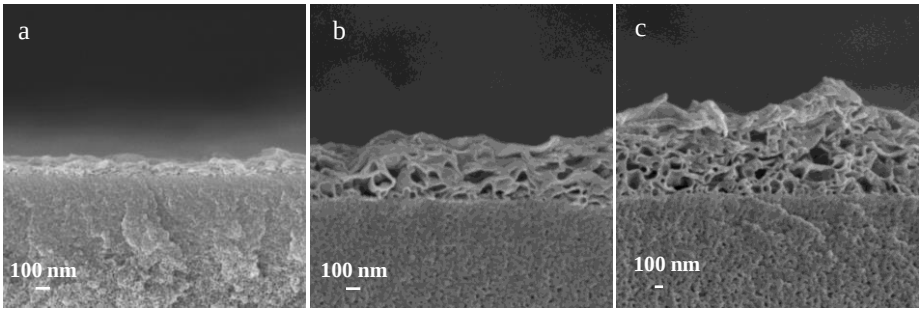

Figure 5-5: SEM images of the polyamide selective layer from modules with various scales. (a) P5; (b) P500; (c) P1500

XPS was used to analyse the changes in inner surface elemental composition of P500 and P1500 after IP reaction and illustrated in Figure 5-6. As observed in Figure 5-6 (a, b and c), the elemental N peaks for P500 and P1500 are similar to that of P5. In addition, the elemental O peaks as shown in Figure 5-6 (d, e and f) are also comparable. Since it has been established in the previous chapter that the selective layer on P5 is an MPD-based polyamide layer, this indicates that the layers formed on P500 and P1500 after the IP reaction are indeed the same.

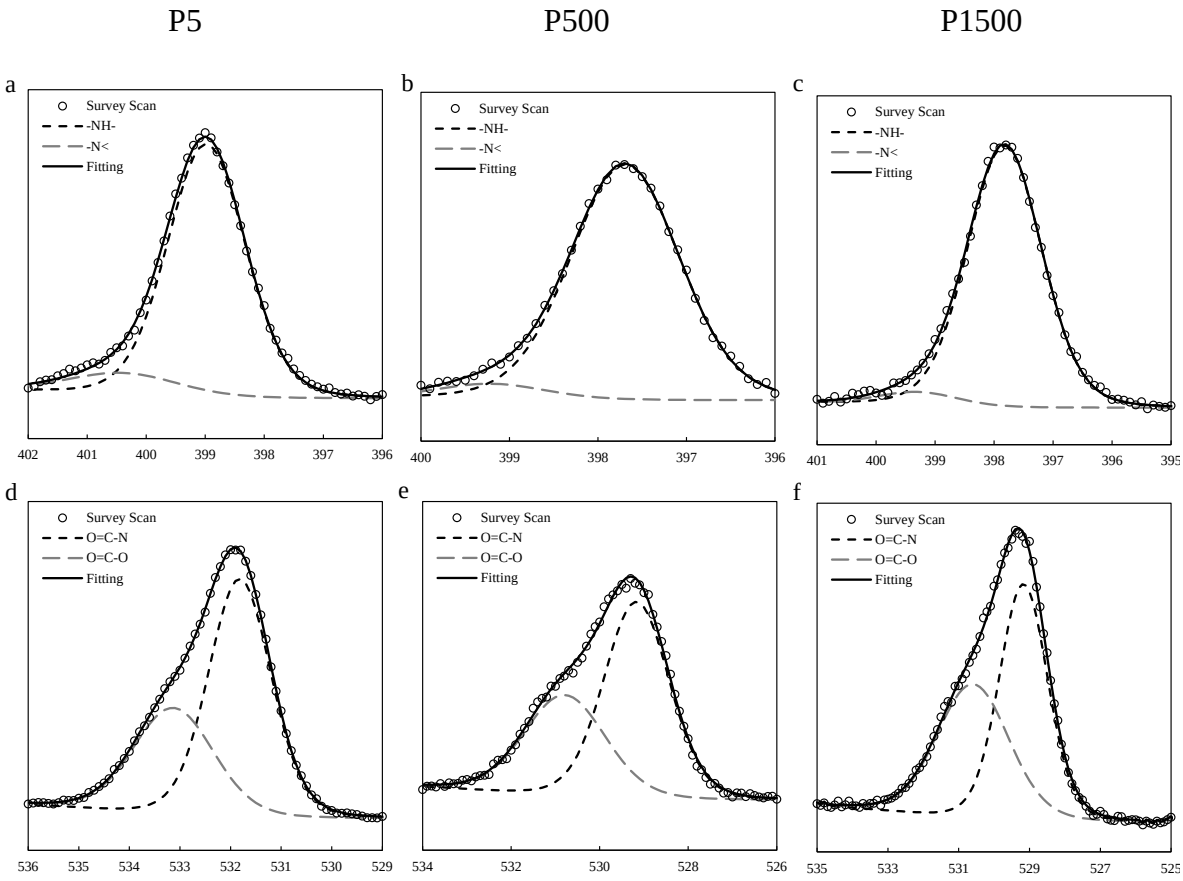

Figure 5-6: XPS spectra of (a) P5 N1s; (b) P500 N1s; (c) P1500 N1s; (d) P5 O1s; (e) P500 O1s; (f) P1500 O1s

5.3.2 Effect of upscaling on membrane performances

Hollow fibre modules with 5, 500 and 1500 fibres were successfully fabricated and the cross-sections of the scaled-up modules are shown in Figure 5-7. Subsequently, a selective layer was synthesized onto the lumen of the fibres. To ensure that the selective layers were properly synthesized, the crossflow velocities of the solvents used during the IP reaction process were adjusted accordingly. A higher crossflow velocity was used for P500 and P1500 modules due to longer module length and increase in fibres. Cyclohexane was introduced into the lumen for a longer time to ensure that the aqueous phase was completely purged from the surface of the membrane.

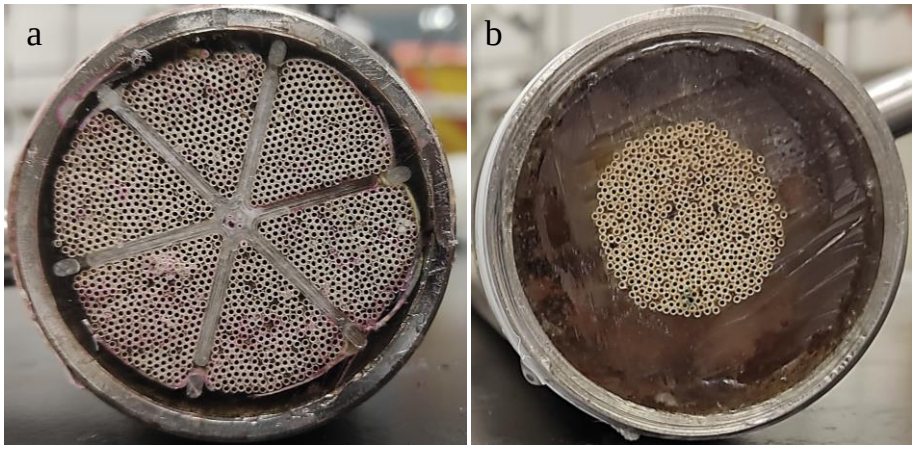

Figure 5-7: Cross-section of scaled-up hollow fibre module. (a) P1500; (b) P500

The effective surface areas and nominal packing densities of the modules were calculated and compared with commercial membranes of similar dimensions in Table 5-2. When the module was scaled from P5 to P1500, the effective surface area of the module increased by 575 times from 0.00235 m^2 to 1.41 m^2. This is more than twice the effective surface area of the two commercial modules (PuraMem 280 and TW30) of similar sizes. As such, P1500 achieved a packing density of 1510 m^2/m^3 while the commercial membranes have a packing density of 300 – 600 m^2/m^3. This aptly illustrates the advantage of hollow fibre membranes as the higher packing density allows for higher output for a given module size. In addition, the free-standing nature of hollow fibre membranes also eliminate the need for spacers and supports that are compatible with organic solvents.

Table 5-2: Module properties

Module	**Effective surface area (m^2)**	**Packing density (m^2/m^3)**
P5	0.00235	n.a
P500	0.470	503

P1500	1.41	1510
PuraMem 280 (2520) [108]	0.6	372
TW30 (2514) [193]	0.65	577

From Figure 5-7 (a), it can be observed that the fibres were packed relatively close to one another with minimal gap between fibres. In addition, the spacers were able to separate the bundles evenly, introducing more pathways that the epoxy can flow around the fibres. Theoretically, a total of 2300 such fibres could be potted into each 2-in modules for maximum packing density of up to 2300 m^2/m^3. However, this introduces much more engineering challenges when scaling up. For example, the creeping of epoxy resin onto the fibres through capillary action could be exacerbated due to tighter packing, reducing the effective length of fibres in the module [160, 194]. In addition, an even longer pathway is required for the epoxy resin to completely seal the ends of the module, increasing the likelihood of a leakage. A tighter packing will also increase the likelihood of fibres being damaged during the potting process, thereby introducing unnecessary complications for scaling up. Another issue with higher packing density is an increase in flow restriction at the shell-side for FO process. More severe headloss will increasing pumping losses and also exacerbate concentration polarisation, thus reducing its performance. Overall, this demonstrates the scalability of the hollow fibre membranes fabricated in Chapter 4.

As much higher flow rates were required for the scaled-up modules, a larger crossflow filtration system was used. The modules were tested for their performances similar to that described in Chapter 4 and the results are shown in Figure 5-8 and Figure 5-9. As observed in Figure 5-8, P5 achieved the highest solvent permeabilities for all modules. On the other hand, solvent permeabilities of P500 and P1500 were similar and 20 – 40% lower than P5. This trend of solvent permeabilities decreasing when membranes were scaled-up was also observed in

Chapter 4, Section 4.3.3, where a 100-piece module was fabricated. This might be caused by slightly different parameters used in the IP reactions on the scaled-up modules. Nonetheless, the similar performances of P500 and P1500 demonstrates that the increase in fibres for the same module dimension does not affect its performance. From Figure 5-9, it is observed that the selectivity of all modules remained in a similar range, regardless of the number of fibres and module dimensions. In addition, the membranes were able to achieve more than 91% rejection for methyl red, indicating a MWCOs of less than that of 269 Da. For separation and recovery of high-value solutes like APIs and other KOMs, a membrane with such high selectivity is thus desirable. The performance of P1500 was also compared with commercial OSN membranes as shown in Table 5-3. Permeabilities of tested solvents were much higher for P1500 compared to the commercial membranes. Given the much higher packing density of the hollow fibre module, these factors allow a much smaller module to produce the same output in a given system, lowering the footprint of the OSN system. The selectivity of P1500 membrane was also comparable to most of the commercial membranes, thereby eliminating the traditional trade-offs associated with permeability and selectivity in membrane fabrication.

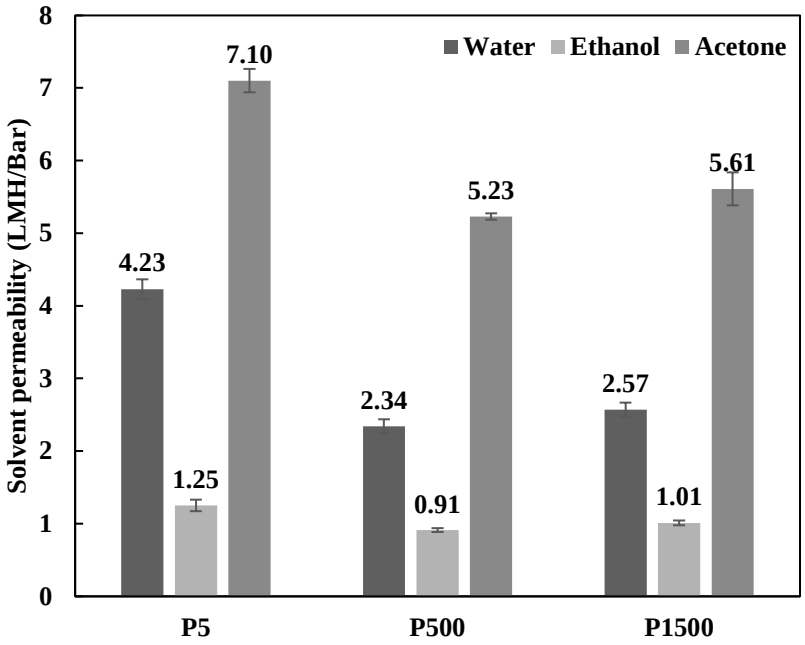

Figure 5-8: Solvent permeabilities of thin film composite membranes

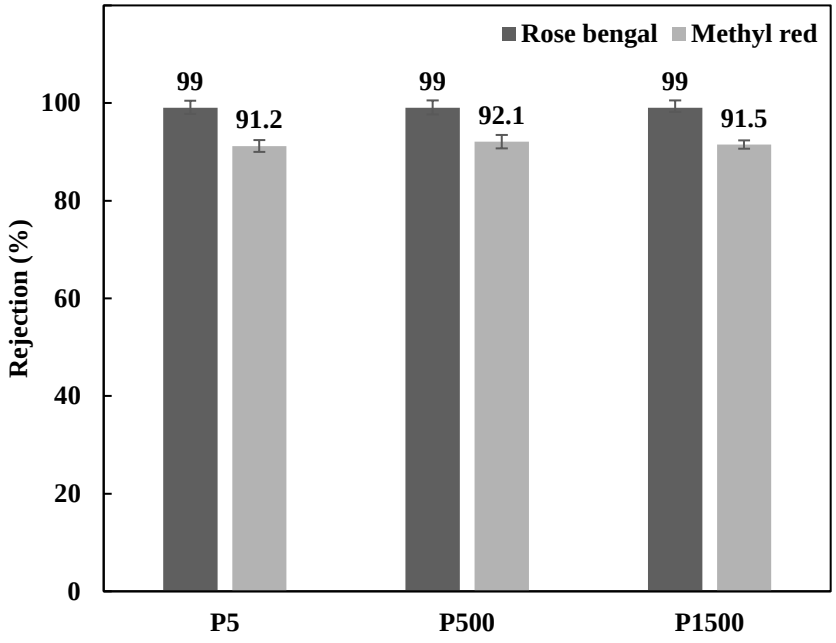

Figure 5-9: Rejection of dyes in ethanol

Table 5-3: Performances of various commercial OSN membranes

Membrane	**Material**	**Membrane type**	**Solvent permeability (LMH/Bar)**	**Rejection (MW; %)**	**Ref**
Duramem 300	Cross-linked Polyimide	Integrally skinned	Acetone; 0.15 ± 0.03 Ethanol; 0.27 ± 0.02	200 Da; 90 -	[195]
Puramem 280	Uncross-linked Polyimide	Integrally skinned	Toluene; 0.6 Ethanol; 0.65 ± 0.03	280 Da; 90 -	[195, 196]
GMT-oNF2	Silicone composite	Thin-film composite	Toluene; 2 Acetone; 1.01 Ethanol; 0.15	507 Da; 98 - -	[196]
SolSep BV 010206	Polyimide	Integrally skinned	Acetone; 1	300 Da; 95	[196]
P1500	Polyimide	Thin-film composite	Acetone; 5.61 Ethanol; 1.01	- 269 Da; 91.5	This work

5.3.3 Extended filtration test for P500

To evaluate the stability of the scaled-up TFC module P500, a 10-day filtration experiment was done using 50 ppm methyl red dissolved in ethanol. The permeabilities and rejections were measured periodically throughout the length of experiment and illustrated in Figure 5-10. The module was able to maintain the ethanol permeability at about 0.9 LMH/Bar throughout the 10 days. Slight fluctuation in solvent permeabilities might be caused by the evaporation of the solvent collected during measurements. Otherwise, the membrane displayed excellent stability in the solvent. In addition, methyl red rejection was kept relatively constant at 91% throughout the experiment. This indicates that the membrane can be utilized for prolonged OSN applications. As such, a subsequent experiment was done to evaluate its OSN performance.

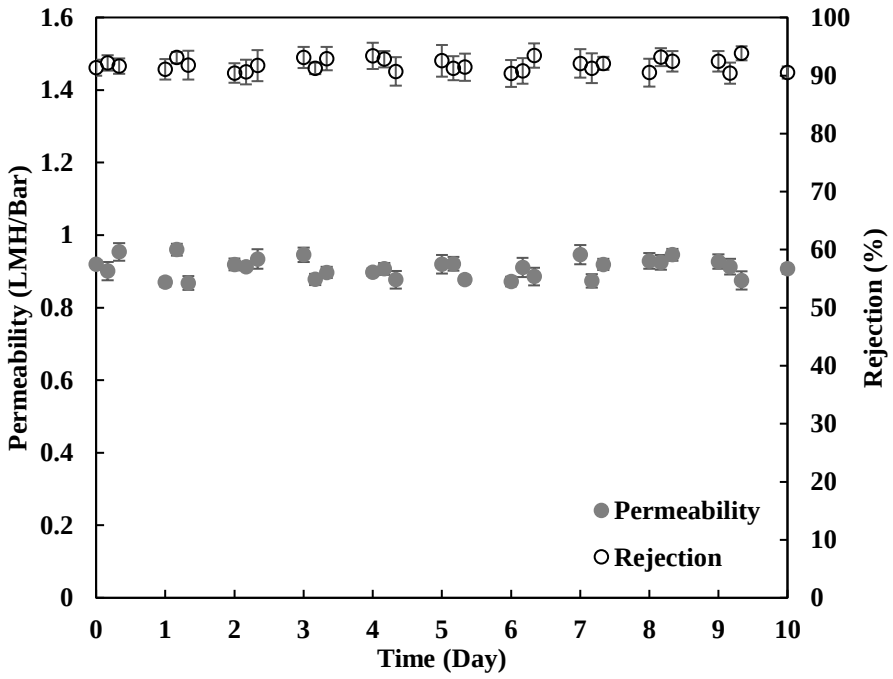

Figure 5-10: Stability test of P500 module for OSN performance. 50 ppm methyl red dissolved in ethanol

5.3.4 Performance in OSN application

To evaluate the OSN performance of the scaled-up module, P500 was used to recover acetone and concentrate levofloxacin simultaneously in a crossflow set-up. The reason for using P500 instead of P1500 for the experiment was due to the large amount of solvents required for the experiment. Otherwise, the performances of P500 and P1500 should be similar as examined in Chapter 5, section 5.3.2. The performance was then compared with P5 and illustrated in Figure 5-11. Since the time taken for the experiments to complete were different, the time axis was normalised to provide a clearer comparison between the 2 modules. Initially, the acetone permeabilities of P5 and P500 were about 5 and 6.8 LMH/Bar, respectively. As these were batch experiments, the concentration of levofloxacin nearly doubles every time the volumes of feed were halved. This explains the rapidly increasing concentrations of levofloxacin at the end of the experiments. As the feeds were concentrated, the acetone permeabilities gradually decreased and at the last 15% of time, the permeabilities dropped drastically. A similar observation can be made for the selectivities of the modules as the experiment progressed. Initial levofloxacin rejections remained about 99% but underwent a sudden decline near the end to 96%. This might be caused by concentration polarisation on the membrane surface due to the increasing concentrations of levofloxacin in the feed. Overall, both experiments were able to concentrate levofloxacin from 500 ppm to about 9000 ppm and more than 90% of acetone was recovered. From this study, it demonstrated that the polyimide based TFC hollow fibre membrane can be scaled up without much impact on performance. The permeability was slightly reduced as a trade-off to obtain a defect-free selective layer, which is evident from the high selectivity of the scaled-up module.

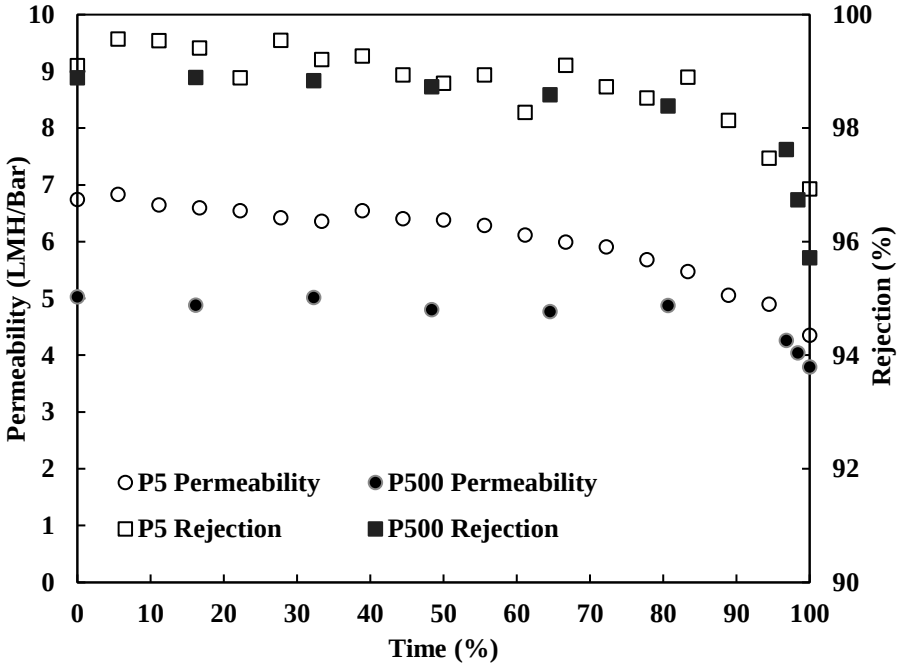

Figure 5-11: Simultaneous pharmaceutical concentration and solvent recovery for P5 and P500 modules

5.4 Conclusions

This study has demonstrated that the thin-film composite hollow fibre membrane can be scaled to commercial sizes for OSN application. The scaled-up modules exhibited superior packing densities compared to commercial spiral wound modules of similar sizes. This evidently shows the benefit of hollow fibre membranes compared to spiral wound modules. A tight selective layer was applied onto the lumen of the membranes and tested for performance. The scaled-up modules suffered slight reduction in permeability compared to lab-scale modules (acetone, 7.1 to 5.6 LMH/Bar) but was able to maintain its exceptional selectivity (269 Da, >91%). Comparing its performance to commercially available OSN membranes, it exhibited excellent solvent permeabilities with comparable selectivity. A 10-day filtration experiment also demonstrated the stability of the scaled-up module. A pharmaceutical concentration and solvent recovery experiment also showed potential for the scaled-up module to be used in OSN applications.

Chapter 6 Organic solvent forward osmosis membrane

6.1 Introduction

In Chapter 4, OSN membrane was used to simultaneously concentrate pharmaceutical products and recover organic solvent. However, higher pressure was required by the OSN membrane to achieve higher solute concentration, potentially adding more operating and maintenance costs. In addition, the fouling propensity of OSN membranes inhibited its performance drastically as demonstrated in Chapter 4 and Chapter 5. Thus, a more viable alternative is required to further concentrate solutes in an organic solvent. Organic solvent forward osmosis (OSFO) has received much attention in recent years as a membrane separation process for pharmaceutical and food industry. Essentially, OSFO utilises the difference in osmotic pressure between the draw and feed solution to generate solvent flux across a semi-permeable membrane. Depending on the purpose of the OSFO application, the solute in the feed can be concentrated to high levels of purity. With a suitable draw solution, the solvent can then be recovered from the draw solution using an appropriate regenerative process [53, 197, 198].

In this chapter, an OSFO thin-film composite hollow fibre membrane was fabricated. The dope composition and spinning parameters of the substrate were altered to improve the physical properties of the substrate for FO processes. Subsequently, an m-phenylenediamine (MPD)-based polyamide selective layer was synthesized onto the substrate through interfacial polymerisation (IP) to achieve high selectivity. The performance of the TFC FO membrane was evaluated by standard FO tests. The OSFO performance was also investigated using a non-toxic draw solution. Lastly, an active pharmaceutical ingredient (API) dissolved in an organic solvent was concentrated to demonstrate the application of OSFO in the pharmaceutical industry.

6.2 Materials and methods

6.2.1 Materials and chemicals

Polyimide (P84 Lenzing) was used to fabricate the substrate. 1-Methyl-2-pyrrolidinone (NMP, >99%) purchased from Merck and diethylene glycol (DG, >99.5%) purchased from Sigma Aldrich were used in the phase inversion process. Isopropanol (IPA, >99.5%), polyethylene glycol 400 (PEG 400) and hexamethylene diamine (HDA, >98%) purchased from Sigma Aldrich were used for post-treatment and storage of membranes. For the IP reaction, m-phenylenediamine (MPD, >99%, Sigma Aldrich), cyclohexane (>99%, VWR) and benzene tricarbonyl trichloride (TMC, >98%, Sigma Aldrich) were used.

To evaluate the selectivity of the TFC membranes, rose bengal (1017 Da in MW, >95%, Sigma Aldrich), methyl red (269 Da in MW, Sigma Aldrich), magnesium chloride hexahydrate (>99%, Merck), sodium chloride (>99%, Merck) and levofloxacin (361 Da in MW, >98%, Sigma Aldrich) were used. Deionized (DI) water, acetone (>95%, Sigma Aldrich), ethanol (>99.5%, Sigma Aldrich) and isopropanol (>99.5%, Sigma Aldrich) were used as solvents.

6.2.2 Fabrication of thin-film composite hollow fibre membrane

The hollow fibre substrates were fabricated via dry-jet wet spinning process. The dope was prepared in a similar manner described in the previous work [122], but the dope composition and spinning parameters were changed as illustrated in Table 6-1, to improve its performance for use as OSFO substrate. The substrate was then cross-linked by immersing it into a solution of 20 g/l of HDA in IPA for 18 hours to achieve solvent resistance. The cross-linked membranes were then stored in 40/60 wt% PEG 400/IPA solution to preserve the pores. The fibres were subsequently potted into modules with dimensions as shown in Table 6-2.

Table 6-1: Spinning parameters of hollow fibre substrate

	This work	**Previous work [122]**
Dope composition P84/DG/NMP (wt%)	16/8/76	20/8/72
Dope flow rate (ml/min)	3	3.5
Bore fluid	DI water	DI water
Bore fluid flow rate (ml/min)	3	3.5
External coagulant	Tap water	Tap water
Air gap (cm)	<1	5
Drum speed (cm/s)	6	3.75

Table 6-2: Dimensions of module for hollow fibre FO membranes

Module	**Number of Fibres**	**Module length (cm)**	**Module diameter (inch)**	**Membrane Area (cm^2)**
P5	5	26	~ 3/8	22
P500	500	50	~ 2	4145

A polyamide selective layer was synthesized on the lumen side of the fibres through interfacial polymerisation. The membranes were first soaked in an aqueous solution containing MPD and then purged with cyclohexane to remove excess aqueous solution. Subsequently, a cyclohexane solution containing TMC was pumped through the lumens to initiate the IP reaction, forming a thin polyamide layer on the substrate. Afterwards, the reaction was quenched and the modules were stored in DI water before use.

6.2.3 Membrane characterisation and performance evaluation

The chemical and physical properties of the hollow fibre substrate and the selective layer were examined using a series of standardised characterisation tests. The cross-section and surface morphologies of the polyimide substrate and TFC membrane were examined using Zeiss EVO 50 Scanning Electron Microscope (SEM). The prepared hollow fibre samples were coated with platinum using EMITECH SC7620 sputter coater for the SEM preparation.

To evaluate the cross-linking of the polyimide substrate, Fourier Transform Infrared Spectroscopy (FTIR) was carried out using Prestige-21 spectrophotometer from Shimadzu. Polyimide bands at 1780 cm^{-1} and 1711 cm^{-1} (C=O), 1361 cm^{-1} (C-N), and amide bands at 1634 cm^{-1} (C=O) and 1525 cm^{-1} (C-N) of the pristine and cross-linked substrate were compared to evaluate the changes in the polymer structure. The porosity (ε) of the hollow fibre substrate can be determined by gravimetric method [199]. The inner surface of the TFC membrane was examined by X-ray photoelectron spectroscopy (XPS) using a Kratos AXIS Ultra to confirm the presence of polyamide layer after IP.

A crossflow setup was used to test the membrane in RO mode. The permeability of water, ethanol and acetone for the polyimide substrate and TFC membranes was evaluated by pressurizing the solvents from the lumen side at 2 bar. Measurements were taken after the system has stabilised and the performance were calculated using equation (6.1), where J_i (LMH/Bar) is the solvent permeability, m_i is the mass of solvent collected, ΔP (bar) is the transmembrane pressure, A (m^2) is the effect area of the membrane, ρ_i (g cm^{-3}) is the density of solvent, and t (h) is the time taken for permeate collection.

$$J_i = \frac{m_i}{\Delta P \times A \times \rho_i \times t} \qquad (6.1)$$

The molecular weight cut-off (MWCO) of the substrate was evaluated using standardised test with a dextran aqueous solution [200]. The selectivity of the TFC membrane was determined using aqueous salt solutions consisting of 2000 ppm NaCl and $MgCl_2$. 50 ppm of rose bengal and methyl red dissolved in ethanol, separately, were used to investigate its OSN performance. The concentrations of salts and dyes were determined using a conductivity meter (Myron L Company, Canada) and UV-1650 PC UV–Vis spectrophotometer (Shimadzu, Japan), respectively [29, 125]. The rejection (R) of dextran, salts and dyes were determined using equation (6.2), where C_f and C_p are the concentrations of the solutes in the feed and permeate, respectively.

$$R = \frac{C_f - C_p}{C_f} \times 100 \qquad (6.2)$$

A bench-scale FO setup was utilized to study the FO performance of the TFC membranes in the active layer facing feed solution (AL-FS) orientation, as shown Figure 6-1. Solutions with 0.5 – 1.5 M $MgCl_2$ were used as draw solutions while DI water was used as the feed.

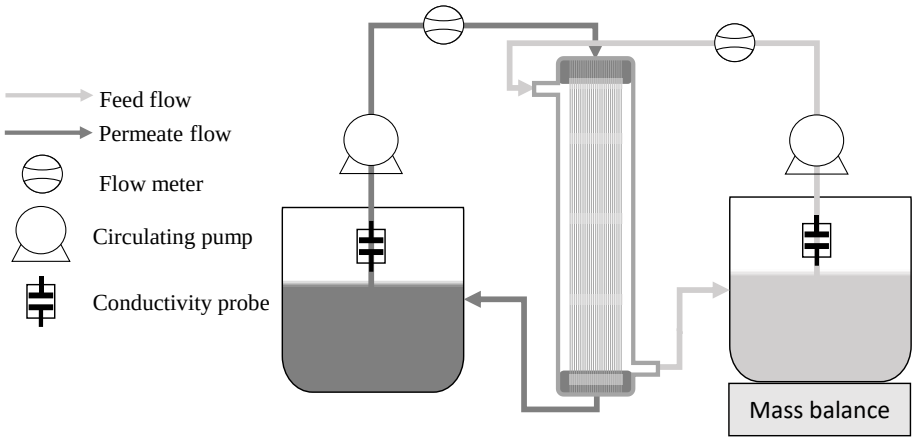

Figure 6-1: Schematic diagram of forward osmosis experimental setup

To determine the FO performance, the water flux J_w, (l m^{-2} h^{-1}, LMH) was determined using equation (6.3), where Δw (g) is the change in feed mass over a time interval Δt (h), A_m (m^2) is the effective membrane area and ρ_w (g/l) is the density of water.

$$J_w = \frac{\Delta w}{A_m \rho_w \Delta t} \qquad (6.3)$$

The reverse solute flux (RSF), J_s, (g m^{-2} h^{-1}, gMH) was examined according to equation (6.4), where C_0 (g/l) and V_0 (l) are salt concentration and feed volume at time 0, C_t and V_t indicate the final salt concentration and feed volume over a time interval (Δt), respectively.

$$J_s = \frac{C_t V_t - C_0 V_0}{A_m \Delta_t} \qquad (6.4)$$

Subsequently, the specific RSF (J_s/J_w), (g/l), was plotted against draw solution concentration. The performance of P5 and P500 modules were then compared to evaluate the scalability of the TFC membrane.

The structural parameter (S) of the TFC membrane was then measured using equation (6.5), where D_s is the diffusion coefficient for $MgCl_2$, approximated to 1.06 x 10^{-9} m^2 s^{-1} [201], Π_D is the osmotic pressure of the bulk draw solution, Π_F is the osmotic pressure of the feed solution at the membrane surface. A and B are the pure water and salt permeability coefficients, respectively.

$$S = \frac{D_s}{J_w} ln \left[\frac{A\pi_D + B}{A\pi_F + J_w + B}\right] \qquad (6.5)$$

6.2.4 Organic solvent forward osmosis application

The scaled-up (P500) module was tested for OSFO performance in the AL-FS orientation. The setup illustrated in Figure 6-1 was used for the OSFO experiments by replacing the fittings and tubes with solvent resistant ones. IPA and acetone were used as solvents and the respective solvent fluxes were measured using 0.5 – 2 M PEG 400 as draw solutions. PEG 400 concentrations in the feed and draw solutions were measured using total organic carbon (TOC) analyser (Shimadzu, Japan). A known volume of solution containing PEG 400 was first oven dried at 60ºC to completely remove the solvent and then diluted with water for TOC analysis. The solvent fluxes, RSF and specific RSF were measured similarly as described in section 6.2.3. A concentric cylinder (CC-27) rheometer from Anton Paar was used to examine the viscosities of the draw solutions. A shear rate (τ) of 2000 s^{-1} was used to obtain the values.

To demonstrate the OSFO capability of the P500 module, a solution of levofloxacin in acetone was concentrated. 2 M PEG 400 in acetone was used as the draw solution while 1000 ppm levofloxacin dissolved in acetone was used as the feed solution. The feed and draw solutions were circulated in the AL-FS orientation and the draw solution was constantly dosed to maintain its concentration. The concentration of levofloxacin in the feed was determined using UV-1650 PC UV–Vis spectrophotometer (Shimadzu, Japan) at a wavelength of 292 nm [202]. The solution was appropriately diluted before measuring to obtain an accurate reading.

6.3 Results and discussion

6.3.1 Characterisation of polyimide substrate

P84 polyimide hollow fibre substrate was spun in-house and cross-linked with HDA to achieve organic solvent resistance. The MWCO of the cross-linked substrate was then determined to be about 90 kDa using a dextran standard solution. Subsequently, the physical properties of the membrane after cross-linking were measured and shown in Table 6-3. Compared to the substrate fabricated in the previous work, the inner diameter, outer diameter and thickness of the membrane were significantly reduced. This was achieved by reducing the polymer concentration in the dope and increasing the uptake speed of the drum [115]. The lower polymer concentration reduces the viscosity of the dope solution, thereby having a less pronounced die swelling at the exit of the spinneret. The higher drum uptake speed also increased the elongation of the fibre, further reducing the fibre dimension. In addition, the decrease in bore and dope flow rates also contributed to a thinner fibre obtained for this study [109, 117].

Table 6-3: Physical properties of polyimide substrate before and after cross-linking

	This work	**Previous work [122]**
Inner diameter (μm)	573.7 ± 8.7	640.5 ± 5.2
Outer diameter (μm)	823.6 ± 10.8	920.4 ± 12.3
Thickness (μm)	125.0 ± 4.1	139.9 ± 7.7
Porosity (%)	79	68

The morphology of the cross-linked substrate was also examined using SEM imaging as shown in Figure 6-2. It can be observed that a thin skin layer (Figure 6-2 (c & e)) was formed on the outer and inner surfaces of the membrane through rapid phase inversion via using hard bore fluid and external coagulant [50, 109]. The thin skin layer allows for a defect-free polyamide selective layer to be synthesized onto the surface while reducing the overall intrinsic membrane resistance for higher solvent permeability [137, 178]. It can also be seen that the finger-like structures developed extensively towards the centre of the membrane, separated by a sponge-like polymer matrix as shown in Figure 6-2 (b). This was achieved by using a hard bore fluid and lower air gap (see Table 6-1) [50, 109]. The extensive finger-like structures resulted in an increase in porosity from 68% to 79%. Consequently, the thinner and more porous membrane would improve the structural parameter of the membrane and reduce the effects of ICP [50, 129]. Overall, the fabricated hollow fibre substrate showed desirable characteristics of a FO membrane.

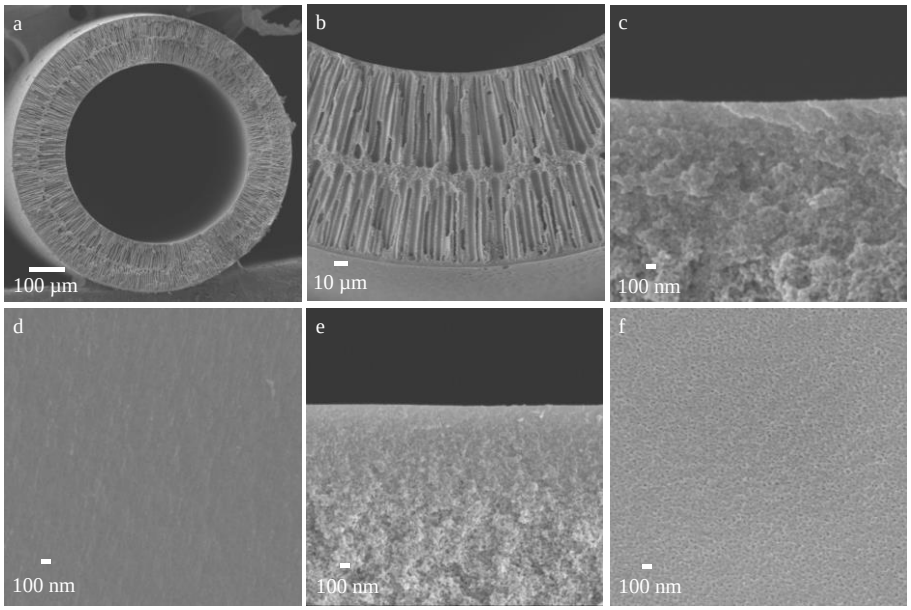

Figure 6-2: SEM images of cross-linked hollow fibre substrate. (a) Cross-section; (b) enlarged cross-section; (c) cross-section of inner surface; (d) inner surface; (e) cross-section of outer surface; (f) outer surface

Figure 6-3 illustrates the solvent permeability of the membrane fabricated in this study and the previous work [122]. It was found that the solvent permeability of the membrane fabricated in this work is much higher than that obtained from the previous work. The permeability for water, ethanol and acetone improved by about 61%, 79% and 91%, respectively. The improvements were mainly attributed to the reduction in membrane thickness and the increase in the porosity of the hollow fibre substrate. Overall, the substrate fabricated in this work showed significant improvement in its physical properties that are potentially beneficial in FO process.

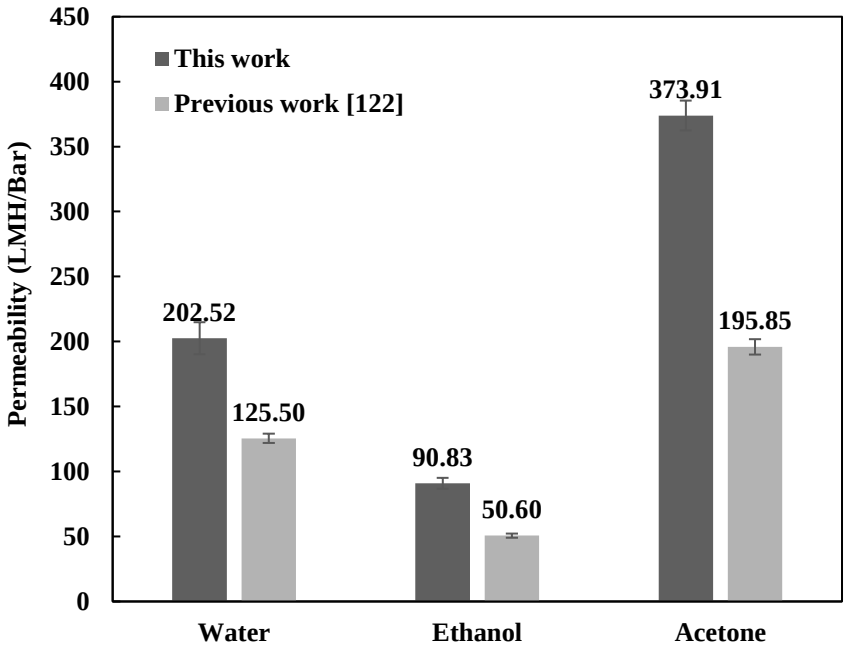

Figure 6-3: Solvent permeability of hollow fibre substrates in various solvents

The chemical composition of the substrate before and after cross-linking were also analysed by FTIR as presented in Figure 6-4. The characteristic peaks of imide groups at 1361 cm^{-1} (C=O), 1711 cm^{-1} (C=O) and 1780 cm^{-1} (C-N) diminished significantly after cross-linking. On the other hand, the amide peaks, 1634 cm^{-1} (C=O) and 1525 cm^{-1} (C-N), became more intense through the formation of amide bonds. These observations are consistent with previous works and thus, the solvent resistance of the fabricated substrate should perform similarly [29, 122]. The hollow fibre substrate was potted into two types of modules, P5 and P500, and used for subsequent experiments.

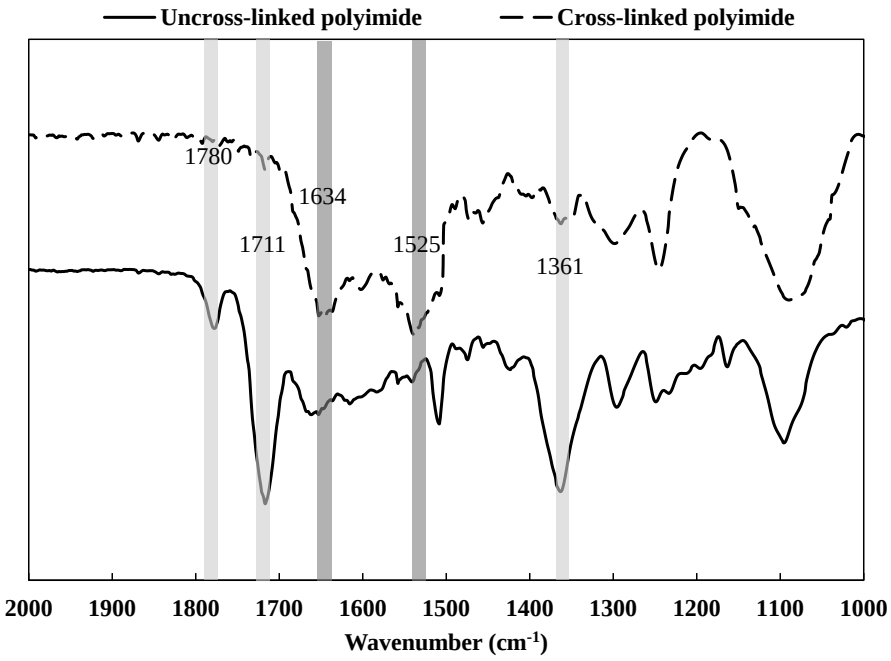

Figure 6-4: FTIR spectrum of uncross-linked and cross-linked polyimide substrates.

6.3.2 Characterisation of selective layer

A polyamide selective layer was synthesized on the lumens of the hollow fibre substrates in P5 and P500 modules via interfacial polymerisation. The SEM images in Figure 6-5 show the morphology of the inner surface and cross-section of the membrane after IP. As observed in Figure 6-5 (a), the inner surface of the membrane was covered by a ridge-and-valley like texture, the characteristic of a typical MPD-based polyamide layer. Looking at Figure 6-5 (c), the cross-section shows a selective layer thickness of about 150 nm. A thinner selective layer could potentially improve solvent permeability. However, as the OSFO membrane was used to concentrate high value pharmaceutical products, a TFC membrane with higher selectivity was favoured.

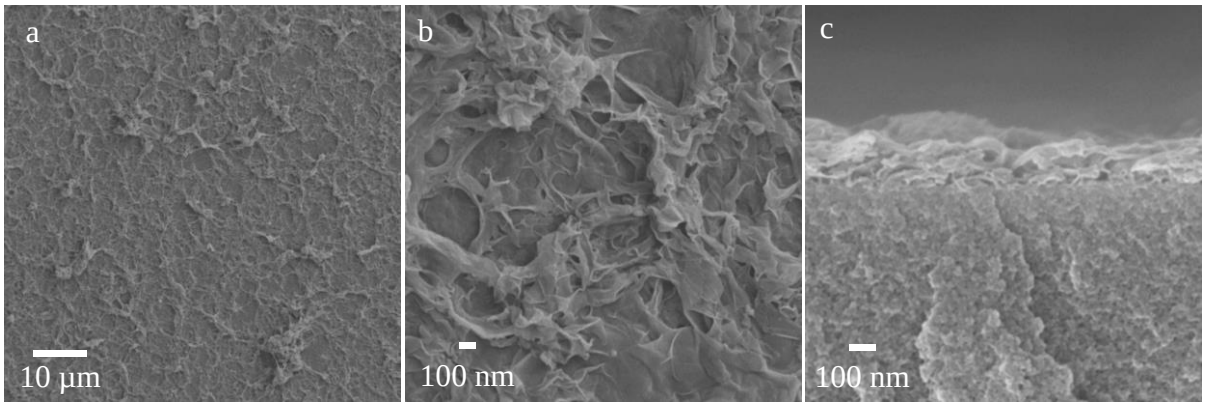

Figure 6-5: SEM images of thin-film composite hollow fibre membranes, (a) inner surface; (b) enlarged inner surface; (c) cross-section

The changes in surface chemistry of the membrane after IP were analysed using XPS. The N1s and O1s peaks of the polyimide substrate and TFC were deconvoluted respectively and illustrated in Figure 6-6. As observed from Figure 6-6 (a and b), the amide bonds increased after the selective layer was synthesized onto the substrate. From Figure 6-6 (c and d), it can also be seen that the deconvoluted O1s peaks for the membrane changed. The C=O peak of the substrate was no long present and a new O=C-O peak was detected. These observations were also made in previous works and thus suggests that the polyamide selective layer was successfully synthesized onto the substrates [29, 122].

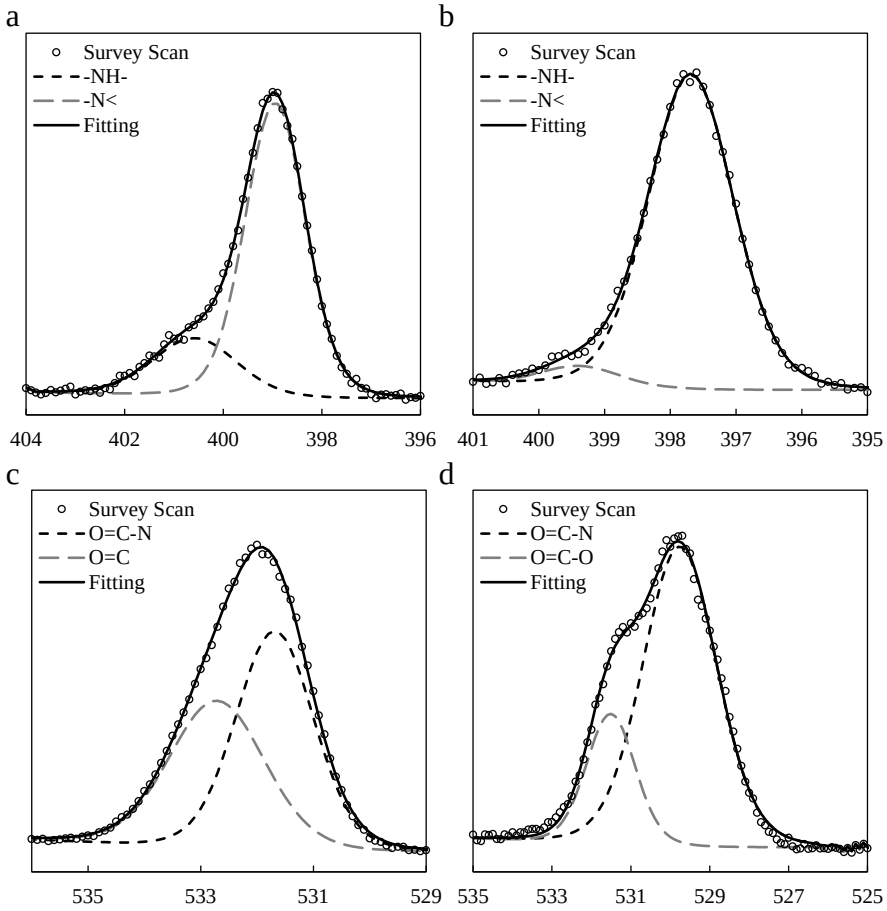

Figure 6-6: XPS spectra of (a) substrate N1s, (b) TFC N1s, (c) substrate O1s and (d) TFC O1s

The OSN performance of P5 and P500 TFC modules were evaluated using a cross-flow setup and the results are illustrated in Figure 6-7 and Figure 6-8, respectively. Ethanol permeability of P5 module was measured at 1.65 LMH/Bar while the corresponding permeability for P500 module was lower at 1.04 LMH/Bar. This trend is similar to that reported in the previous work, where the scaled-up membrane suffered from lower solvent permeability due to possible non-uniform IP layer coating [122]. The increase in module length (from 30 cm to 50 cm) and enlarged module cross-sectional area (from 3/8 inch to 2 inch) might have caused uneven distribution of liquids during the IP process and formed less ideal selective layer. On the other hand, the selectivity of P500 module was very similar to P5 module, which indicates that the selective layer was synthesized onto the membrane without any defects. As observed from Figure 6-8, P500 module showed slightly higher salt rejections of $MgCl_2$ and NaCl at 99.1% and 95.4%, respectively. The membranes also achieved excellent methyl red rejection of over 92%. This suggests that the selective layer can serve well as a RO-like barrier for small solutes in FO operation.

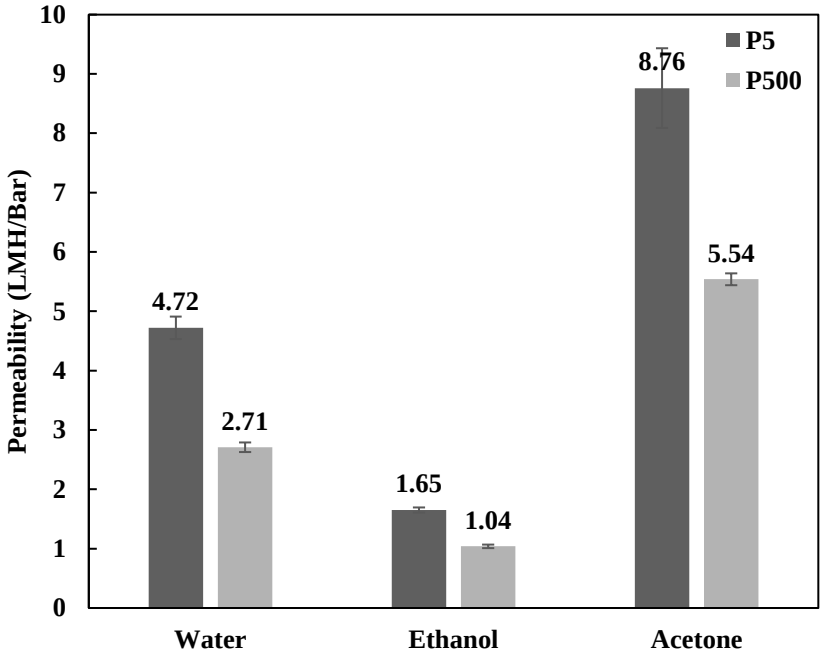

Figure 6-7: Solvent permeabilities for P5 and P500 thin-film composite modules

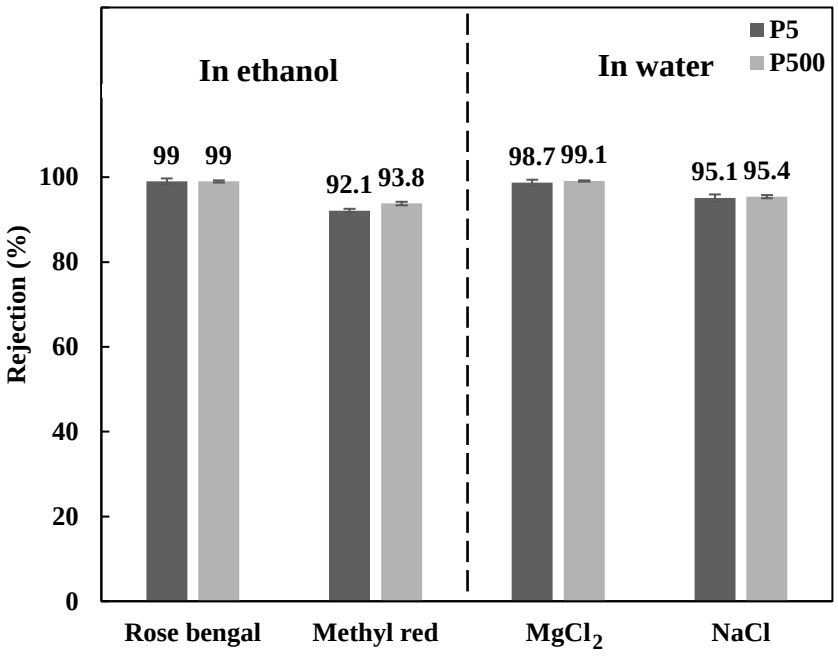

Figure 6-8: Solute rejections of P5 and P500 modules in ethanol and water

6.3.3 FO performance of lab-scale and scaled-up modules

The modules were tested for their FO performances in the AL-FS orientation using the setup illustrated in Figure 6-1. Varied concentrations of $MgCl_2$ were used as the draw solution while DI water was used as the feed solution. The water flux (J_w), RSF (J_s) and calculated specific RSF (J_s/J_w) were obtained and reported in Figure 6-9. As seen from Figure 6-9 (a), the water flux of P5 module increased from 25.6 LMH to 42.9 LMH when the concentration of $MgCl_2$ in the draw solution increased from 0.5 M to 1.5 M. On the other hand, P500 module achieved water flux of 23.0 LMH and 33.2 LMH when 0.5 M and 1.0 M of $MgCl_2$ was used (Figure 6-9 (A)). The comparatively lower J_w of P500 module can be attributed to its relatively lower intrinsic water permeability than P5 module, which is expected from the solvent permeability test in Figure 6-7. It can also be observed from Figure 6-9 (a) that there is a diminishing increase in flux when the concentration of draw solution further increased. This suggests that dilutive ICP is much more noticeable at a higher concentration of draw solution [130, 203]. As seen from Figure 6-9 (b and B), the estimated specific RSF of P5 module was higher than P500 module. This suggests that the polyamide layer synthesized on P500 module was more selective than that on P5 module. This observation can also be verified by the higher solute rejections as illustrated in Figure 6-8. Nevertheless, both P5 and P500 modules exhibited excellent selectivity with very low specific RSF values. It is interesting to see that the specific RSFs of P5 and P500 modules at 0.5 M, 1.0 M and 1.5 M $MgCl_2$ draw solutions were relatively constant. This phenomenon is consistent with several FO studies, where the specific RSF was found to be independent of the concentration of draw solution [130, 204]. Overall, the performance of the membrane in FO mode demonstrated consistent trends with that reported in RO mode.

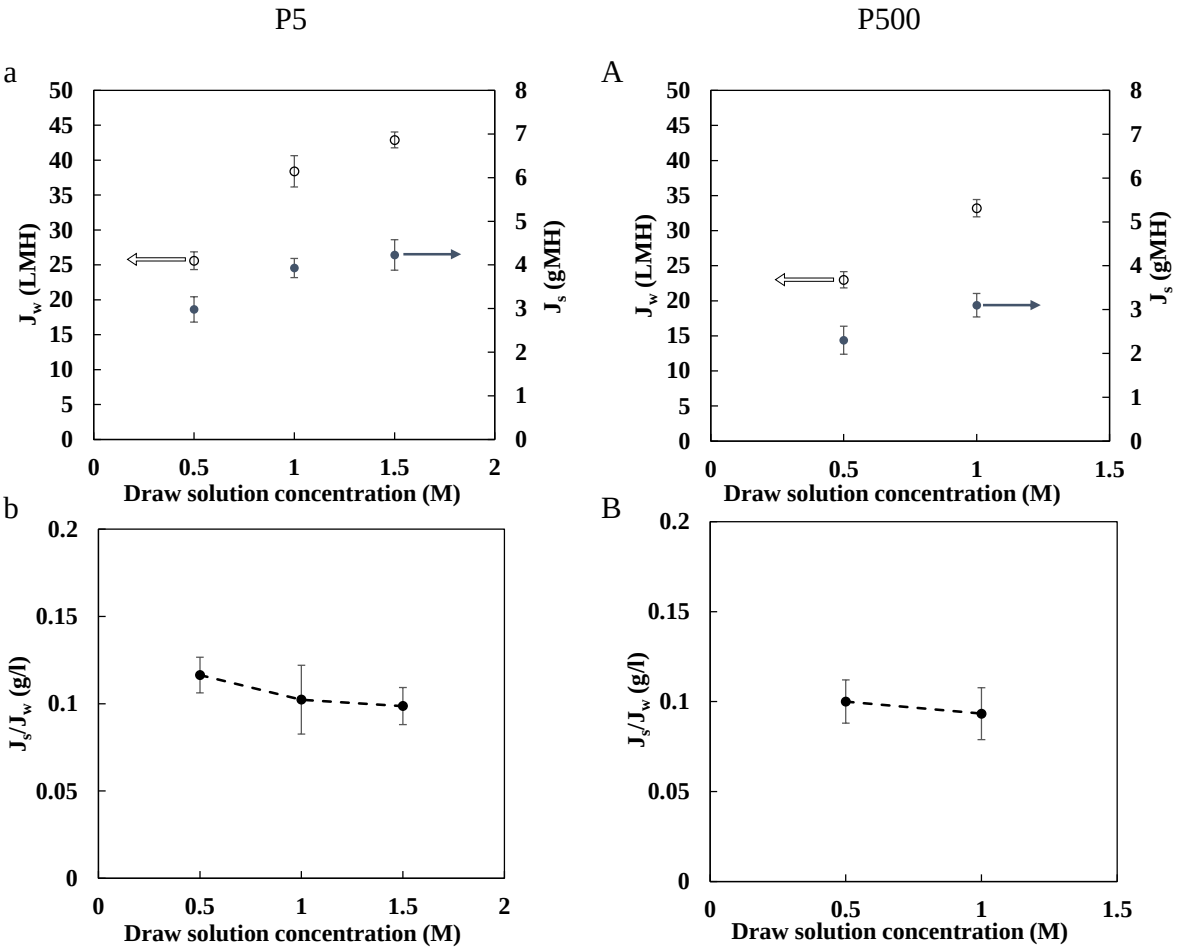

Figure 6-9: FO performance of P5 and P500 modules in AL-FS orientation. (a) and (A) Water flux (*Jw*) and RSF (*Js*); (b) and (B) Specific RSF (*Js/Jw*)

6.3.4 OSFO performance tests for P500 module

The organic solvent forward osmosis performance of P500 module was evaluated with a number of solvents and draw solutions. 0.5 – 2M of PEG 400 were used as draw solutes to investigate acetone and IPA fluxes of the module in the AL-FS orientation. Figure 6-10 illustrates the solvent fluxes and RSF when varied concentrations of draw solution were used. As observed from Figure 6-10 (a), the acetone flux increased steadily from 5.1 LMH to 13.9 LMH when the concentration of PEG 400 draw solution increased from 0.5 M to 2 M. The RSF of PEG 400 also increased as a function of draw solution concentration. This phenomenon is in line with that observed in recent studies on OSFO [54, 55]. In addition, this observation is also similar to that obtained in the FO study, which suggests that the solute transport mechanism for OSFO is similar to FO process [59]. From Figure 6-10 (A), the IPA flux and RSF also increased with increasing concentration of draw solution. However, IPA fluxes (0.22 LMH to 0.63 LMH) were much lower than acetone even though the same concentrations of draw solutions were used. This is consistent with OSN experiments, where ethanol and IPA were reported to have much lower permeability than acetone [29, 122]. One possible explanation is that IPA has significantly higher viscosity (8.15 mPa.s) compared to acetone (2.24 mPa.s) as shown in Table 6-4. The hydrophilic membrane also has a higher affinity to the more polar acetone [205]. In addition, the difference in Hansen solubility parameter (R_a) of acetone to the substrate (5.04 $MPa^{0.5}$) is smaller than IPA to the substrate (11.57 $MPa^{0.5}$), which also contributed to a comparatively higher mass transport of acetone [206].

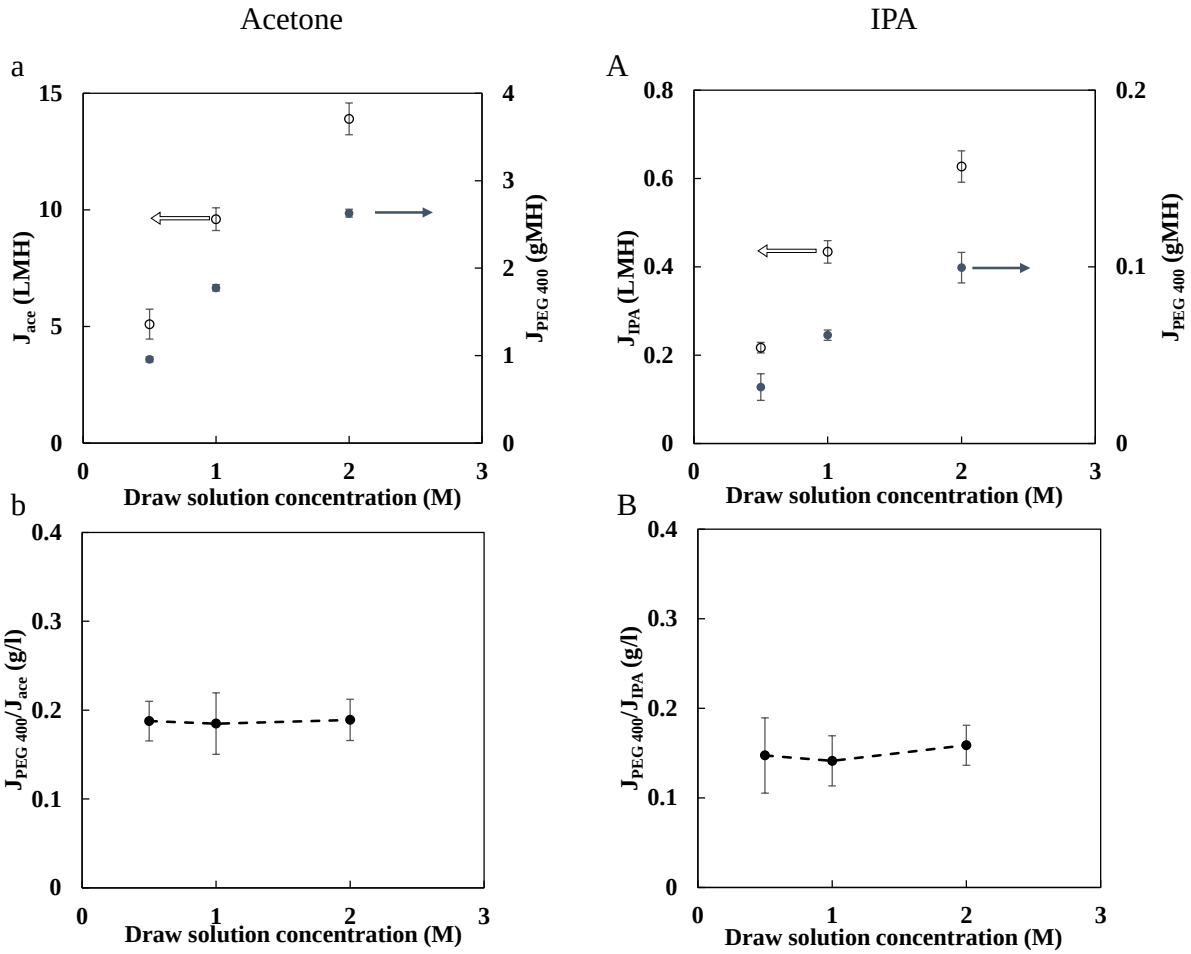

Figure 6-10: Effect of draw solution concentration on organic solvent forward osmosis performance. (a) Acetone flux (J_{ace}) and RSF ($J_{PEG\ 400}$); (A) IPA flux (J_{IPA}) and RSF ($J_{PEG\ 400}$); (b) and (B) Specific solute flux of PEG 400

Table 6-4: Viscosity of different solutions

Solvent	Draw solute	Viscosity (mPa.s)
Acetone	Pure solvent	2.24
	0.5 M PEG 400	4.79
	1 M PEG 400	7.70
	2 M PEG 400	20.0
IPA	Pure solvent	8.15
	0.5 M PEG 400	13.1
	1 M PEG 400	17.8
	2 M PEG 400	26.3

The solvent flux and RSF also increased at a diminishing rate as the concentrations of draw solutions increased. This is even more apparent when IPA was used as the solvent. As the membrane was tested in the AL-FS orientation, this suggests that there were significant ICP occurring when higher concentrations of draw solutions were used [203]. This might be caused by substantially higher viscosities of the draw solutions when higher concentrations of PEG 400 were used, as shown in Table 6-4. The increase in viscosity can potentially inhibit the diffusion of the bulk draw solution into the substrate due to a thicker boundary layer, which resulted in a more severe ICP phenomenon [131, 207]. As shown in Figure 6-10 (b and B), the specific RSF of PEG 400 in acetone (~0.1877 g/l) is higher than IPA (~0.1527 g/l). Since specific RSF is an intrinsic parameter of the selective layer, this indicates that the selectivity of the membrane changed in different organic solvents. One possible explanation is that acetone caused the substrate and selective layer to swell slightly, which reduced its selectivity [208]. Similar observations were made in a previous OSN study, where solute rejections of Starmem^{TM} 122 and Puramem^{TM} 280 were dependent on the extent of membrane swelling and solute solubility parameter in the particular solvent [209]. Studies have also shown that the

diffusivity of solutes are influenced by solvent properties [210, 211]. Consequently, the type of solvent used in a draw solution will affect the reverse solute diffusion [59, 204]. This finding suggests a new challenge for OSFO research such that the performance obtained for different solute-solvent systems might not be comparable, adding to the complexity of reviewing literature for analysis.

The P500 module was subsequently used to concentrate levofloxacin using 2 M PEG 400 as draw solution. Acetone was used as solvent for both the feed and draw solutions. The solvent flux and RSF were plotted against feed concentration as illustrated in Figure 6-11. The initial levofloxacin feed of 1000 ppm was gradually concentrated to approximately 16,000 ppm, a concentration factor of about 16. As observed from Figure 6-11 (a), the initial acetone flux is slightly lower than that when pure acetone was used as feed. It also decreased at an increasing rate when the feed got more concentrated. This might be caused by the increase in severity of concentrative external concentration polarisation (ECP), where levofloxacin built up on the membrane surface at the feed side [203, 204]. This phenomenon can be diminished by increasing the cross-flow velocity of the feed stream, thereby reducing the effect of ECP on OSFO performance. Studies have also shown that an FO membrane with high permeate flux can intensify the phenomenon of ECP [72, 203]. Thus, a draw solution with lower osmotic pressure can be used to minimize this effect. Similarly, the RSF decreased as the concentration of feed gradually increased. This is expected as RSF is proportional to solvent flux [59, 204]. From Figure 6-11 (b), the specific RSF stayed relatively constant when the feed was gradually concentrated. This implies that this parameter is independent of external factors such as feed concentration and draw solution concentrations. Instead, it was shown to be dependent on the intrinsic selectivity of the membrane for a particular solute-solvent system [59, 204].

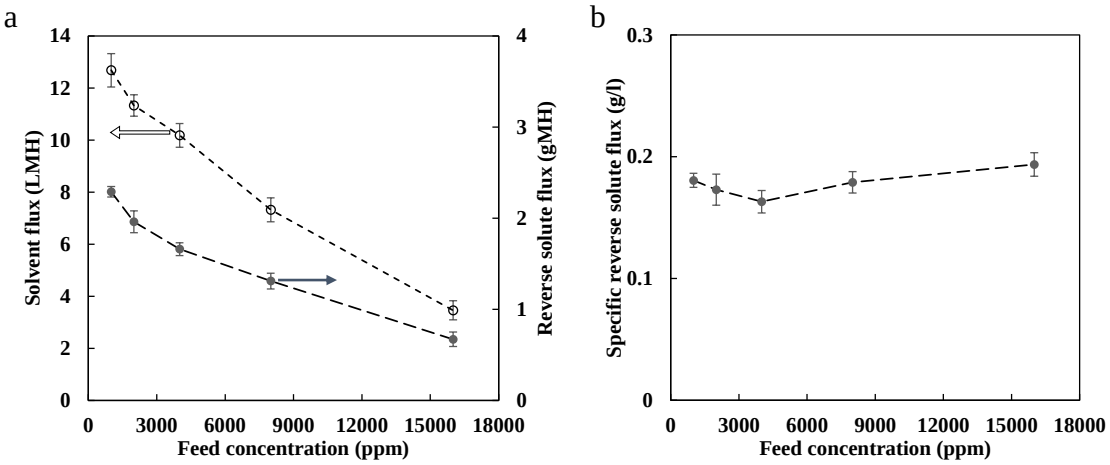

Figure 6-11: Concentration of levofloxacin in AL-FS orientation. Effects of feed concentration on (a) solvent and RSF; (b) specific RSF

The levofloxacin concentration process was listed together with existing membrane-based concentration experiments in solute-solvent systems reported in literature (Table 6-5). As publications on OSFO applications are very limited, the concentration applications by OSN were also included for illustration. The concentration factors reported had a wide variation from 2 to 40 times. Notably, the OSN process developed by R Wang et al was able to achieve concentration factor of as high as 40 times [122]. From the table, the closest reference that could be made is an OSFO study by Chung et al [54]. In the study, tetracycline (444 Da in molecular weight) dissolved in ethanol was concentrated from 1000 ppm to 10,000 ppm using 2 M LiCl as draw solution. On the other hand, the OSFO study conducted in current work concentrated levofloxacin (361 Da in molecular weight) in acetone to a concentration of 16,000 ppm, showing promising performance of this process. However, it is clear that OSFO is still at a very early stage of study. The real feeds in pharmaceutical industry are much more sophisticated than single solute-solvent systems, which pose great challenges to OSFO for practical application. Thus, future work should focus on testing OSFO membranes with a feed that closely resembles the pharmaceutical feed streams. Likewise, the challenge of draw

solution regeneration should also be addressed in order for OSFO systems to be competitive to existing purification processes.

Table 6-5: Concentrating feed in solvent streams using membrane-based separation processes

Process	Feed system	Driving force	Feed concentration	Final concentration	Concentration factor	Ref Year
3-stage OSN	Rosmarinic acid in ethanol	20 – 40 bar	0.118 g/l	0.346 g/l	~ 3	[212] 2011
2-stage OSN	Roxithromycin in methanol	30 bar	~ 120 ppm	~ 210 ppm	~ 2	[213] 2014
OSFO	Tetracycline in ethanol	2 M LiCl in ethanol	1000 ppm	10,000 ppm	~ 10	[54] 2018
OSN	Levofloxacin in acetone	<10 bar	500 ppm	20,000 ppm	~ 40	[122] 2021
OSFO	Levofloxacin in acetone	2 M PEG 400 in acetone	1000 ppm	16,000 ppm	~ 16	This work

6.4 Conclusions

In this work, a scaled-up thin-film composite hollow fibre membrane module with a membrane surface area of 4,145 cm^2 was developed for organic solvent forward osmosis process. The spinning parameters and dope composition used for membrane substrate fabrication were optimised to decrease the mass transport resistance of the substrate with high porosity and low structural parameter. Subsequently, a polyamide selective layer was synthesized on the lumen of the substrate. The resultant P500 module showed promising OSFO results with high IPA and acetone fluxes of 0.63 LMH and 13.9 LMH, respectively, using 2 M PEG 400 as draw solute. The membrane also achieved low specific RSF using PEG 400 as draw solute for both solvent systems, which indicated that the selectivity was maintained in both organic solvent environments. In the pharmaceutical concentration experiment, levofloxacin in acetone was concentrated with 2 M PEG 400 as draw solution using P500 module. A concentration factor of 16 can be achieved while maintaining high selectivity. This study demonstrated promising potential of OSFO to be used in the pharmaceutical industry for API concentration. Further studies should focus on using feeds with compositions similar to real pharmaceutical feeds to evaluate the feasibility of using OSFO process in the pharmaceutical industry. In addition, identifying suitable draw solutes for the myriad of solute-solvent combinations present in the pharmaceutical industry is also an important task.

Chapter 7 Conclusions and recommendations

7.1 Overall conclusion

The thesis focused on the development of thin-film composite hollow fibre membranes for organic solvent membrane separation processes. By modifying the dope composition and spinning parameters, different hollow fibre substrates were fabricated with various properties specific for targeted applications. The hollow fibre substrates achieved solvent resistance through chemical cross-linking, which was demonstrated to be facile and scalable. The interfacial polymerisation process was also modified accordingly to tune the selectivity of the polyamide TFC membranes. In addition, the scalability of the hollow fibre membrane was also studied. The major findings of the thesis are summarised as follows:

In Chapter 3, a TFC hollow fibre membrane was fabricated for low pressure organic solvent nanofiltration. LiCl and DG were investigated as dope additives in the spinning process and DG was found to enhance the physical properties of the substrate, thereby improving solvent permeabilities. HDA was used as a cross-linker for the post treatment process, resulting in a substrate that was resistant to several organic solvents. However, the cross-linked substrate is still susceptible to excessive swelling in harsher organic solvents such as DMF. Through the use of a mixture of PEI and PIP, a mix-polyamide layer was synthesized on the lumen of the substrate. The resultant selective layer exhibited excellent selectivity for solutes in the nanofiltration range while demonstrating exceptional solvent permeabilities.

In Chapter 4, the hollow fibre substrate was further improved to enhance its scalability. In addition, a highly selective layer was synthesized on the substrate using MPD as the monomer in IP reaction. The resulting selective layer was able to achieve about 91% rejection for methyl

red (273 Da). Subsequently, the permeability was significantly enhanced through solvent activation while selectivity was maintained. A 100-piece module was also fabricated to demonstrate the scalability of the membrane. The membrane modules were also subjected to a 7-day test and demonstrated stable performance. Finally, the 100-piece module was used to concentrate a pharmaceutical product while the solvent was recovered simultaneously.

In Chapter 5, the TFC hollow fibre membrane was further scaled-up to match that of a commercial membrane, with an effective membrane area of about 1.4 m^2. In comparison, a commercial spiral-wound module of similar size has an effective membrane area of about 0.6 – 0.7 m^2. This demonstrated the key advantage of hollow fibre membrane compared to flat sheets. The scaled-up modules were tested for OSN performance and showed little impact on performance when further scaled-up. A 10-day filtration test on the module indicated high stability for the OSN membrane. The module also underwent the same pharmaceutical concentration test described in Chapter 4 and showed promising results for OSN application.

In Chapter 6, a TFC hollow fibre membrane was fabricated specifically for OSFO application. The substrate was further fine-tuned to improve its porosity, thickness and ultimately, structural parameters to enhance its solvent flux in FO mode. An RO-like, MPD-based, polyamide selective layer was synthesized onto the lumen of the membrane to achieve high solute rejection. The membrane was also scaled-up like previous study (Chapter 5) and tested for FO and OSFO performance. The membrane exhibited excellent solvent permeabilities with low specific RSF for salts and PEG 400. In addition, the membrane was able to concentration levofloxacin from 1000 ppm to 16,000 ppm using 2M PEG 400 in acetone as draw solution, demonstrating its OSFO capabilities.

7.2 Recommendations for future research

7.2.1 OSN performance tests

From this study, it has been shown that cross-linked polyimide substrates are chemically stable in various organic solvents like acetone, isopropanol and acetonitrile. However, there are many other commonly used organic solvents in the pharmaceutical industry such as dimethylformamide, dimethyl sulfoxide and tetrahydrofuran. Therefore, the performance and chemical stability of the polyimide substrate and thin film composite should also be rigorously tested in these organic solvents. As the selectivity of membranes can be affected by the type of organic solvent used, performance tests should be done in organic solvents from various categories (ketones, alcohols, aromatic, aliphatic, aprotic etc.). This enable researchers to have a more comprehensive understanding of performance based on various organic solvents, while appropriate comparisons can be made with membranes reported in the literature.

In the pharmaceutical industry, the feed streams are much more complex than those used in current research. Pharmaceutical feed and waste streams may contain high concentration of salt, mixture of solvents, as well as presence of numerous solutes of similar molecular weight. These can severely affect the selectivity and permeability of membranes due to their complex interaction with the material. Thus, future work should use synthetic feeds that closely resemble real industrial feeds to obtain better representation of membrane performance.

7.2.2 Concentration polarisation

Another challenge that researchers face in membrane separation processes is the effect of concentration polarisation. Currently, it is still not widely addressed in OSN and OSFO due to its complexity, especially for organic solvent separation processes where a wide range of solute-solvent systems are present. For the case of OSN, the increasing concentration of APIs intensify the effects of ECP, thereby reducing solvent permeability and lowering membrane selectivity. This observation was made in this work and needs to be addressed urgently. The issue can be mitigated by optimising the cross-flow setup, as well as improving the surface morphology of the selective layer. For OSFO, the use of high draw solution concentration increases ICP in the substrate. Consequently, the effective osmotic pressure is significantly reduced. Improvements should be made to the design of the substrate to further improve its structural parameter to alleviate ICP. In addition, the module design can also be optimised to improve the flow distribution of draw solution at the shell-side.

7.2.3 Draw solution for OSFO

As OSFO is still at its infancy, there are many issues that are not yet addressed by the scientific community. One such challenge is the choice of draw solution in an OSFO system. A desirable draw solution should exhibit high osmotic pressure in the selected organic solvent and easily regenerated with minimum energy input. In addition, the diffusion of draw solute through the membrane should be low to minimize contamination of the feed stream. In the case of OSFO application in the pharmaceutical industry, the diffusion of draw solute into the feed stream may render the concentrated feed unsuitable for further use, due to the low tolerance of contamination required for pharmaceuticals. This issue is also prevalent in the food industry due to its stringent standards. Thus, draw solutes that are non-toxic or compatible and with

extremely low permeability should be evaluated. Studies should focus on understanding the mechanism that affects the osmotic pressure of draw solution in organic solvents. As the osmotic pressure of different solutes may be different in various organic solvents, the method for determining osmotic pressure of a draw solution should be standardised.

Another challenge for OSFO is the regeneration of draw solution after it has been diluted. As many commonly used organic solvents such as hexane, acetone and IPA have relatively low boiling points, a potential energy source to regenerate the draw solution is the waste heat from nearby plant processes. Vacuum-assisted distillation can be utilised to regenerate the draw solution at temperatures below its boiling point, while simultaneously recovering the organic solvent for reuse. This can potentially reduce the input of useful energy required for the OSFO process. However, the regeneration process may be too slow and required larger operating footprint due to the low heat value provided by waste heat sources. In addition, high solute concentrations typically found in draw solutes drastically increases the energy required to heat the solution. Thus, research should also focus on evaluating options to regenerate draw solution for OSFO.

References

[1] E.M. Renkin, Filtration, diffusion, and molecular sieving through porous cellulose membranes, The Journal of general physiology, 38 (1954) 225-243.
[2] J.G. Wijmans, R.W. Baker, The solution-diffusion model: a review, Journal of Membrane Science, 107 (1995) 1-21.
[3] A.W. Mohammad, Y.H. Teow, W.L. Ang, Y.T. Chung, D.L. Oatley-Radcliffe, N. Hilal, Nanofiltration membranes review: Recent advances and future prospects, Desalination, 356 (2015) 226-254.
[4] S. Loeb, S. Sourirajan, Sea Water Demineralization by Means of an Osmotic Membrane, in: Saline Water Conversion—II, AMERICAN CHEMICAL SOCIETY, 1963, pp. 117-132.
[5] W. Banks, A. Sharples, Studies on desalination by reverse osmosis. III. Mechanism of solute rejection, Journal of Applied Chemistry, 16 (1966) 153-158.
[6] R.W. Baker, Future directions of membrane gas separation technology, Industrial & engineering chemistry research, 41 (2002) 1393-1411.
[7] A. Alkhudhiri, N. Darwish, N. Hilal, Membrane distillation: A comprehensive review, Desalination, 287 (2012) 2-18.
[8] K.P. Lee, T.C. Arnot, D. Mattia, A review of reverse osmosis membrane materials for desalination—development to date and future potential, Journal of Membrane Science, 370 (2011) 1-22.
[9] F. Meng, S.-R. Chae, A. Drews, M. Kraume, H.-S. Shin, F. Yang, Recent advances in membrane bioreactors (MBRs): membrane fouling and membrane material, Water research, 43 (2009) 1489-1512.
[10] P. Le-Clech, V. Chen, T.A. Fane, Fouling in membrane bioreactors used in wastewater treatment, Journal of membrane science, 284 (2006) 17-53.
[11] L.F. Greenlee, D.F. Lawler, B.D. Freeman, B. Marrot, P. Moulin, Reverse osmosis desalination: water sources, technology, and today's challenges, Water research, 43 (2009) 2317-2348.
[12] W. Suwaileh, N. Pathak, H. Shon, N. Hilal, Forward osmosis membranes and processes: A comprehensive review of research trends and future outlook, Desalination, 485 (2020) 114455.
[13] N. Akther, A. Sodiq, A. Giwa, S. Daer, H.A. Arafat, S.W. Hasan, Recent advancements in forward osmosis desalination: A review, Chemical Engineering Journal, 281 (2015) 502-522.
[14] K. Lutchmiah, A.R.D. Verliefde, K. Roest, L.C. Rietveld, E.R. Cornelissen, Forward osmosis for application in wastewater treatment: A review, Water Research, 58 (2014) 179-197.
[15] R.P. Lively, D.S. Sholl, From water to organics in membrane separations, Nature Materials, 16 (2017) 276-279.
[16] P. Marchetti, M.F. Jimenez Solomon, G. Szekely, A.G. Livingston, Molecular separation with organic solvent nanofiltration: A critical review, Chemical Reviews, 114 (2014) 10735-10806.
[17] Y.H. See Toh, F.W. Lim, A.G. Livingston, Polymeric membranes for nanofiltration in polar aprotic solvents, Journal of Membrane Science, 301 (2007) 3-10.
[18] D.S. Sholl, R.P. Lively, Seven chemical separations to change the world, Nature, 532 (2016) 435-437.
[19] P. Vandezande, L.E.M. Gevers, I.F.J. Vankelecom, Solvent resistant nanofiltration: separating on a molecular level, Chemical Society Reviews, 37 (2008) 365-405.

[20] K. Vanherck, G. Koeckelberghs, I.F.J. Vankelecom, Crosslinking polyimides for membrane applications: A review, Progress in Polymer Science, 38 (2013) 874-896.
[21] S.K. Lim, K. Goh, T.-H. Bae, R. Wang, Polymer-based membranes for solvent-resistant nanofiltration: A review, Chinese Journal of Chemical Engineering, 25 (2017) 1653-1675.
[22] K. Grodowska, A. Parczewski, Organic solvents in the pharmaceutical industry, Acta poloniae pharmaceutica, 67 (2010) 3-12.
[23] D. Fritsch, P. Merten, K. Heinrich, M. Lazar, M. Priske, High performance organic solvent nanofiltration membranes: Development and thorough testing of thin film composite membranes made of polymers of intrinsic microporosity (PIMs), Journal of Membrane Science, 401-402 (2012) 222-231.
[24] C. Li, S. Li, L. Lv, B. Su, M.Z. Hu, High solvent-resistant and integrally crosslinked polyimide-based composite membranes for organic solvent nanofiltration, Journal of Membrane Science, 564 (2018) 10-21.
[25] Evonik, DURAMEM® AND PURAMEM® MEMBRANES FOR ORGANIC SOLVENT NANOFILTRATION, in.
[26] H. Mariën, I.F.J. Vankelecom, Transformation of cross-linked polyimide UF membranes into highly permeable SRNF membranes via solvent annealing, Journal of Membrane Science, 541 (2017) 205-213.
[27] M.F. Jimenez Solomon, Y. Bhole, A.G. Livingston, High flux membranes for organic solvent nanofiltration (OSN)—Interfacial polymerization with solvent activation, Journal of Membrane Science, 423-424 (2012) 371-382.
[28] M. Amirilargani, M. Sadrzadeh, E.J.R. Sudhölter, L.C.P.M. de Smet, Surface modification methods of organic solvent nanofiltration membranes, Chemical Engineering Journal, 289 (2016) 562-582.
[29] K.S. Goh, J.Y. Chong, Y. Chen, W. Fang, T.-H. Bae, R. Wang, Thin-film composite hollow fibre membrane for low pressure organic solvent nanofiltration, Journal of Membrane Science, 597 (2020) 117760.
[30] B. Khorshidi, T. Thundat, B.A. Fleck, M. Sadrzadeh, Thin film composite polyamide membranes: parametric study on the influence of synthesis conditions, RSC Advances, 5 (2015) 54985-54997.
[31] B. Khorshidi, T. Thundat, B.A. Fleck, M. Sadrzadeh, A Novel Approach Toward Fabrication of High Performance Thin Film Composite Polyamide Membranes, Scientific Reports, 6 (2016) 22069.
[32] J.H. Kim, S.J. Moon, S.H. Park, M. Cook, A.G. Livingston, Y.M. Lee, A robust thin film composite membrane incorporating thermally rearranged polymer support for organic solvent nanofiltration and pressure retarded osmosis, Journal of Membrane Science, 550 (2018) 322-331.
[33] P. Marchetti, L. Peeva, A. Livingston, The Selectivity Challenge in Organic Solvent Nanofiltration: Membrane and Process Solutions, Annual Review of Chemical and Biomolecular Engineering, 8 (2017) 473-497.
[34] H.A. Le Phuong, C.F. Blanford, G. Szekely, Reporting the unreported: the reliability and comparability of the literature on organic solvent nanofiltration, Green Chemistry, 22 (2020) 3397-3409.
[35] Y.H. See Toh, X.X. Loh, K. Li, A. Bismarck, A.G. Livingston, In search of a standard method for the characterisation of organic solvent nanofiltration membranes, Journal of Membrane Science, 291 (2007) 120-125.
[36] X.J. Yang, A.G. Livingston, L. Freitas dos Santos, Experimental observations of nanofiltration with organic solvents, Journal of Membrane Science, 190 (2001) 45-55.
[37] C.A. Nayak, N.K. Rastogi, Forward osmosis for the concentration of anthocyanin from Garcinia indica Choisy, Separation and Purification Technology, 71 (2010) 144-151.

[38] K.Y. Wang, M.M. Teoh, A. Nugroho, T.-S. Chung, Integrated forward osmosis–membrane distillation (FO–MD) hybrid system for the concentration of protein solutions, Chemical Engineering Science, 66 (2011) 2421-2430.
[39] S. Herbig, J. Cardinal, R. Korsmeyer, K. Smith, Asymmetric-membrane tablet coatings for osmotic drug delivery, Journal of Controlled Release, 35 (1995) 127-136.
[40] G. Santus, R.W. Baker, Osmotic drug delivery: a review of the patent literature, journal of controlled release, 35 (1995) 1-21.
[41] B. Jiao, A. Cassano, E. Drioli, Recent advances on membrane processes for the concentration of fruit juices: a review, Journal of food engineering, 63 (2004) 303-324.
[42] K.J. Park, A. Bin, F.P.R. Brod, T.H.K.B. Park, Osmotic dehydration kinetics of pear D'anjou (Pyrus communis L.), Journal of Food Engineering, 52 (2002) 293-298.
[43] M.B. Uddin, P. Ainsworth, Ş. İbanoğlu, Evaluation of mass exchange during osmotic dehydration of carrots using response surface methodology, Journal of food engineering, 65 (2004) 473-477.
[44] K.B. Petrotos, H.N. Lazarides, Osmotic concentration of liquid foods, Journal of food engineering, 49 (2001) 201-206.
[45] E. Cornelissen, D. Harmsen, E. Beerendonk, J. Qin, H. Oo, K. De Korte, J. Kappelhof, The innovative osmotic membrane bioreactor (OMBR) for reuse of wastewater, Water Science and Technology, 63 (2011) 1557-1565.
[46] A. Achilli, T.Y. Cath, E.A. Marchand, A.E. Childress, The forward osmosis membrane bioreactor: a low fouling alternative to MBR processes, Desalination, 239 (2009) 10-21.
[47] E. Cornelissen, D. Harmsen, K. De Korte, C. Ruiken, J.-J. Qin, H. Oo, L. Wessels, Membrane fouling and process performance of forward osmosis membranes on activated sludge, Journal of membrane science, 319 (2008) 158-168.
[48] T.Y. Cath, A.E. Childress, M. Elimelech, Forward osmosis: Principles, applications, and recent developments, Journal of Membrane Science, 281 (2006) 70-87.
[49] R. Wang, L. Shi, C.Y. Tang, S. Chou, C. Qiu, A.G. Fane, Characterization of novel forward osmosis hollow fiber membranes, Journal of Membrane Science, 355 (2010) 158-167.
[50] L. Shi, S.R. Chou, R. Wang, W.X. Fang, C.Y. Tang, A.G. Fane, Effect of substrate structure on the performance of thin-film composite forward osmosis hollow fiber membranes, Journal of Membrane Science, 382 (2011) 116-123.
[51] M. Qasim, N.A. Darwish, S. Sarp, N. Hilal, Water desalination by forward (direct) osmosis phenomenon: A comprehensive review, Desalination, 374 (2015) 47-69.
[52] R. Valladares Linares, Z. Li, S. Sarp, S.S. Bucs, G. Amy, J.S. Vrouwenvelder, Forward osmosis niches in seawater desalination and wastewater reuse, Water Res, 66 (2014) 122-139.
[53] S. Zhao, L. Zou, D. Mulcahy, Brackish water desalination by a hybrid forward osmosis–nanofiltration system using divalent draw solute, Desalination, 284 (2012) 175-181.
[54] Y. Cui, T.-S. Chung, Pharmaceutical concentration using organic solvent forward osmosis for solvent recovery, Nature Communications, 9 (2018) 1426.
[55] Y. Wei, Y. Wang, L. Wang, H. Yang, H. Jin, P. Lu, Y. Li, Simultaneous phase-inversion and crosslinking in organic coagulation bath to prepare organic solvent forward osmosis membranes, Journal of Membrane Science, 620 (2021) 118829.
[56] B. Mi, M. Elimelech, Organic fouling of forward osmosis membranes: Fouling reversibility and cleaning without chemical reagents, Journal of membrane science, 348 (2010) 337-345.
[57] B. Mi, M. Elimelech, Chemical and physical aspects of organic fouling of forward osmosis membranes, Journal of membrane science, 320 (2008) 292-302.
[58] R.V. Linares, V. Yangali-Quintanilla, Z. Li, G. Amy, Rejection of micropollutants by clean and fouled forward osmosis membrane, Water research, 45 (2011) 6737-6744.

[59] W.A. Phillip, J.S. Yong, M. Elimelech, Reverse Draw Solute Permeation in Forward Osmosis: Modeling and Experiments, Environmental Science & Technology, 44 (2010) 5170-5176.
[60] S.-i. Nakao, Determination of pore size and pore size distribution: 3. Filtration membranes, Journal of Membrane Science, 96 (1994) 131-165.
[61] W. Shu-Sen, Effect of solution viscosity on ultrafiltration flux, Journal of Membrane Science, 39 (1988) 187-194.
[62] K.H.I.F.J. Vankelecom, Solvent-Resistant Nanofiltration Membranes, in: Encyclopedia of Membrane Science and Technology, 2013.
[63] H. Yasuda, A. Peterlin, Diffusive and bulk flow transport in polymers, Journal of Applied Polymer Science, 17 (1973) 433-442.
[64] H.K. Lonsdale, U. Merten, R.L. Riley, Transport properties of cellulose acetate osmotic membranes, Journal of Applied Polymer Science, 9 (1965) 1341-1362.
[65] H.Y. Ng, W. Tang, W.S. Wong, Performance of Forward (Direct) Osmosis Process: Membrane Structure and Transport Phenomenon, Environmental Science & Technology, 40 (2006) 2408-2413.
[66] P. Silva, S. Han, A.G. Livingston, Solvent transport in organic solvent nanofiltration membranes, Journal of Membrane Science, 262 (2005) 49-59.
[67] J.R. Werber, A. Deshmukh, M. Elimelech, The Critical Need for Increased Selectivity, Not Increased Water Permeability, for Desalination Membranes, Environmental Science & Technology Letters, 3 (2016) 112-120.
[68] W.R. Bowen, A.O. Sharif, Transport through microfiltration membranes - Particle hydrodynamics and flux reduction, Journal of Colloid And Interface Science, 168 (1994) 414-421.
[69] D.o.R. Machado, D. Hasson, R. Semiat, Effect of solvent properties on permeate flow through nanofiltration membranes. Part I: investigation of parameters affecting solvent flux, Journal of Membrane Science, 163 (1999) 93-102.
[70] L.G. Peeva, E. Gibbins, S.S. Luthra, L.S. White, R.P. Stateva, A.G. Livingston, Effect of concentration polarisation and osmotic pressure on flux in organic solvent nanofiltration, Journal of Membrane Science, 236 (2004) 121-136.
[71] S. Singh, K.C. Khulbe, T. Matsuura, P. Ramamurthy, Membrane characterization by solute transport and atomic force microscopy, Journal of Membrane Science, 142 (1998) 111-127.
[72] J.R. Mccutcheon, M. Elimelech, Modeling water flux in forward osmosis: Implications for improved membrane design, AIChE Journal, 53 (2007) 1736-1744.
[73] R. Bian, K. Yamamoto, Y. Watanabe, The effect of shear rate on controlling the concentration polarization and membrane fouling, Desalination, 131 (2000) 225-236.
[74] M.C. Porter, Concentration Polarization with Membrane Ultrafiltration, Product R&D, 11 (1972) 234-248.
[75] V. Gekas, B. Hallström, Mass transfer in the membrane concentration polarization layer under turbulent cross flow: I. Critical literature review and adaptation of existing sherwood correlations to membrane operations, Journal of Membrane Science, 30 (1987) 153-170.
[76] S.S. Sablani, M.F.A. Goosen, R. Al-Belushi, M. Wilf, Concentration polarization in ultrafiltration and reverse osmosis: a critical review, Desalination, 141 (2001) 269-289.
[77] B.S. Lalia, V. Kochkodan, R. Hashaikeh, N. Hilal, A review on membrane fabrication: Structure, properties and performance relationship, Desalination, 326 (2013) 77-95.
[78] S. Luque, D. Gómez, J.R. Álvarez, Industrial Applications of Porous Ceramic Membranes (Pressure-Driven Processes), in: Membrane Science and Technology, Elsevier, 2008, pp. 177-216.

[79] M. Padaki, R. Surya Murali, M.S. Abdullah, N. Misdan, A. Moslehyani, M.A. Kassim, N. Hilal, A.F. Ismail, Membrane technology enhancement in oil–water separation. A review, Desalination, 357 (2015) 197-207.
[80] B.A. Pulido, C. Waldron, M.G. Zolotukhin, S.P. Nunes, Porous polymeric membranes with thermal and solvent resistance, Journal of Membrane Science, 539 (2017) 187-196.
[81] X.Q. Cheng, Y.L. Zhang, Z.X. Wang, Z.H. Guo, Y.P. Bai, L. Shao, Recent Advances in Polymeric Solvent-Resistant Nanofiltration Membranes, Advances in Polymer Technology, 33 (2014) n/a-n/a.
[82] M.H. Davood Abadi Farahani, T.-S. Chung, Solvent resistant hollow fiber membranes comprising P84 polyimide and amine-functionalized carbon nanotubes with potential applications in pharmaceutical, food, and petrochemical industries, Chemical Engineering Journal, 345 (2018) 174-185.
[83] D.W. Mangindaan, N.M. Woon, G.M. Shi, T.S. Chung, P84 polyimide membranes modified by a tripodal amine for enhanced pervaporation dehydration of acetone, Chemical Engineering Science, 122 (2015) 14-23.
[84] H. Mariën, I.F.J. Vankelecom, Transformation of cross-linked polyimide UF membranes into highly permeable SRNF membranes via solvent annealing, Journal of Membrane Science, 541 (2017) 205-213.
[85] H. Siddique, Y. Bhole, L.G. Peeva, A.G. Livingston, Pore preserving crosslinkers for polyimide OSN membranes, Journal of Membrane Science, 465 (2014) 138-150.
[86] L.S. White, A.R. Nitsch, Solvent recovery from lube oil filtrates with a polyimide membrane, Journal of Membrane Science, 179 (2000) 267-274.
[87] P.S. Tin, T.S. Chung, Y. Liu, R. Wang, S.L. Liu, K.P. Pramoda, Effects of cross-linking modification on gas separation performance of Matrimid membranes, Journal of Membrane Science, 225 (2003) 77-90.
[88] G. Szekely, M.F. Jimenez-Solomon, P. Marchetti, J.F. Kim, A.G. Livingston, Sustainability assessment of organic solvent nanofiltration: from fabrication to application, Green Chemistry, 16 (2014) 4440-4473.
[89] J. Campbell, R.P. Davies, D.C. Braddock, A.G. Livingston, Improving the permeance of hybrid polymer/metal-organic framework (MOF) membranes for organic solvent nanofiltration (OSN) - development of MOF thin films via interfacial synthesis, Journal of Materials Chemistry A, 3 (2015) 9668-9674.
[90] X.Q. Cheng, Y.L. Zhang, Z.X. Wang, Z.H. Guo, Y.P. Bai, L. Shao, Recent advances in polymeric solvent‐resistant nanofiltration membranes, Advances in Polymer Technology, 33 (2014).
[91] E.J. Kappert, M.J.T. Raaijmakers, K. Tempelman, F.P. Cuperus, W. Ogieglo, N.E. Benes, Swelling of 9 polymers commonly employed for solvent-resistant nanofiltration membranes: A comprehensive dataset, Journal of Membrane Science, 569 (2019) 177-199.
[92] Y. Li, T. Verbiest, I. Vankelecom, Improving the flux of PDMS membranes via localized heating through incorporation of gold nanoparticles, Journal of Membrane Science, 428 (2013) 63-69.
[93] K. Ebert, J. Koll, M.F.J. Dijkstra, M. Eggers, Fundamental studies on the performance of a hydrophobic solvent stable membrane in non-aqueous solutions, Journal of Membrane Science, 285 (2006) 75-80.
[94] X. Li, B. Chen, W. Cai, T. Wang, Z. Wu, J. Li, Highly stable PDMS–PTFPMS/PVDF OSN membranes for hexane recovery during vegetable oil production, RSC advances, 7 (2017) 11381-11388.
[95] A.K. Hołda, I.F. Vankelecom, Understanding and guiding the phase inversion process for synthesis of solvent resistant nanofiltration membranes, Journal of Applied Polymer Science, 132 (2015).

[96] D. Chen, S. Yu, H. Zhang, X. Li, Solvent resistant nanofiltration membrane based on polybenzimidazole, Separation and Purification Technology, 142 (2015) 299-306.
[97] J. da Silva Burgal, L.G. Peeva, S. Kumbharkar, A. Livingston, Organic solvent resistant poly(ether-ether-ketone) nanofiltration membranes, Journal of Membrane Science, 479 (2015) 105-116.
[98] Hui M. Tham, K.Y. Wang, D. Hua, S. Japip, T.-S. Chung, From ultrafiltration to nanofiltration: Hydrazine cross-linked polyacrylonitrile hollow fiber membranes for organic solvent nanofiltration, Journal of Membrane Science, 542 (2017) 289-299.
[99] I.B. Valtcheva, P. Marchetti, A.G. Livingston, Crosslinked polybenzimidazole membranes for organic solvent nanofiltration (OSN): Analysis of crosslinking reaction mechanism and effects of reaction parameters, Journal of Membrane Science, 493 (2015) 568-579.
[100] A. Asadi Tashvigh, T.-S. Chung, Robust polybenzimidazole (PBI) hollow fiber membranes for organic solvent nanofiltration, Journal of Membrane Science, 572 (2019) 580-587.
[101] I.B. Valtcheva, S.C. Kumbharkar, J.F. Kim, Y. Bhole, A.G. Livingston, Beyond polyimide: Crosslinked polybenzimidazole membranes for organic solvent nanofiltration (OSN) in harsh environments, Journal of Membrane Science, 457 (2014) 62-72.
[102] Y. Liu, T.-S. Chung, R. Wang, D.F. Li, M.L. Chng, Chemical Cross-Linking Modification of Polyimide/Poly(ether sulfone) Dual-Layer Hollow-Fiber Membranes for Gas Separation, Industrial & Engineering Chemistry Research, 42 (2003) 1190-1195.
[103] J.C. Scaiano, A.F. Becknell, R.D. Small, Photochemistry of a benzophenone-containing bisimide: a model for inherently photosensitive polyimides, Journal of Photochemistry and Photobiology A: Chemistry, 44 (1988) 99-110.
[104] K. Vanherck, P. Vandezande, S.O. Aldea, I.F.J. Vankelecom, Cross-linked polyimide membranes for solvent resistant nanofiltration in aprotic solvents, Journal of Membrane Science, 320 (2008) 468-476.
[105] K. Vanherck, A. Cano-Odena, G. Koeckelberghs, T. Dedroog, I. Vankelecom, A simplified diamine crosslinking method for PI nanofiltration membranes, Journal of Membrane Science, 353 (2010) 135-143.
[106] F. Van Vught, W.F.C. Kools, B. te Hoogstraten, Membrane formation by phase inversion in multicomponent polymer system, in, PhD Thesis, University of Twente, 1998.
[107] H. Strathmann, K. Kock, The formation mechanism of phase inversion membranes, Desalination, 21 (1977) 241-255.
[108] A.K. Hołda, I.F.J. Vankelecom, Understanding and guiding the phase inversion process for synthesis of solvent resistant nanofiltration membranes, Journal of Applied Polymer Science, 132 (2015).
[109] M. Rahbari-sisakht, A.F. Ismail, T. Matsuura, Effect of bore fluid composition on structure and performance of asymmetric polysulfone hollow fiber membrane contactor for CO2 absorption, Separation and Purification Technology, 88 (2012) 99-106.
[110] L. K. Wang, J. Chen, Y.-T. Hung, N. Shammas, Membrane and Desalination Technologies, 2011.
[111] J.-J. Qin, J. Gu, T.-S. Chung, Effect of wet and dry-jet wet spinning on the shear-induced orientation during the formation of ultrafiltration hollow fiber membranes, Journal of Membrane Science, 182 (2001) 57-75.
[112] H. Adib, S. Hassanajili, D. Mowla, F. Esmaeilzadeh, Fabrication of integrally skinned asymmetric membranes based on nanocomposite polyethersulfone by supercritical CO2 for gas separation, The Journal of Supercritical Fluids, 97 (2015) 6-15.
[113] T.S. Chung, Z.L. Xu, W. Lin, Fundamental understanding of the effect of air - gap distance on the fabrication of hollow fiber membranes, Journal of applied Polymer science, 72 (1999) 379-395.

[114] I. Soroko, M.P. Lopes, A. Livingston, The effect of membrane formation parameters on performance of polyimide membranes for organic solvent nanofiltration (OSN): Part A. Effect of polymer/solvent/non-solvent system choice, Journal of Membrane Science, 381 (2011) 152-162.
[115] X. Li, C.H. Loh, R. Wang, W. Widjajanti, J. Torres, Fabrication of a robust high-performance FO membrane by optimizing substrate structure and incorporating aquaporin into selective layer, Journal of Membrane Science, 525 (2017) 257-268.
[116] H. Pang, H. Gong, M. Du, Q. Shen, Z. Chen, Effect of non-solvent additive concentration on CO2 absorption performance of polyvinylidenefluoride hollow fiber membrane contactor, Separation and Purification Technology, 191 (2018) 38-47.
[117] J. Qin, T.-S. Chung, Effect of dope flow rate on the morphology, separation performance, thermal and mechanical properties of ultrafiltration hollow fibre membranes, Journal of Membrane Science, 157 (1999) 35-51.
[118] D.-M. Wang, J.-Y. Lai, Recent advances in preparation and morphology control of polymeric membranes formed by nonsolvent induced phase separation, Current Opinion in Chemical Engineering, 2 (2013) 229-237.
[119] C. Dizman, M.A. Tasdelen, Y. Yagci, Recent advances in the preparation of functionalized polysulfones, Polymer International, 62 (2013) 991-1007.
[120] I. Soroko, A. Livingston, Impact of TiO2 nanoparticles on morphology and performance of crosslinked polyimide organic solvent nanofiltration (OSN) membranes, Journal of Membrane Science, 343 (2009) 189-198.
[121] J.-H. Kim, K.-H. Lee, Effect of PEG additive on membrane formation by phase inversion, Journal of Membrane Science, 138 (1998) 153-163.
[122] K.S. Goh, Y. Chen, J.Y. Chong, T.H. Bae, R. Wang, Thin film composite hollow fibre membrane for pharmaceutical concentration and solvent recovery, Journal of Membrane Science, 621 (2021) 119008.
[123] W.J. Lau, S. Gray, T. Matsuura, D. Emadzadeh, J. Paul Chen, A.F. Ismail, A review on polyamide thin film nanocomposite (TFN) membranes: History, applications, challenges and approaches, Water Research, 80 (2015) 306-324.
[124] L. Lin, R. Lopez, G.Z. Ramon, O. Coronell, Investigating the void structure of the polyamide active layers of thin-film composite membranes, Journal of Membrane Science, 497 (2016) 365-376.
[125] W. Fang, L. Shi, R. Wang, Interfacially polymerized composite nanofiltration hollow fiber membranes for low-pressure water softening, Journal of Membrane Science, 430 (2013) 129-139.
[126] W. Fang, L. Shi, R. Wang, Mixed polyamide-based composite nanofiltration hollow fiber membranes with improved low-pressure water softening capability, Journal of Membrane Science, 468 (2014) 52-61.
[127] S. Karan, Z. Jiang, A.G. Livingston, Sub–10 nm polyamide nanofilms with ultrafast solvent transport for molecular separation, Science, 348 (2015) 1347-1351.
[128] A. Ismail, M. Padaki, N. Hilal, T. Matsuura, W. Lau, Thin film composite membrane—Recent development and future potential, Desalination, 356 (2015) 140-148.
[129] B. Kim, G. Gwak, S. Hong, Review on methodology for determining forward osmosis (FO) membrane characteristics: Water permeability (A), solute permeability (B), and structural parameter (S), Desalination, 422 (2017) 5-16.
[130] C.Y. Tang, Q. She, W.C.L. Lay, R. Wang, A.G. Fane, Coupled effects of internal concentration polarization and fouling on flux behavior of forward osmosis membranes during humic acid filtration, Journal of Membrane Science, 354 (2010) 123-133.
[131] S. Zhao, L. Zou, Relating solution physicochemical properties to internal concentration polarization in forward osmosis, Journal of Membrane Science, 379 (2011) 459-467.

[132] G. Han, S. Zhang, X. Li, T.-S. Chung, Progress in pressure retarded osmosis (PRO) membranes for osmotic power generation, Progress in Polymer science, 51 (2015) 1-27.
[133] S.S. Manickam, J.R. McCutcheon, Understanding mass transfer through asymmetric membranes during forward osmosis: A historical perspective and critical review on measuring structural parameter with semi-empirical models and characterization approaches, Desalination, 421 (2017) 110-126.
[134] J.R. McCutcheon, R.L. McGinnis, M. Elimelech, A novel ammonia—carbon dioxide forward (direct) osmosis desalination process, Desalination, 174 (2005) 1-11.
[135] M. Park, J.J. Lee, S. Lee, J.H. Kim, Determination of a constant membrane structure parameter in forward osmosis processes, Journal of Membrane Science, 375 (2011) 241-248.
[136] J. Wang, D.S. Dlamini, A.K. Mishra, M.T.M. Pendergast, M.C. Wong, B.B. Mamba, V. Freger, A.R. Verliefde, E.M. Hoek, A critical review of transport through osmotic membranes, Journal of Membrane Science, 454 (2014) 516-537.
[137] N.Y. Yip, A. Tiraferri, W.A. Phillip, J.D. Schiffman, M. Elimelech, High Performance Thin-Film Composite Forward Osmosis Membrane, Environmental Science & Technology, 44 (2010) 3812-3818.
[138] S. Chou, R. Wang, L. Shi, Q. She, C. Tang, A.G. Fane, Thin-film composite hollow fiber membranes for pressure retarded osmosis (PRO) process with high power density, Journal of membrane science, 389 (2012) 25-33.
[139] Y. Liu, G.H. Koops, H. Strathmann, Characterization of morphology controlled polyethersulfone hollow fiber membranes by the addition of polyethylene glycol to the dope and bore liquid solution, Journal of Membrane Science, 223 (2003) 187-199.
[140] M.L. Yeow, Y.T. Liu, K. Li, Morphological study of poly(vinylidene fluoride) asymmetric membranes: Effects of the solvent, additive, and dope temperature, Journal of Applied Polymer Science, 92 (2004) 1782-1789.
[141] Z. Berk, Chapter 10 - Membrane processes, in: Z. Berk (Ed.) Food Process Engineering and Technology, Academic Press, San Diego, 2009, pp. 233-257.
[142] H. Strathmann, L. Giorno, E. Drioli, An Introduction to Membrane Science and Technology, 2011.
[143] J. Schwinge, P.R. Neal, D.E. Wiley, D.F. Fletcher, A.G. Fane, Spiral wound modules and spacers: Review and analysis, Journal of Membrane Science, 242 (2004) 129-153.
[144] P. Wang, T.-S. Chung, Recent advances in membrane distillation processes: Membrane development, configuration design and application exploring, Journal of membrane science, 474 (2015) 39-56.
[145] M.G. Buonomenna, J. Bae, Organic Solvent Nanofiltration in Pharmaceutical Industry, Separation & Purification Reviews, 44 (2015) 157-182.
[146] D. Ormerod, B. Sledsens, G. Vercammen, D. Van Gool, T. Linsen, A. Buekenhoudt, B. Bongers, Demonstration of purification of a pharmaceutical intermediate via organic solvent nanofiltration in the presence of acid, Separation and Purification Technology, 115 (2013) 158-162.
[147] J. Vanneste, D. Ormerod, G. Theys, D. Van Gool, B. Van Camp, S. Darvishmanesh, B. Van der Bruggen, Towards high resolution membrane-based pharmaceutical separations, Journal of Chemical Technology & Biotechnology, 88 (2013) 98-108.
[148] D. Ott, D. Kralisch, I. Denčić, V. Hessel, Y. Laribi, P.D. Perrichon, C. Berguerand, L. Kiwi-Minsker, P. Loeb, Life Cycle Analysis within Pharmaceutical Process Optimization and Intensification: Case Study of Active Pharmaceutical Ingredient Production, ChemSusChem, 7 (2014) 3521-3533.
[149] J.P. Sheth, Y. Qin, K.K. Sirkar, B.C. Baltzis, Nanofiltration-based diafiltration process for solvent exchange in pharmaceutical manufacturing, Journal of Membrane Science, 211 (2003) 251-261.

[150] A. LIVINGSTON, L. PEEVA, S. HAN, D. NAIR, S.S. LUTHRA, L.S. WHITE, L.M. FREITAS DOS SANTOS, Membrane Separation in Green Chemical Processing, Annals of the New York Academy of Sciences, 984 (2003) 123-141.
[151] I.M. Smallwood, Solvent recovery handbook, CRC Press, 2002.
[152] J. Geens, B. De Witte, B. Van der Bruggen, Removal of API's (active pharmaceutical ingredients) from organic solvents by nanofiltration, Separation Science and Technology, 42 (2007) 2435-2449.
[153] I. Sereewatthanawut, F.W. Lim, Y.S. Bhole, D. Ormerod, A. Horvath, A.T. Boam, A.G. Livingston, Demonstration of molecular purification in polar aprotic solvents by organic solvent nanofiltration, Organic Process Research & Development, 14 (2010) 600-611.
[154] S.R. Maddula, M. Kharkar, K. Manudhane, S. Kale, A. Bhori, A. Lali, P. Dubey, K.J. Sarma, A. Bhattacharya, R. Bandichhor, Preparative chromatography technique in the removal of isostructural genotoxic impurity in rizatriptan: use of physicochemical descriptors of solute and adsorbent, Organic Process Research & Development, 13 (2009) 683-689.
[155] B. Van der Bruggen, J. Schaep, D. Wilms, C. Vandecasteele, Influence of molecular size, polarity and charge on the retention of organic molecules by nanofiltration, Journal of Membrane Science, 156 (1999) 29-41.
[156] B. Li, Y. Cui, S. Japip, Z. Thong, T.-S. Chung, Graphene oxide (GO) laminar membranes for concentrating pharmaceuticals and food additives in organic solvents, Carbon, 130 (2018) 503-514.
[157] Y. Xu, F. You, H. Sun, L. Shao, Realizing Mussel-Inspired Polydopamine Selective Layer with Strong Solvent Resistance in Nanofiltration toward Sustainable Reclamation, ACS Sustainable Chemistry & Engineering, 5 (2017) 5520-5528.
[158] N.F.D. Aba, J.Y. Chong, B. Wang, C. Mattevi, K. Li, Graphene oxide membranes on ceramic hollow fibers – Microstructural stability and nanofiltration performance, Journal of Membrane Science, 484 (2015) 87-94.
[159] R. Mukherjee, P. Bhunia, S. De, Long term filtration modelling and scaling up of mixed matrix ultrafiltration hollow fiber membrane: a case study of chromium(VI) removal, Journal of Membrane Science, 570-571 (2019) 204-214.
[160] Y. Chen, C.H. Loh, L. Zhang, L. Setiawan, Q. She, W. Fang, X. Hu, R. Wang, Module scale-up and performance evaluation of thin film composite hollow fiber membranes for pressure retarded osmosis, Journal of Membrane Science, 548 (2018) 398-407.
[161] P.G. Ingole, W.K. Choi, G.B. Lee, H.K. Lee, Thin-film-composite hollow-fiber membranes for water vapor separation, Desalination, 403 (2017) 12-23.
[162] L. Setiawan, R. Wang, K. Li, A.G. Fane, Fabrication of novel poly(amide–imide) forward osmosis hollow fiber membranes with a positively charged nanofiltration-like selective layer, Journal of Membrane Science, 369 (2011) 196-205.
[163] S.-P. Sun, T.-S. Chung, K.-J. Lu, S.-Y. Chan, Enhancement of flux and solvent stability of Matrimid® thin-film composite membranes for organic solvent nanofiltration, AIChE Journal, 60 (2014) 3623-3633.
[164] S.K. Lim, L. Setiawan, T.-H. Bae, R. Wang, Polyamide-imide hollow fiber membranes crosslinked with amine-appended inorganic networks for application in solvent-resistant nanofiltration under low operating pressure, Journal of Membrane Science, 501 (2016) 152-160.
[165] Z. Wang, B. Zhang, H. Yu, L. Sun, C. Jiao, W. Liu, Microporous polyimide networks with large surface areas and their hydrogen storage properties, Chemical Communications, 46 (2010) 7730-7732.
[166] S.-J. Yang, W. Jang, C. Lee, Y.G. Shul, H. Han, The effect of crosslinked networks with poly(ethylene glycol) on sulfonated polyimide for polymer electrolyte membrane fuel cell, Journal of Polymer Science Part B: Polymer Physics, 43 (2005) 1455-1464.

[167] N.K. Saha, S.V. Joshi, Performance evaluation of thin film composite polyamide nanofiltration membrane with variation in monomer type, Journal of Membrane Science, 342 (2009) 60-69.
[168] S.-H. Park, Y.-S. Ko, S.-J. Park, J.S. Lee, J. Cho, K.-Y. Baek, I.T. Kim, K. Woo, J.-H. Lee, Immobilization of silver nanoparticle-decorated silica particles on polyamide thin film composite membranes for antibacterial properties, Journal of Membrane Science, 499 (2016) 80-91.
[169] J. Zuo, Y. Wang, S.P. Sun, T.-S. Chung, Molecular design of thin film composite (TFC) hollow fiber membranes for isopropanol dehydration via pervaporation, Journal of Membrane Science, 405-406 (2012) 123-133.
[170] L. Li, S. Zhang, X. Zhang, Preparation and characterization of poly(piperazineamide) composite nanofiltration membrane by interfacial polymerization of 3,3′,5,5′-biphenyl tetraacyl chloride and piperazine, Journal of Membrane Science, 335 (2009) 133-139.
[171] C.M. Hansen, 50 Years with solubility parameters - Past and future, Progress in Organic Coatings, 51 (2004) 77-84.
[172] H.M. Tham, K.Y. Wang, D. Hua, S. Japip, T.S. Chung, From ultrafiltration to nanofiltration: Hydrazine cross-linked polyacrylonitrile hollow fiber membranes for organic solvent nanofiltration, Journal of Membrane Science, 542 (2017) 289-299.
[173] G. Falca, V.-E. Musteata, A.R. Behzad, S. Chisca, S.P. Nunes, Cellulose hollow fibers for organic resistant nanofiltration, Journal of Membrane Science, 586 (2019) 151-161.
[174] S. Jeon, A. Nishitani, L. Cheng, L.-F. Fang, N. Kato, T. Shintani, H. Matsuyama, One-step fabrication of polyamide 6 hollow fibre membrane using non-toxic diluents for organic solvent nanofiltration, RSC Advances, 8 (2018) 19879-19882.
[175] S.-P. Sun, S.-Y. Chan, W. Xing, Y. Wang, T.-S. Chung, Facile Synthesis of Dual-Layer Organic Solvent Nanofiltration (OSN) Hollow Fiber Membranes, ACS Sustainable Chemistry & Engineering, 3 (2015) 3019-3023.
[176] S.-P. Sun, S.-Y. Chan, T.-S. Chung, A slow–fast phase separation (SFPS) process to fabricate dual-layer hollow fiber substrates for thin-film composite (TFC) organic solvent nanofiltration (OSN) membranes, Chemical Engineering Science, 129 (2015) 232-242.
[177] J.A. Whu, B.C. Baltzis, K.K. Sirkar, Nanofiltration studies of larger organic microsolutes in methanol solutions, Journal of Membrane Science, 170 (2000) 159-172.
[178] A. Tiraferri, N.Y. Yip, W.A. Phillip, J.D. Schiffman, M. Elimelech, Relating performance of thin-film composite forward osmosis membranes to support layer formation and structure, Journal of Membrane Science, 367 (2011) 340-352.
[179] D.o.R. Machado, D. Hasson, R. Semiat, Effect of solvent properties on permeate flow through nanofiltration membranes: Part II. Transport model, Journal of Membrane Science, 166 (2000) 63-69.
[180] A.K. Ghosh, E.M.V. Hoek, Impacts of support membrane structure and chemistry on polyamide–polysulfone interfacial composite membranes, Journal of Membrane Science, 336 (2009) 140-148.
[181] Y. Chen, L. Setiawan, S. Chou, X. Hu, R. Wang, Identification of safe and stable operation conditions for pressure retarded osmosis with high performance hollow fiber membrane, Journal of Membrane Science, 503 (2016) 90-100.
[182] A. Buekenhoudt, F. Bisignano, G. De Luca, P. Vandezande, M. Wouters, K. Verhulst, Unravelling the solvent flux behaviour of ceramic nanofiltration and ultrafiltration membranes, Journal of Membrane Science, 439 (2013) 36-47.
[183] S. Darvishmanesh, J. Degrève, B. Van der Bruggen, Mechanisms of solute rejection in solvent resistant nanofiltration: the effect of solvent on solute rejection, Physical Chemistry Chemical Physics, 12 (2010) 13333-13342.

[184] M.F. Jimenez Solomon, Y. Bhole, A.G. Livingston, High flux hydrophobic membranes for organic solvent nanofiltration (OSN)—Interfacial polymerization, surface modification and solvent activation, Journal of Membrane Science, 434 (2013) 193-203.
[185] S. Wang, D. Mahalingam, B. Sutisna, S.P. Nunes, 2D-dual-spacing channel membranes for high performance organic solvent nanofiltration, Journal of Materials Chemistry A, 7 (2019) 11673-11682.
[186] Y.C. Xu, Y.P. Tang, L.F. Liu, Z.H. Guo, L. Shao, Nanocomposite organic solvent nanofiltration membranes by a highly-efficient mussel-inspired co-deposition strategy, Journal of Membrane Science, 526 (2017) 32-42.
[187] J. Aburabie, K.-V. Peinemann, Crosslinked poly(ether block amide) composite membranes for organic solvent nanofiltration applications, Journal of Membrane Science, 523 (2017) 264-272.
[188] F.M. Sukma, P.Z. Çulfaz-Emecen, Cellulose membranes for organic solvent nanofiltration, Journal of Membrane Science, 545 (2018) 329-336.
[189] S. Yuan, J. Swartenbroekx, Y. Li, J. Zhu, F. Ceyssens, R. Zhang, A. Volodine, J. Li, P. Van Puyvelde, B. Van der Bruggen, Facile synthesis of Kevlar nanofibrous membranes via regeneration of hydrogen bonds for organic solvent nanofiltration, Journal of Membrane Science, 573 (2019) 612-620.
[190] Y. Feng, M. Weber, C. Maletzko, T.-S. Chung, Fabrication of organic solvent nanofiltration membranes via facile bioinspired one-step modification, Chemical Engineering Science, 198 (2019) 74-84.
[191] S. Yang, H. Li, X. Zhang, S. Du, J. Zhang, B. Su, X. Gao, B. Mandal, Amine-functionalized ZIF-8 nanoparticles as interlayer for the improvement of the separation performance of organic solvent nanofiltration (OSN) membrane, Journal of Membrane Science, 614 (2020) 118433.
[192] H. Yan, X. Miao, J. Xu, G. Pan, Y. Zhang, Y. Shi, M. Guo, Y. Liu, The porous structure of the fully-aromatic polyamide film in reverse osmosis membranes, Journal of Membrane Science, 475 (2015) 504-510.
[193] I. APPLIED MEMBRANES, Dow Filmtec Commercial RO Elements, in, APPLIED MEMBRANES, INC, 2020, pp. Specification of DOW RO membranes.
[194] D. Li, R. Wang, T.-S. Chung, Fabrication of lab-scale hollow fiber membrane modules with high packing density, Separation and Purification Technology, 40 (2004) 15-30.
[195] G.M. Shi, M.H. Davood Abadi Farahani, J.Y. Liu, T.-S. Chung, Separation of vegetable oil compounds and solvent recovery using commercial organic solvent nanofiltration membranes, Journal of Membrane Science, 588 (2019) 117202.
[196] Z.-X. Low, J. Shen, Determining stability of organic solvent nanofiltration membranes by cross-flow aging, Separation and Purification Technology, 256 (2021) 117840.
[197] R.K. McGovern, J.H. Lienhard V, On the potential of forward osmosis to energetically outperform reverse osmosis desalination, Journal of Membrane Science, 469 (2014) 245-250.
[198] O.A. Bamaga, A. Yokochi, B. Zabara, A.S. Babaqi, Hybrid FO/RO desalination system: Preliminary assessment of osmotic energy recovery and designs of new FO membrane module configurations, Desalination, 268 (2011) 163-169.
[199] C. Feng, R. Wang, B. Shi, G. Li, Y. Wu, Factors affecting pore structure and performance of poly(vinylidene fluoride-co-hexafluoro propylene) asymmetric porous membrane, Journal of Membrane Science, 277 (2006) 55-64.
[200] S. Mochizuki, A.L. Zydney, Dextran transport through asymmetric ultrafiltration membranes: Comparison with hydrodynamic models, Journal of Membrane Science, 68 (1992) 21-41.
[201] D.G. Miller, J.A. Rard, L.B. Eppstein, J.G. Albright, Mutual diffusion coefficients and ionic transport coefficients lij of magnesium chloride-water at 25.degree.C, The Journal of Physical Chemistry, 88 (1984) 5739-5748.

[202] M. Maleque, M.R. Hasan, F. Hossen, S. Safi, Development and validation of a simple UV spectrophotometric method for the determination of levofloxacin both in bulk and marketed dosage formulations, Journal of Pharmaceutical Analysis, 2 (2012) 454-457.
[203] J.R. McCutcheon, M. Elimelech, Influence of concentrative and dilutive internal concentration polarization on flux behavior in forward osmosis, Journal of Membrane Science, 284 (2006) 237-247.
[204] C. Suh, S. Lee, Modeling reverse draw solute flux in forward osmosis with external concentration polarization in both sides of the draw and feed solution, Journal of Membrane Science, 427 (2013) 365-374.
[205] S. Darvishmanesh, A. Buekenhoudt, J. Degrève, B. Van der Bruggen, General model for prediction of solvent permeation through organic and inorganic solvent resistant nanofiltration membranes, Journal of Membrane Science, 334 (2009) 43-49.
[206] S. Araki, D. Gondo, S. Imasaka, H. Yamamoto, Permeation properties of organic compounds from aqueous solutions through hydrophobic silica membranes with different functional groups by pervaporation, Journal of Membrane Science, 514 (2016) 458-466.
[207] M. Xie, W.E. Price, L.D. Nghiem, M. Elimelech, Effects of feed and draw solution temperature and transmembrane temperature difference on the rejection of trace organic contaminants by forward osmosis, Journal of Membrane Science, 438 (2013) 57-64.
[208] E. Dražević, K. Košutić, V. Freger, Permeability and selectivity of reverse osmosis membranes: Correlation to swelling revisited, Water Research, 49 (2014) 444-452.
[209] P. Schmidt, T. Köse, P. Lutze, Characterisation of organic solvent nanofiltration membranes in multi-component mixtures: Membrane rejection maps and membrane selectivity maps for conceptual process design, Journal of Membrane Science, 429 (2013) 103-120.
[210] T. Chan, I. Lee, K. Chan, Effect of Solvent on Diffusion: Probing with Nonpolar Solutes, The Journal of Physical Chemistry B, 118 (2014) 10945-10955.
[211] A.J. Easteal, L.A. Woolf, Solute–solvent interaction effects on tracer diffusion coefficients, Journal of the Chemical Society, Faraday Transactions 1: Physical Chemistry in Condensed Phases, 80 (1984) 1287-1295.
[212] D. Peshev, L.G. Peeva, G. Peev, I.I.R. Baptista, A.T. Boam, Application of organic solvent nanofiltration for concentration of antioxidant extracts of rosemary (Rosmarinus officiallis L.), Chemical Engineering Research and Design, 89 (2011) 318-327.
[213] L. Peeva, J.d.S. Burgal, I. Valtcheva, A.G. Livingston, Continuous purification of active pharmaceutical ingredients using multistage organic solvent nanofiltration membrane cascade, Chemical Engineering Science, 116 (2014) 183-194.